

This article appeared in a journal published by Elsevier. The attached copy is furnished to the author for internal non-commercial research and education use, including for instruction at the authors institution and sharing with colleagues.

Other uses, including reproduction and distribution, or selling or licensing copies, or posting to personal, institutional or third party websites are prohibited.

In most cases authors are permitted to post their version of the article (e.g. in Word or Tex form) to their personal website or institutional repository. Authors requiring further information regarding Elsevier's archiving and manuscript policies are encouraged to visit:

<http://www.elsevier.com/authorsrights>



Contents lists available at ScienceDirect

Physics Reports

journal homepage: www.elsevier.com/locate/physrep



Tunable transport with broken space–time symmetries



Sergey Denisov^{a,b,f,*}, Sergej Flach^c, Peter Hänggi^{b,d,e}

^a Sumy State University, Rimsky-Korsakov Street 2, 40007 Sumy, Ukraine

^b Institut für Physik, Universität Augsburg, Universitätsstr.1, 86135 Augsburg, Germany

^c New Zealand Institute for Advanced Study, Centre for Theoretical Chemistry and Physics, Massey University, Private Bag 102 904 NSMCS, 0746 Auckland, New Zealand

^d Center for Phononics and Thermal Energy Science, School of Physics Science and Engineering, Tongji University, 200092 Shanghai, China

^e Nanosystems Initiative Munich, Schellingstr. 4, D-80799 München, Germany

^f Department of Radiophysics, Nizhny Novgorod University, Gagarin Avenue 23, 603950 Nizhny Novgorod, Russia

ARTICLE INFO

Article history:

Accepted 21 January 2014

Available online 4 February 2014

editor: J. Eichler

Keywords:

Nonlinear dynamics
Ratchet effect
Hamiltonian chaos
Floquet theory
Quantum optics

ABSTRACT

Transport properties of particles and waves in spatially periodic structures that are driven by external time-dependent forces manifestly depend on the space–time symmetries of the corresponding equations of motion. A systematic analysis of these symmetries uncovers the conditions necessary for obtaining directed transport. In this work we give a unified introduction into the symmetry analysis and demonstrate its action on the motion in one-dimensional periodic, both in time and space, potentials. We further generalize the analysis to quasi-periodic drives, higher space dimensions, and quantum dynamics. Recent experimental results on the transport of cold and ultracold atomic ensembles in ac-driven optical potentials are reviewed as illustrations of theoretical considerations.

© 2014 Elsevier B.V. All rights reserved.

Contents

1. Introduction.....	78
2. Symmetries in a nutshell	79
2.1. Symmetries of periodic functions.....	79
2.2. Symmetries of quasiperiodic functions.....	80
2.3. An example: Hamiltonian ratchets.....	80
3. Directed transport in one spatial dimension.....	81
3.1. Symmetry analysis.....	82
3.2. The role of initial conditions	83
3.3. Special cases	83
3.3.1. Additive driving	83
3.3.2. Multiplicative driving.....	84
3.3.3. Traveling potentials.....	85
3.3.4. Gating ratchets.....	85
3.4. Extension to quasiperiodic driving.....	85
3.5. Dynamics	86
3.5.1. Hamiltonian ratchets revisited	86

* Corresponding author at: Institut für Physik, Universität Augsburg, Universitätsstr.1, 86135 Augsburg, Germany. Tel.: +49 821 598 3228.

E-mail addresses: sergey.denisov@physik.uni-augsburg.de (S. Denisov), Hanggi@physik.uni-augsburg.de (P. Hänggi).

3.5.2.	Transport with dissipation	89
3.5.3.	Transport in the overdamped limit	89
3.6.	Transport with noise and fluctuations	90
3.6.1.	Molecular chaos assumption and the Boltzmann equation	92
3.6.2.	From Langevin dynamics to the Fokker–Planck equation	92
3.7.	Experiments with cold atoms	94
3.7.1.	Cold atom ratchets with periodic driving	95
3.7.2.	Cold atom ratchets with quasiperiodic driving	97
4.	Directed transport in two and three spatial dimensions	98
4.1.	Symmetry analysis	99
4.2.	Applications: numerical studies	101
4.3.	Experiments with cold atoms	104
5.	Quantum ratchets	106
5.1.	Symmetry analysis	107
5.2.	Applications: numerical studies	110
5.3.	Experiments with Bose–Einstein condensates	111
6.	Extensions and outlook	113
	Acknowledgments	117
	References	117

1. Introduction

The last decade has witnessed a large number of studies on nonequilibrium, fluctuation-induced transport in potentials and confinements of different shapes and geometries, where ubiquitous fluctuations included colored or idealized white noise or/and regular time-periodic components [1–4]. The main subject of these studies, the so-called *ratchet* effect, occurs due to the violation of the thermal equilibrium so that the Second Law of Thermodynamics no longer applies. With no restriction imposed by the Second Law there are no constraints on the appearance of a steady transport, even in the absence of constant forces or gradients. The issue was recognized already back in 1912, when Marian von Smoluchowski posed the question concerning the (im)possibility to extract work from a ratchet-toothed wheel placed into a heat bath [5]. Fifty years later, it had been revived and popularized by Richard Feynman [6], and since the late 1990s the studies of the ratchet phenomenon proceeded along many research tracks in statistical mechanics, condensed matter, chemistry and biophysics [3,4,7,8].

The majority of ratchet studies typically focuses on systems acting in a noisy and viscous environment, so that the resulting dynamics emerges to be essentially stochastic and dissipative. The corresponding evolution, being hampered by the thermal noise and/or other sorts of random nonequilibrium fluctuations, is characterized by space–time correlations that are restricted to short ranges. This extends also to quantum ratchets, see Refs. [9–13]. A large variety of strongly dissipative stochastic models was put forward in order to describe intracellular transport and to serve as blue-prints for synthetic molecular motors, microfluidic pumps, and colloidal separators. Most of them can be unified under the name ‘*Brownian motors*’ [3,4,7]. A recent comprehensive review by one of the authors [8] provides an up-to-date information on such Brownian machinery.

Fast progress in experimental manipulations with cold- and ultra-cold atoms [14,15] has created a new testing ground for the ratchet concept. The corresponding physical systems, ensembles of atoms kept in optical or magnetic confinements [16,17], evolve without being subjected to strong external noise. The resulting dynamics appears to be coherent on time scales much larger than the typical time scale set by the characteristic frequency of the potential. As it is known from the theory [18], the evolution of a fully coherent system may be governed by several co-existing invariant manifolds, e.g. multiple attractors in the limit of weak dissipation [19,20], regular and chaotic regions in the classical Hamiltonian limit [20] and eigenstates in the case of quantum evolution [21]. Asymptotic regimes appear as interference patterns to which different invariant manifolds contribute simultaneously. Even the presence of weak fluctuations cannot erase the interference effects completely [22]. The functioning of Hamiltonian and weakly dissipative ratchets, therefore, is essentially different from that of Brownian motors, in which the presence of strong ambient noise induces an effective averaging over the system phase space and erases the memory on initial states, or, more generally, on initial preparations [1,4].

Various interpretations of the ratchet effect have been introduced, including Maxwell daemons, harmonic mixing, nonlinear response, to name but a few among others [1,2,4,3,8]. However, often evaluation of a particular ratchet system does not allow for an in-depth analytical treatment but calls for direct numerical simulations [23,24]. The focus of this review, the *symmetry analysis* [25,26], allows to predict and control the rectification outcome avoiding computational studies of the system dynamics. The latter can become rather cumbersome when chaotic motion, and thus a sensitivity to initial conditions, are at work. The analysis can be performed systematically on various levels of description, ranging from microscopic equations of motion to kinetic equations governing the evolution of probability distributions. To be more specific, the symmetry analysis does produce a list of symmetries which *prevent* rectification. The corresponding symmetries include operations on the system variables and time. A proper choice of control parameters, especially of the driving field,

leads to the destruction of all relevant ‘no-go’ symmetries which forbid rectification. The review focuses on that relationship between the appearance of *directed transport* and the *symmetries of the equations* describing the evolution of the system.

The structure of the review is as follows: Section 2 introduces the main ideas which underpin the symmetry analysis. In Section 3 we apply the symmetry analysis in the context of classical one-dimensional transport, while in Section 4 we step into higher dimensions and discuss multi-directional currents and the generation of vortices. We next discuss the extension of the ratchet concept to the case of coherent quantum dynamics in Section 5. In all these sections, the theoretical analysis is supplemented with the outcomes of numerical studies and recent results from the field of cold- and ultracold-atom experimental physics. Finally, in Section 6 we briefly touch upon applications of the analysis to other systems, such as Josephson junctions and spins, and conclude the review with a discussion on issues that constitute promising directions for further applications of the symmetry analysis.

2. Symmetries in a nutshell

Consider a set of differential equations, which governs the evolution of a system,

$$\dot{\Psi} = \mathcal{F}_{\theta}(\Psi, t) = \mathcal{F}_{\theta}(\Psi, t + T), \quad (1)$$

where Ψ is a vector describing the state of the system. Examples are a finite set of coordinates and momenta, $\Psi = \{x, y, \dots, v_x, v_y, \dots\}$, or a vector in a Hilbert space describing a state of a quantum system, or a probability density function whose evolution is governed by the Fokker–Planck equation. Here $\dot{\Psi}$ denotes the derivative of Ψ with respect to time. The vector function $\mathcal{F}_{\theta}(\Psi, t)$ is explicitly time-periodic with period T and may depend on a set of control parameters $\theta = \{\theta_1, \theta_2, \dots, \theta_D\}$. Consider an observable $A(t) = \mathcal{A}[\Psi(t)]$, where \mathcal{A} is an operator or functional over the phase space of the system. Is it possible to tune the control parameter(s) θ in such a way that the evolving system yields a nonzero value of the time-averaged observable, $\bar{A} = \lim_{t \rightarrow \infty} (1/t) \int_0^t A(s) ds \neq 0$? To answer the question, we follow the *symmetry analysis protocol* [26]:

1. Identify all possible transformations, $\hat{S} : \{\Psi, t\} \rightarrow \{\Psi', t'\}$, which change the sign of the observable, $\tilde{A}(t') = \mathcal{A}[\Psi'(t')] = -A(t) = -\mathcal{A}[\Psi(t)]$, and at the same time leave Eq. (1) invariant. Then the time evolution of the observable, $\tilde{A}(t') = \mathcal{A}[\Psi'(t')]$, is supported by a solution of (1), i.e. a certain trajectory in the system phase space. Transformations may include, for example, time reversal, $t \rightarrow t' = -t$, a time shift, $t \rightarrow t' = t + \tau$, similar operations on the space variables, or/and other operations on system variables, including, for example, permutations [27].
2. Consider contributions from the original trajectory yielding an observable $A(t)$ and the symmetry-related trajectory, which yields $\tilde{A}(t') = -A(t)$. If both are parts of the same long trajectory, or if they belong to different trajectories, which have identical statistical weights, the average expectation value of the observable vanishes exactly, $\bar{A} = 0$.
3. Choose control parameters in such a way as to destroy *all* the symmetries. Then, in general, the rectification effect would appear, with $\bar{A} \neq 0$, in agreement with Curie's principle [28].

2.1. Symmetries of periodic functions

Consider two periodic functions,

$$E(t + T) = E(t), \quad f(x + L) = f(x), \quad (2)$$

with the temporal period $T = 2\pi/\omega$ and spatial period $L = 2\pi/k$, and both with zero mean

$$\int_0^T E(t) dt = \int_0^L f(x) dx = 0. \quad (3)$$

The functions can be *symmetric* around certain values of their arguments,

$$E_s(t - t') = E_s(-t - t'), \quad f_s(x - x') = f_s(-x - x'). \quad (4)$$

After proper shifts the functions, being expanded in Fourier series, reduce to a cosine series.

The functions can be *antisymmetric* around certain values of their arguments,

$$E_a(t - t') = -E_a(-t - t'), \quad f_a(x - x') = -f_a(-x - x'). \quad (5)$$

After proper shifts, the Fourier expansions of the functions reduce to a sine series.

The functions can be *shift-symmetric*, in that case they change their signs after the shift of the argument by half of the period,¹

$$E_{sh}(t + T/2) = -E_{sh}(t), \quad f_{sh}(x + L/2) = -f_{sh}(x). \quad (6)$$

¹ In the context of nonlinear oscillations the shift-symmetric property is also referred to as ‘anti-periodicity’, see Ref. [29] and references therein.

The Fourier expansion of shift-symmetric functions contains odd harmonics only.

Henceforth, we mark these three symmetries by labels “s”, “a” and “sh” respectively. A periodic function of zero-mean may have neither of the symmetries, exactly one of them, or all three. For example, $E(t) = \cos(t)$ possesses all three symmetries, for it is symmetric around zero, antisymmetric around $t = \pi/2$, and evidently shift-symmetric. Function $f(x) = \cos(x) + \cos(3x + \Delta)$ is shift-symmetric, and in addition becomes symmetric and antisymmetric for $\Delta = 0, \pi$. Finally, function $E(t) = \cos(t) + \cos(2t + \theta)$ does not possess any of the symmetries except for $\theta = 0, \pi$ (symmetric) and $\theta = \pm\pi/2$ (antisymmetric). Differentiation preserves shift symmetry and exchanges symmetry with antisymmetry (and vice versa).

2.2. Symmetries of quasiperiodic functions

A quasiperiodic function $E(t)$ can be viewed as a function that depends on N different variables t_i . The latter are linear functions of the variable t but with different coefficients, i.e. frequencies:

$$E(t) \equiv \tilde{E}(t_1, t_2, \dots, t_N), \quad \frac{dt_i}{dt} = \omega_i. \quad (7)$$

The frequencies are mutually incommensurate, with all the ratios ω_i/ω_j being irrational numbers when $i \neq j$. The function \tilde{E} is periodic in every of these variables, $\tilde{E}(t_1, t_2, \dots, t_i + 2\pi, \dots, t_N) = \tilde{E}(t_1, t_2, \dots, t_i, \dots, t_N)$, for all i .

A quasiperiodic function $E(t)$ is *symmetric* if

$$\tilde{E}_s(-t_1, -t_2, \dots, -t_N) = \tilde{E}_s(t_1, t_2, \dots, t_N), \quad (8)$$

and *antisymmetric* if

$$\tilde{E}_a(-t_1, -t_2, \dots, -t_N) = -\tilde{E}_a(t_1, t_2, \dots, t_N). \quad (9)$$

Note that these two symmetry operations necessarily involve simultaneous actions on all N variables t_i .

Finally, the quasiperiodic function $E(t)$ can be *shift-symmetric* on a subset of indices $\{i, \dots, j\}$, if

$$\tilde{E}_{sh}(t_1, \dots, t_i + \pi, \dots, t_j + \pi, \dots, t_N) = -\tilde{E}_{sh}(t_1, \dots, t_i, \dots, t_j, \dots, t_N). \quad (10)$$

Note that shift-symmetry may involve actions on one, two, and so on up to all N variables.

Topologically, the function $\tilde{E}(t)$ evolves on a N -dimensional torus, $\{t_1, \dots, t_N\}$. The incommensurability of the frequencies guarantees that, in the course of time, the torus surface is scanned in an ergodic manner [19,20], and will be covered with uniform density in the asymptotic limit $t \rightarrow \infty$.

2.3. An example: Hamiltonian ratchets

Let us consider a dissipationless, point-like particle of mass m , which moves in a spatially periodic potential. In addition, the potential is periodically modulated in time, e. g. because the particle is electrical charged and exposed to a time-periodic spatially-homogeneous electric field. The position of the particle is governed by the following equation of motion [19]:

$$m\ddot{x} = \cos(x) + E(t). \quad (11)$$

The driving function $E(t)$ is periodic, $E(t + T) = E(t)$, and has zero mean, $\langle E(t) \rangle = (1/T) \int_0^T E(\tau) d\tau = 0$. Let us find the conditions when the driving field sets the particle into motion with a nonzero average velocity.

The relevant observable is

$$\bar{v} = \langle \dot{x} \rangle = \lim_{t \rightarrow \infty} x(t)/t. \quad (12)$$

We search for transformations of the system variables, $\hat{S} : \{x, t\} \rightarrow \{\tilde{x}, \tilde{t}\}$, that change the sign of the observable, $\bar{v}(\tilde{x}, \tilde{t}) = -\bar{v}(x, t)$, while leaving the equation of motion (11) invariant.

There are two possibilities to change the sign of \dot{x} . Namely, either to change the sign of x and, in case of a need, perform additional shifts, $\tilde{x} = -x + \chi$, $\tilde{t} = t + \tau$, or change the sign of time, $\tilde{t} = -t + \tau$, with an additional spatial shift $\tilde{x} = x + \chi$, if needed. Thus we have two possible transformations:

$$\hat{S}_x[\chi, \tau] : x \rightarrow \tilde{x} = -x + \chi, \quad t \rightarrow \tilde{t} = t + \tau, \quad (13)$$

$$\hat{S}_t[\chi, \tau] : x \rightarrow \tilde{x} = x + \chi, \quad t \rightarrow \tilde{t} = -t + \tau. \quad (14)$$

Transformation \hat{S}_x changes the sign of \ddot{x} on the lhs of Eq. (11). Additional shifts in time and space have to be performed, such that the rhs terms change their signs as well. The force term will change sign by setting $\chi = \pi$. The drive must be *shift-symmetric*, with $\tau = T/2$, $E(t + T/2) = -E(t)$, and only in this case symmetry \hat{S}_x will hold. In order to break this symmetry, we can simply choose a function $E(t)$ which is not shift-symmetric (note, however, that we could also choose a

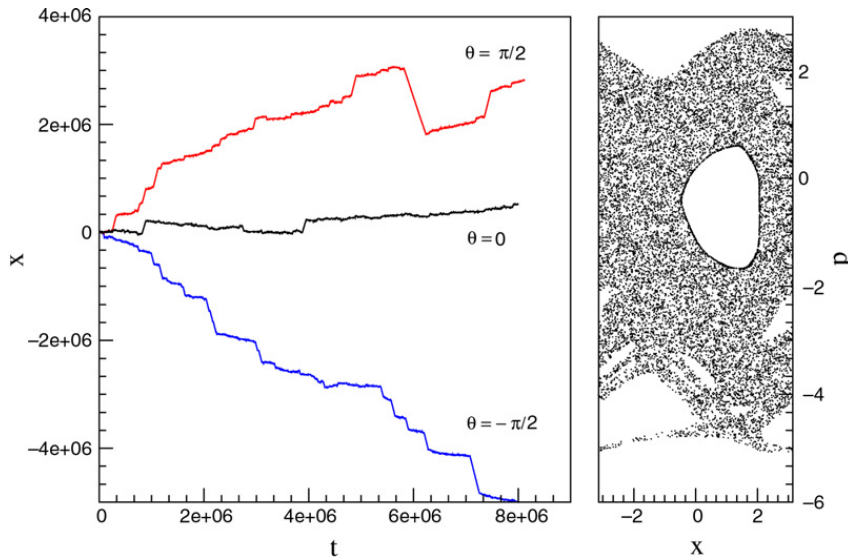


Fig. 1. (Color online) Left panel: Dependence $x(t)$ vs. t for Eq. (11), with $m = 1$ and initial conditions $\{x = \pi, \dot{x} = 0, t = 0\}$. Right panel: Poincaré section for $\theta = -\pi/2$ plotted at time instances $t = 0, T, \dots, 10^4 T$. The parameters of the driving function, Eq. (15), are $E_1 = E_2 = 2$ and $\omega = 2$.

more complicated ratchet potential which alone could violate this symmetry). The simplest choice of a driving function that violates shift-symmetry is a bi-harmonic combination,

$$E(t) = E_1 \cos(\omega t) + E_2 \cos(2\omega t + \theta). \quad (15)$$

Transformation \hat{S}_t does not change the sign of \ddot{x} . Reversal of time does not affect the first term on the rhs of Eq. (11), $\cos(x)$, either. However, the reversal affects the driving term, $E(t)$. Then, for the symmetry \hat{S}_t to hold, the driving function should be symmetric, $E(-t - \tau) = E(t)$. To break this symmetry we have to choose a function $E(t)$ which is not symmetric. For the bi-harmonic function (15) this holds with $\theta \neq 0, \pm\pi$. Therefore, a bi-harmonic driving function alone can destroy both symmetries.

The dynamics of the system (11) allows both for regular (periodic and quasiperiodic) solutions and chaotic trajectories embedded into the chaotic layer around the line $\dot{x} = 0$ [20]. Note that ergodicity holds in the layer. Therefore the average velocity will be the same for all trajectories from the chaotic layer, at the asymptotic limit $t \rightarrow \infty$. If any of the symmetries, \hat{S}_x or \hat{S}_t , holds, then, when it applied to a chaotic trajectory, it will generate a new trajectory, also embedded inside the layer and therefore chaotic. Consequently the average velocity vanishes inside the layer.

In the absence of both symmetries, with a properly set parameter θ , a directed transport within the stochastic layer will emerge. This was observed in numerical simulations, see, for example, Ref. [25]. Fig. 1 depicts several trajectories launched from the same initial point, $\{x(0), \dot{x}(0)\}$, chosen in the layer area and then propagated in time.² The numerical results are in a full agreement with the theory. Asymptotic transport is negligible when $\theta = 0$ and symmetry \hat{S}_t is present. There is a steady transport in positive (negative) direction when $\theta = \pi/2$ ($-\pi/2$) and both key symmetries are broken. This is a typical performance of *Hamiltonian ratchets*³ [11,25,30,32,33], see for a further discussion in Section 3.5.1.

3. Directed transport in one spatial dimension

In this section we consider the general case of a point-like particle moving in a time-modulated spatially periodic potential V ,

$$m\ddot{x} + \gamma\dot{x} = g(x, t), \quad g(x, t) = -\partial_x V(x, t). \quad (16)$$

Zero-mean force function $g(x, t)$ is periodic in both x and t :

$$g(x, t) = g(x, t + T) = g(x + L, t), \quad \int_0^T \int_0^L g(x, t) dt dx = 0. \quad (17)$$

Eq. (16) can be rewritten as a set of three autonomous differential equations of first order,

$$\dot{x} = p/m, \quad (18)$$

² Attention should be paid to the choice of the long-run propagation algorithm, which needs to be symplectic in the case of Hamiltonian systems, see Refs. [11,25,30].

³ A Hamiltonian ratchet is an ac-driven Hamiltonian system which is able to exhibit regimes of directed transport in absence of a bias [4,11,24,30–32].

$$\dot{p} = -\gamma p/m + g(x, \Omega), \quad (19)$$

$$\dot{\Omega} = \omega, \quad (20)$$

where $\omega = 2\pi/T$. Therefore, the phase space of the system is three-dimensional.

The function $g(x, t)$ can be continuous or discontinuous, smooth or non-smooth, etc. Examples of discontinuous functions are trains of delta-like peaks [32,34,35], while piecewise-linear sawtooth potentials [4,36,37] constitute a good example of non-smooth functions. The symmetry analysis applies equally well to all situations though below we will focus mainly on the smooth functions consisting of a few harmonics only. This is a reasonable choice in the context of manipulations with cold atoms in optical potentials because it allows to build an experimental set-up with a minimal number of lasers and acousto-optical modulators [16,38,39].

3.1. Symmetry analysis

Transport in the system (16) is characterized by the velocity of the particle, \dot{x} . The total current is defined by means of averaging over the phase space:

$$J(t) = \langle \dot{x} \rangle_t. \quad (21)$$

Here $\langle \dots \rangle_t$ stands for the phase space averaging with some distribution function, which needs to be specified in order to define the problem entirely (we will discuss this issue in Section 3.2). The asymptotic current is given by:

$$J = \langle J(t) \rangle_t, \quad \langle \dots \rangle_t \equiv \lim_{t-t_0 \rightarrow \infty} \left[\frac{1}{t-t_0} \int_{t_0}^t dt' (\dots) \right]. \quad (22)$$

Our aim now is to figure out the necessary conditions for J to acquire non-zero values. To this end, we first will find the sufficient conditions which prevent from this and then will discuss how to violate them.

Let assume that there is a trajectory which contributes to J , i.e. it has been taken into account when performing the averaging over the phase space, Eq. (21). Suppose now that there is a transformation of the equation of motion (18)–(20), which maps parts of the phase space onto each other. The symmetry operation transforms the trajectory into another one—but with opposite velocity. If at least one symmetry exists, then the contributions of the trajectory and its symmetry-related twin will cancel each other after the averaging provided that both trajectories contribute to the quantity given by Eq. (21) with equal statistical weights. Finally, if the symmetry-based cancellation mechanism works for all trajectories, one may conclude that the asymptotic current J is strictly zero. Evidently, a nonzero current can only appear when all the symmetries are broken. There might be other specific mechanisms, aside of the trajectory-by-trajectory cancellation, which prohibit the appearance of a directed current. However, we again remind that the absence of the symmetries is a *necessary* but not *sufficient* condition for the rectification effect to appear.

As before, there are only two possibilities to change the sign of the velocity \dot{x} . The corresponding symmetry transformations were obtained in the previous section:

$$\hat{S}_x[\chi, \tau] : x \rightarrow -x + \chi, \quad t \rightarrow t + \tau, \quad (23)$$

$$\hat{S}_t[\chi, \tau] : x \rightarrow x + \chi, \quad t \rightarrow -t + \tau, \quad (24)$$

where χ and τ are some appropriate shifts, which depend on the shape of the function $g(x, t)$ and the friction strength parameter γ .

Now we briefly address different dynamical regimes of the system (16), which differ with respect to the friction strength γ and mass m .

- *Hamiltonian case*, $m > 0$, $\gamma = 0$. The corresponding equation of motion is

$$m\ddot{x} = g(x, t). \quad (25)$$

In this case both symmetries \hat{S}_x and \hat{S}_t can be present, as it has been shown in Section 2.3. Namely,

$$\hat{S}_x \text{ holds if } g(-x - \chi, t + \tau) = -g(x, t), \quad (26)$$

$$\hat{S}_t \text{ holds if } g(x + \chi, -t - \tau) = g(x, t). \quad (27)$$

Note that χ and τ are used to shift the function to the relevant inversion points in time or space. These parameters can take, in principle, any values. However, the shifts which are not accompanied by a sign change, e.g. τ for (26) and χ for (27) are restricted to $\tau = \pm T/2$ or 0, and $\chi = L/2$ or 0, correspondingly.

- *Dissipative case*, $m, \gamma > 0$. The corresponding equation of motion is

$$m\ddot{x} + \gamma\dot{x} = g(x, t). \quad (28)$$

In this case the time-reversal symmetry \hat{S}_t is broken by the simultaneous presence of the dissipative and inertia terms in the equation of motion. Symmetry \hat{S}_x , however, can hold:

$$\hat{S}_x \text{ holds if } g(-x - \chi, t + \tau) = -g(x, t), \quad (29)$$

- *Overdamped limit*, $m = 0$, $\gamma > 0$. The corresponding equation of motion is

$$\gamma \dot{x} = g(x, t). \quad (30)$$

Here both symmetries, \widehat{S}_x and \widehat{S}_t , can be present. The conditions for the symmetry \widehat{S}_x to hold remain the same as for the Hamiltonian case, Eq. (26), while the condition for \widehat{S}_t is modified:

$$\widehat{S}_x \text{ holds if } g(-x - \chi, t + \tau) = -g(x, t), \quad (31)$$

$$\widehat{S}_t \text{ holds if } g(x + \chi, -t - \tau) = -g(x, t). \quad (32)$$

The presence of the time-reversal antisymmetry in the overdamped limit was first noticed in Ref. [25] and was explained then in Ref. [40].

The presence of either of the symmetries (23)–(24) in the Hamiltonian or the dissipative cases guarantees that for any trajectory with a nonzero velocity the phase space contains its image, i.e., another trajectory with the velocity opposite to the velocity of the original trajectory. Assuming that both trajectories contribute equally to the system evolution, we arrive at the conclusion that the overall current produced by the system equals zero.⁴ Thus, in order to obtain a nonzero directed current, we should choose a function $g(x, t)$ which does not satisfy either of the symmetries.

Finally, it is noteworthy that all relevant symmetries can be re-formulated in terms of the original potential, $V(x, t)$, by noting that $g(x, t) = -\partial V(x, t)/\partial x$ and taking into account the modifications of the symmetries of a function by the differentiation operation, see Section 2.1.

3.2. The role of initial conditions

As we discussed in the introduction, the phase space of a coherent, noise-free system may consist of several invariant manifolds. The co-existence of many invariant manifolds is the general case for ac-driven Hamiltonian systems, so the corresponding phase space is conventionally called ‘mixed phase space’ [20]. The co-existence of attractors is a typical situation in weakly-damped systems [19], and, sometimes, it is the case for overdamped systems [41]. Because of this co-existence, the asymptotic characteristics of a system depend on the form of the initial distribution function, $\mathcal{F}(x_0, p_0, \Omega_0 = t_0)$, and the overall asymptotic current should be calculated as

$$\tilde{J} = \int dx_0 dp_0 d\Omega_0 \mathcal{F}(x_0, p_0, \Omega_0) J(x_0, p_0, \Omega_0), \quad (33)$$

where $J(x_0, p_0, \Omega_0)$ is the asymptotic current, Eq. (22), produced by the trajectory launched from point $\{x_0, p_0, \Omega_0\}$.

Every invariant manifold can be characterized by its asymptotic average velocity, which might be different from zero even when one of the basic symmetries, Eqs. (13)–(14), is present. A symmetry transformation can map two manifolds with nonzero opposite velocities onto each other. By initiating more trajectories on the manifold with the average velocity $v \neq 0$ than on its symmetry-related counterpart, with the velocity $-v$, one will detect a non-zero current in the situation when the corresponding equations of motions are perfectly symmetric. The presence of a symmetry guarantees zero-current output only when symmetry-related trajectories contribute equally to the overall current (33). That happens when the initial distribution function, $\mathcal{F}(x_0, p_0, \Omega_0)$, also satisfies the relevant symmetry. Since the phase space of the system given by Eqs. (18)–(20), (x, p, Ω) , is compact along the variables $x \bmod L$ and $\Omega \bmod T$, a reasonable choice of the initial distribution function is the product of the uniform distributions over the variables $x_0 \bmod L$ and $\Omega_0 \bmod T$, and a symmetric distribution with respect to the momentum variable, $\mathcal{F}(x_0, -p_0, t_0) = \mathcal{F}(x_0, p_0, t_0)$. The latter can be, for example, the Maxwell distribution [25,32]. Such initial distributions possess both fundamental symmetries, Eqs. (23), (14), for any values of χ and τ .

3.3. Special cases

3.3.1. Additive driving

First we consider force functions of the type $g(x, t) = f(x) + E(t)$. It is a sum of two independent, space- and time-dependent functions⁵:

$$m\ddot{x} + \gamma\dot{x} = f(x) + E(t), \quad E(t) = E(t + T), \quad f(x) = f(x + L). \quad (34)$$

Functions $E(t)$ and $f(x)$ both have zero means. Therefore one can classify them with respect to their symmetry properties, as described in Section 2.1. We list in Table 1 the requirements for the functions $f(x)$ and $E(t)$ to satisfy either of the two basic symmetries. Any choice of the functions $f(x)$ and $E(t)$, which does not fall into one of the listed cases, leads to the

⁴ In the overdamped case the situation is more tricky, see Refs. [25,26,40]. We will address this issue in Section 3.6.2.

⁵ In the ratchet literature this is often coined *tilting* or *rocking* ratchet [4,8].

Table 1

(Color online) Conditions for the fundamental symmetries, Eqs. (26)–(27), to hold in the case of additive driving, Eq. (34). Ratchet symbol indicates the cases when both symmetries are broken. Note that any other combination, not included in the tables, also corresponds to the case of broken symmetries.































	HAMILTONIAN			DISSIPATIVE			OVERDAMPED		
	$\gamma = 0, m > 0$			$\gamma, m > 0$			$\gamma > 0, m = 0$		
E_s	\hat{S}_t	\hat{S}_t	\hat{S}_t						
E_a									\hat{S}_t
E_{sh}		\hat{S}_x			\hat{S}_x			\hat{S}_x	
	f_s	f_a	f_{sh}	f_s	f_a	f_{sh}	f_s	f_a	f_{sh}

Table 2

(Color online) Conditions for the fundamental symmetries, Eqs. (26)–(27), to hold in the case of multiplicative driving, Eq. (37). Ratchet symbol indicates the cases when both symmetries are broken. Note that any other combination, not included in the tables, also corresponds to the case of broken symmetries.

	HAMILTONIAN			DISSIPATIVE			OVERDAMPED		
	$\gamma = 0, m > 0$			$\gamma, m > 0$			$\gamma > 0, m = 0$		
E_s	\hat{S}_t	\hat{S}_t, \hat{S}_x	\hat{S}_t		\hat{S}_x			\hat{S}_x	\hat{S}_t
E_a		\hat{S}_x	\hat{S}_t		\hat{S}_x		\hat{S}_t	\hat{S}_t, \hat{S}_x	\hat{S}_t
E_{sh}	\hat{S}_x	\hat{S}_x		\hat{S}_x	\hat{S}_x			\hat{S}_x	
	f_s	f_a	f_{sh}	f_s	f_a	f_{sh}	f_s	f_a	f_{sh}

symmetry breaking. The appearance of the directed current in systems of the type (34) has been verified both analytically, numerically and experimentally [4,8]. In the dissipative regime, the following choice of potential force [41–44,25,45]:

$$f(x) = f_1 \sin x + f_2 \sin(2x + \Delta), \quad (35)$$

guarantees the violation of symmetry \hat{S}_x if $f_2 \neq 0$, $\Delta \neq 0, \pm\pi$. Therefore, the presence of a bi-harmonic ratchet potential is a sufficient condition to obtain directed current when $\gamma > 0$ and $m \neq 0$, see the only entry in the corresponding table. Note, however, that this is not yet enough to guarantee the violation of the time-reversal symmetry \hat{S}_t in the Hamiltonian and overdamped limits.

The bi-harmonic driving function,

$$E(t) = E_1 \cos \omega t + E_2 \cos(2\omega t + \theta) \quad (36)$$

allows one to violate the fundamental symmetries in the Hamiltonian, dissipative, and overdamped limits, by tuning parameter θ . Moreover, even in the case of a single-harmonic potential, $f_2 = 0$ in Eq. (35), the bi-harmonic driving alone can break both symmetries [43,44,25,26,45,31,33,46].

3.3.2. Multiplicative driving

Another frequently used setup corresponds to a spatial potential with its amplitude periodically modulated in time,⁶

$$m\ddot{x} + \gamma\dot{x} = f(x)E(t), \quad f(x) = f(x + L), \quad E(t) = E(t + T). \quad (37)$$

Because of the condition (17), at least one the functions, $f(x)$ and $E(t)$, has to be of zero mean. For example, while the function $E(t)$ may have a nonzero constant component, the average potential, $g(x, t) = \sin(x)[E_0 + \sin(\omega t)]$, remains unbiased.

The corresponding symmetry conditions are given in Table 2. Note that when, for example, function $f(x)$ is antisymmetric, Eq. (37) remains invariant with respect to the symmetry \hat{S}_x for any choice of the driving function $E(t)$. This, and a larger

⁶ In the literature often referred to as *pulsating* or *flashing* ratchet [4,8].

overall number of possible symmetries as compared to the previous case of additive driving, are the consequences of multiplicative driving.

A minimal setup, which allows to control all relevant symmetries, consists of bi-harmonic functions, with $f(x)$ and $E(t)$ given by Eqs. (35), (36). This combination has been used in the experimental realization of ac-driven quantum ratchets with a Bose–Einstein condensate [47]. We will review these experiments in more details in Section 5.3.

The overdamped limit of multiplicative ratchets has been extensively studied, see Refs. [48,4]. One of the popular choices was the driving field in the form of dichotomous function, with $E(t) = 1$ or 0 , so the potential is in either “on” or “off” position. [4]. The Hamiltonian limit of the multiplicative set-up has been studied by using different modifications of the kicked-rotor model [19,20]. In these studies the driving field $E(t)$ was represented by a train of delta kicks so that the propagation in time was reduced to iterations of a two-dimensional map [31,32,34,35].

3.3.3. Traveling potentials

A particular setup, named *traveling potential ratchet* [4], has the force function of the form

$$g(x, t) = \sum_k f_k[x + a_k(t)], \quad (38)$$

where $f_k(x)$ and $a_k(t)$ are periodic functions of zero mean. If $f_{k \neq 1} = 0$ and the function $a_1(t) \equiv a(t)$ is periodic in time, then, by using the transformation $x \rightarrow \tilde{x} = x + a(t)$, the equation of motion (16) can be cast in the following form:

$$m\ddot{\tilde{x}} = -\gamma\dot{\tilde{x}} + f(\tilde{x}) - \gamma\dot{a}(t) - m\ddot{a}(t) \quad (39)$$

where both the driving functions, $\dot{a}(t)$ and $\ddot{a}(t)$, have zero means. The asymptotic current is the same in both frames, $J = \langle \dot{x} \rangle_T = \langle \dot{\tilde{x}} \rangle_T$. Therefore, it suffices to perform the analysis in the new frame, $\{\tilde{x}, t\}$. By taking into account that the differentiation operation transforms symmetric functions into antisymmetric ones while leaving the shift-symmetric property invariant, we immediately reduce the symmetry analysis of Eq. (39) to the already considered case of additive driving, Eq. (34). The conditions for the symmetry \hat{S}_x to hold remain the same: $f(x)$ should be antisymmetric, and $a(t)$ shift-symmetric. In the Hamiltonian limit, the same is true for the time-reversal symmetry, \hat{S}_t , which now requires $a(t)$ to be symmetric. The overdamped limit is instructive—for the time-reversal (anti)symmetry to hold, $a(t)$ has to be now symmetric instead of being antisymmetric as before. The force function $g(x, t) = \cos[x - E(t)]$, with $E(t) = E_1 \cos(\omega t) + E_2 \cos(2\omega t + \theta)$, has been used for the realization of rocking ratchets in optical potential with cold atoms [49,38,39,50] and glass microspheres [51]. We will review these experiments in Sections 3.7 and 3.5.3, respectively.

The choice $a_k(t) = v_k t$ corresponds to a so-called *genuine traveling potential ratchet* [4] and mimics the dynamics of a particle interacting with several propagating waves [20]. Each wave drags the particle in the direction of the wave propagation and the asymptotic current appears as a result of competition between the waves. This setup was frequently used in quantum pumps [52,53], and in its simplest form, with $k = 1$, was proposed by Thouless to pump adiabatically electrons [54]. For more efficient non-adiabatic pumping we refer to recent research activities [55,56]. Indeed, consider the traveling-wave potential, $g(x, t) = \cos(x - \Omega t)$. It can be rewritten as $g(x, t) = \sin(x) \cos(\Omega t) + \cos(x) \sin(\Omega t)$ [53]. Applying the symmetry analysis, it is easy to see that all relevant symmetries are broken when $\Omega \neq 0$.

3.3.4. Gating ratchets

Finally, we consider a *gating ratchet* [57],

$$g(x, t) = f(x)a(t) + E(t). \quad (40)$$

Without loss of generality, we assume that $f(x)$ is a function of zero mean while $a(t)$ may have a constant component (the inverse situation can be analyzed in the same manner),

$$f(x) = f \sin(x), \quad a(t) = 1 + \varepsilon \sin(\omega t), \quad E(t) = E \sin(\omega t + \theta). \quad (41)$$

By setting $\theta \neq 0, \pm\pi$, one can break all the symmetries in all the limits with respect to the friction strength. Note that, in this case, there is no need for a second harmonic neither for the force term nor for the drive function. For more analytical and numerical results on the overdamped limit of gating ratchets we refer the reader to Ref. [57]. The gating ratchet setup has also been implemented in experiments with cold atoms [58].

3.4. Extension to quasiperiodic driving

As an example we consider the rocking ratchet (34) with the driving function $E(t) = \tilde{E}(\omega_1 t, \omega_2 t, \dots, \omega_N t)$ [59,60].

First we write the corresponding equations of motion in the following form:

$$\begin{aligned} m\ddot{x} + \gamma\dot{x} - f(x) - E(\phi_1, \phi_2, \dots, \phi_N) &= 0, \\ \dot{\phi}_i &= \omega_i, \quad i = 1, 2, \dots, N. \end{aligned} \quad (42)$$

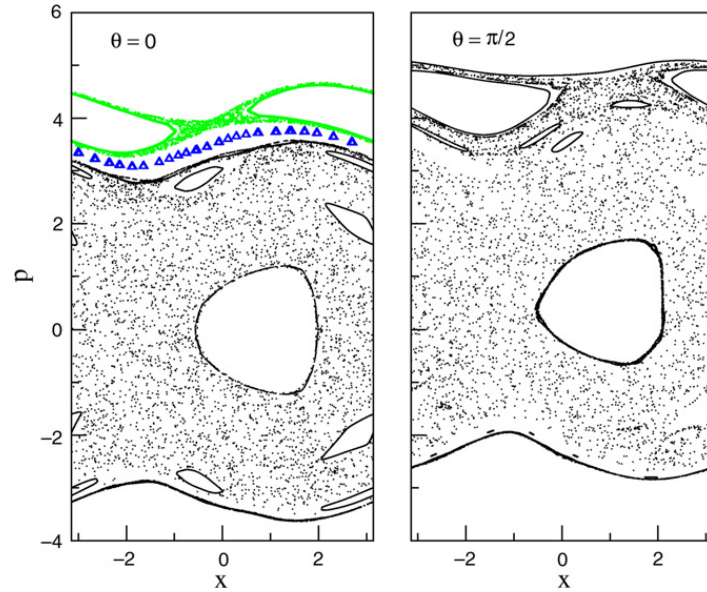


Fig. 2. Poincaré maps of the Hamiltonian system (45), (46) for different values of θ . Due to the time-reversal symmetry $\hat{S}_t[0, 0]$, Eq. (32), the Poincaré map for $\theta = 0$ (left panel) is symmetric at the line $p = 0$. Triangles mark a ballistic invariant manifold, a regular torus with the average velocity $v \approx 1.64$. Bright (green) dots mark another ballistic invariant manifold, a thin chaotic layer enclosing a ballistic regular island. The velocity of the orbits inside the island are equal to the velocity of the periodic orbit at the center of the island, $v = 4$. This is also the average velocity of all orbits inside the ballistic chaotic layer. Symmetry violation results in the overlap between the ballistic resonance and the main stochastic layer as they merge into a single chaotic manifold (right panel). This effect leads to the appearance of a strong positive current within the newly created stochastic layer, see Fig. 3. The parameters are $E_1 = E_2 = 2$ and $\omega = 2$. (For interpretation of the references to color in this figure legend, the reader is referred to the web version of this article.)

It is straightforward to identify the symmetries of the system. There are two types of them,

$$\hat{S}_x^q[\chi, \{i, j, \dots, m\}] : x \rightarrow -x + \chi, \quad \phi_{i, \dots, j} \rightarrow \phi_{i, \dots, j} + \pi, \quad \text{if } \{f_a, E_{sh, \{i, j, \dots, m\}}\}, \quad (43)$$

$$\hat{S}_t^q[\chi] : x \rightarrow x + \chi, \quad t \rightarrow -t, \quad \phi_i \rightarrow -\phi_i, \quad \text{if } \{E_s, \gamma = 0\}. \quad (44)$$

Symmetry $\hat{S}_t^q[\chi]$ is a particular case of the symmetry (14) with $\tau = 0$. Symmetry $\hat{S}_x^q[\chi, \{i, j, \dots, m\}]$ branches into a whole set of symmetry operations, defined by a subset of indices $\{i, \dots, j\}$.

A force function $f(x)$ can also be quasiperiodic, with M spatial harmonics. Generalization of the symmetry analysis to this case is straightforward [60].

3.5. Dynamics

The symmetry analysis tells when a current is absent or *may be* present. However it neither specifies current's value nor its sign. These characteristics can be obtained from reasonable perturbation approaches—at the vicinities of symmetry points in the control parameter space, or by simply performing numerics. In the following subsections we discuss the microscopic dynamical mechanisms underlying the rectification processes in Hamiltonian and dissipative systems.

3.5.1. Hamiltonian ratchets revisited

Let us return to the model introduced in Section 2.3. Both key symmetries, \hat{S}_x and \hat{S}_t , can be violated by using a proper driving function, $E(t)$ [25,26,33,46]. A setup with a single-harmonic potential force and a bi-harmonic drive,

$$m\ddot{x} = \cos(x) + E(t), \quad (45)$$

$$E(t) = E_1 \cos(\omega t) + E_2 \cos(2\omega t + \theta), \quad (46)$$

constitutes the simplest choice. For $E_2 \neq 0$ and $\theta \neq 0, \pi$, both key symmetries are broken so that the appearance of a non-zero current can be expected. Before proceeding further with the analysis of the rectification process, we will briefly discuss some general properties of Hamiltonian chaos [19,20].

A standard way to visualize dynamics of the Hamiltonian system Eqs. (45), (46) is to use the stroboscopic Poincaré map [19]. This can be done by propagating the system in time and plotting the values of coordinate and momentum on the stripe $\{x \bmod L, p\}$ at equidistant instants of time $t_n = nT, n = 1, 2, \dots$. By choosing different initial points in the $\{x, p\}$ plane, we will collect a large set of points $\{x(t_n) \bmod L, p(t_n)\}$, thus resolving the structure of the phase space. Note that the result will depend on the parameter θ . Typical Poincaré maps are depicted in Fig. 2. They reveal that the phase space of the Hamiltonian system is indeed ‘mixed’, i.e. it consists of different invariant manifolds, that are chaotic layers, regular

islands, tori, etc. [20]. Each manifold is characterized by its average velocity $v_i = \langle v_i(t) \rangle_t$. A manifold velocity might be nonzero even when all relevant symmetries hold. For example, if we launch the particle from one of the points marked by triangles on the left panel of Fig. 2, the particle will move ballistically with near constant positive velocity. Therefore the quest for a nonzero current by a Hamiltonian ratchet is intimately related to the choice of initial conditions. If the set of initial conditions overlaps with different manifolds then the corresponding asymptotic current should be calculated as a weighted sum over the velocities of the contributing manifolds, $\tilde{J} = \sum_i p_i v_i$, where p_i is the fraction of the ensemble that overlaps with the i th manifold, $\sum_i p_i = 1$.

Among many different invariant manifolds, the chaotic layer around the line $p = 0$, see Fig. 2, is of particular importance. This manifold is a result of the destruction of the separatrix of the non-driven system (45) when the latter is exposed to the drive. The chaotic layer typically overlaps substantially with an initial ensemble of particles of low-kinetic energies, for example, an ensemble with a low-temperature Maxwell velocity distribution [25,32]. Therefore, the main chaotic layer is the most relevant region of the phase space in the context of cold- and ultra-cold atom experiments [38,39]. The chaotic layer is an ergodic manifold [19,20] and its average velocity, v_{ch} , is the same for all trajectories initiated within the layer. Thus, the asymptotic chaotic current, Eq. (22), is $\tilde{J} = v_{ch}$. When one of the two fundamental symmetries is present, i.e. when Eq. (16) is invariant under either \hat{S}_x or \hat{S}_t , the corresponding transformation maps every trajectory from the layer onto another one, also belonging to the layer but having opposite velocity. Due to mixing [20], both trajectories can be considered as parts of a single infinitely long trajectory. The presence of the symmetry implies that the asymptotic velocity of any trajectory, initiated within the chaotic layer, is strictly zero and thus $v_{ch} = 0$. When both symmetries are broken, like in the case of the set-up (45), (46) with $\theta \neq 0, \pm\pi$, we expect the appearance of a directed current within the layer, $v_{ch} \neq 0$.

There are two possibilities to estimate v_{ch} . The first is straightforward: Calculate v_{ch} by propagating numerically a very long trajectory. We have already resorted to this idea in Section 2.3. However, this brute-force approach has several drawbacks. First, it is a time-consuming task. The trajectory has to be long enough in order to sample the chaotic layer, and it is hard to predict when the average velocity, $\bar{v} = x(t)/t$, will saturate to the asymptotic value v_{ch} within a given accuracy. Often, in order to get a clue about even the direction of the chaotic transport, one has to run trajectory for times which are six to seven orders of magnitude larger than the period of the driving T . Second, a numerical scheme for the propagation of Hamiltonian systems has to account for the symplectic nature of the dynamics. Otherwise accumulations of numerical round-offs will lead to wrong results. Standard schemes, like the Runge–Kutta fourth-order algorithm, are not suitable for this task and one should use symplectic integrators instead.⁷

An alternative approach is based on the so-called ‘sum rule’ [32]. This method is capable of estimating the asymptotic current with a high accuracy while avoiding long-time numerical propagation. The sum rule expresses the averaged velocity in the *chaotic* layer in terms of kinetic characteristics of its adjoining *regular* components. Below we give a brief recipe while referring interested readers to Refs. [32,63] for more detailed explanations.

- Launch a trajectory from a point which belongs to a chaotic layer. A good choice is to use initial momentum value close to zero, and the coordinate value close to a maximum of the potential. It may happen that we will have to perform several short trial runs in order to be sure that we really got into the chaotic layer. Next propagate the trajectory and plot the corresponding Poincaré map. Continue until the chaotic layer structure becomes visible, i.e. its boundaries and inner regular islands are resolved (typically 10^3 – 10^4 periods T are sufficient).
- The obtained chaotic layer is confined between two tori, upper Γ_u and lower Γ_l ones, and occupies a finite area A_{ch} on the Poincaré map. The layer may also enclose different regular islands of areas A_i , see ‘holes’ in Fig. 2. Each island is characterized by an averaged velocity v_i . These velocities can be estimated by launching short trajectories from the interior of the corresponding island. It is not a time-consuming task since the dynamics within islands is regular (quasiperiodic);
- Calculate the average kinetic energies of the border tori, $\bar{K}_{u,l} = \langle p_{u,l}^2(t)/2 \rangle_t$. This can be done by launching trajectories from the initial points that are outside the layer but close to the layer boundaries;
- Finally, calculate the asymptotic current by using the following expression [32],⁸

$$J = \frac{L \cdot [\bar{K}_u - \bar{K}_l] - \sum_i A_i v_i}{A_{ch}}. \quad (47)$$

As an illustration, we apply the sum rule to the system shown in Fig. 2b. The area of the chaotic layer is $A_{ch} \approx 41.1 \pm 0.03$.⁹ The area of the central island, with $v_1 = 0$, and the ballistic island at the top of the layer (of the velocity $v_2 = 4$) are $A_1 = 4.4 \pm 0.01$ and $A_1 = 2.8 \pm 0.01$ correspondingly. Kinetic energies of the boundary tori are $T_u = 10.20 \pm 0.01$ and

⁷ An easy-to-use symplectic scheme which performs extremely well when used to propagate Hamiltonian ratchets of the type (45), (46) [25,26,33], is the Verlet (also coined ‘leap-frog’) algorithm [61]. One can use more sophisticated symplectic integrators [62].

⁸ Note the absence of the factor L in the numerator of the original expression in Refs. [32,63]. When $L = 1$ (which was the case considered in the papers), this absence causes dimensionality problems only. However, in the general case, when $L \neq 1$, it leads to incorrect results.

⁹ We have measured areas of the chaotic region and regular islands by filling them with rectangles, circles and ellipses. We used a free-ware Linux 2d plotting program, *Grace*, <http://plasma-gate.weizmann.ac.il/Grace/>.

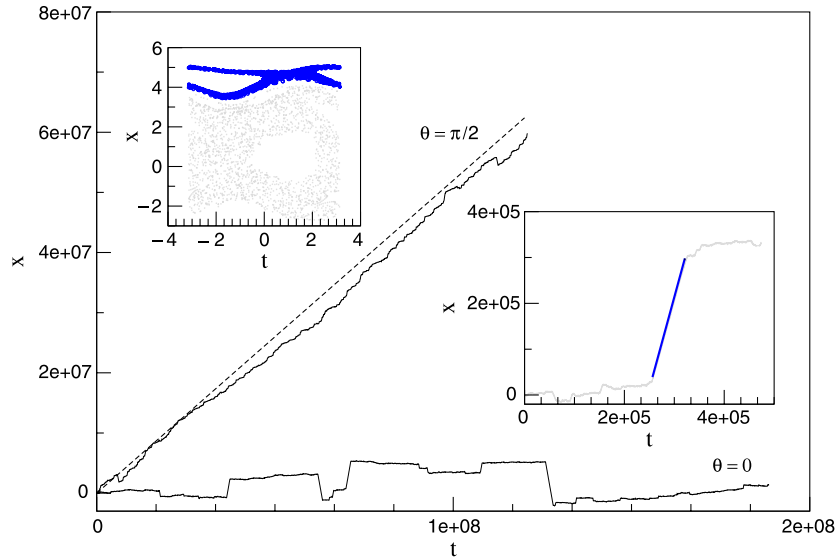


Fig. 3. Left panel: $x(t)$ versus t for the Hamiltonian system (16), (46). The dashed line corresponds to $x = v_{ch}t$, with v_{ch} obtained by using the sum-rule, Eq. (47) Right lower inset: A zoomed part of the trajectory with the thick blue line marking a single ballistic flight with velocity $v = 4$. The gray part corresponds to a diffusive-like dynamics within the chaotic sea. Left upper inset: The Poincaré map corresponding to the trajectory part shown on the right inset. Blue dots correspond to the ballistic flight and gray dots to the diffusion-like part of the trajectory. The parameters are the same as in Fig. 2. (For interpretation of the references to color in this figure legend, the reader is referred to the web version of this article.)

$T_l = 5.05 \pm 0.01$. Finally, the sum rule (47) yields $v_{ch} = 0.521 \pm 0.006$.¹⁰ The obtained value is in a good agreement with the result of the numerical propagation, see the left panel of Fig. 3.

Although being characterized by a uniform invariant density in the asymptotic limit [32,63], the chaotic layer is not uniform on finite time scales. The dynamics of a Hamiltonian system is qualitatively different in different regions of the chaotic sea though all these regions belong to the same, overall ergodic manifold. In particular, the dynamics is nearly regular at the vicinity of embedded regular islands. These regions of the layer are structured by *cantori* [20], which form partial barriers for chaotic trajectories. A trajectory, which entered the region enclosed by a cantorus, can be trapped in the vicinity of the corresponding island for a very long time [20,64]. During this *sticking* event [65], the trajectory reproduces the dynamics of the orbits located inside the island [64,33]. If the corresponding island is transporting, i.e. $v_i \neq 0$, the sticking event produces a ballistic flight, see lower right panel of Fig. 3. A strong current appears when the set of regular islands, submerged into the chaotic layer, is asymmetric, i.e. when there are islands with nonzero velocities which do not have symmetry-related twins. This leads to the violation of the balance between ballistic flights in opposite directions and results in the appearance of a strong current [33]. Functioning of Hamiltonian ratchets relies therefore on the harvesting of long temporal correlations that extend over the time scales much larger than the period of the driving T . Ballistic flights are also responsible for anomalous diffusion [64], when the mean square displacement, $\sigma(t) = \langle x^2(t) \rangle - \langle x(t) \rangle^2$, grows algebraically, $\sigma(t) \propto t^\mu$, with the scaling exponent $\mu > 1$ [66]. Naturally, directed current and superdiffusion represent two facets of the peculiar Hamiltonian kinetics [46,67]. In some limits, however, it may become difficult to separate ballistic flights from non-ballistic chaotic diffusion. This is a typical situation in the regimes of strong driving, when $E_1, E_2 \gg 1$. With the increase of the driving amplitude(s) the chaotic layer starts to inflate, absorbing more and more ballistic islands. The chaotic sea is becoming structured by a network of cantori [20], so that the chaotic dynamics within the layer is far outside of the dichotomous description “unbiased chaotic diffusion vs ballistic flights”.

While the symmetry analysis does not predict sign and value of a ratchet current, it allows to predict when the sign of the current will invert. Namely, either of the following transformations,

$$\theta \rightarrow \theta + \pi, \quad t \rightarrow t + T/2, \quad x \rightarrow -x + \pi, \quad (48)$$

$$\theta \rightarrow -\theta, \quad t \rightarrow -t, \quad x \rightarrow x, \quad (49)$$

reverses the current, $J \rightarrow -J$. Therefore, in order to change the direction of induced transport, it is enough to change the sign of θ or to shift it by π . Evidently, the current is a periodic function of the phase shift θ , $J(\theta + 2\pi) = J(\theta)$. Thus it can be expanded into a Fourier series, $J(\theta) = \sum_k J_k \exp(ik\theta)$. It follows from symmetry (49) that the expansion consists of sine terms only. In addition, symmetry (49) predicts that the Fourier series consists of odd harmonics only, so that $J(\theta) = J_1 \sin(\theta) + J_3 \sin(3\theta) + \dots$. Assuming that the first term of the expansion dominates, we arrive at a simple expression,

$$J(\theta) \propto J_0 \sin(\theta). \quad (50)$$

¹⁰ We neglected the contributions from smaller islands and therefore the actual relative error is larger.

This dependence was detected in the experiments with ac-driven cold [49] and ultracold [47] atom ratchets, see Sections 3.7 and 5.3, respectively.

3.5.2. Transport with dissipation

In the case of finite dissipation, $\gamma/m < \infty$, the only symmetry transformation to take care about is \hat{S}_x , see Table 1. One way to violate this symmetry is to use, for example, the rocking set-up with a potential force $f(x)$ that is not antisymmetric. A bi-harmonic combination, Eq. (35), will do in this case [25,43–45].

In the dissipative regime, similar to the Hamiltonian limit, the asymptotic current is determined by the transport properties of invariant manifolds. There can be several manifolds [68,69] but typically their number is much smaller than that in the Hamiltonian case. There are two kinds of invariant manifolds existing in the phase space of a dissipative system, that are *attractors* and *repellers* [19]. In the asymptotic limit $t \rightarrow \infty$, the dynamics of a noise-free dissipative system is determined by the attractors only. Typically, there is only a few attractors coexisting in the system phase space when the dissipation strength is not too small, $\gamma/m \gtrsim 0.01$. In the simplest case, when only one attractor exists in phase space, all trajectories end up on this manifold independent of their starting points. Therefore, similar to the case of Hamiltonian dynamics, in order to obtain information on the asymptotic transport, one should study the transport properties of the system attractor(s).

There are two types of attractors in periodically driven dissipative system, namely periodic limit cycles and chaotic attractors.¹¹ An attractor is characterized by its average velocity, $v_A = \langle v_A(t) \rangle_t$. A limit-cycle attractor is locked by the driving field $E(t)$, and its transport properties are fully determined by a pair of co-prime integers, m and n , $x(t + mT) = x(t) + Ln$, $p(t + mT) = p(t)$, so that the average velocity is $v_A = nL/mT$. If this is the only attractor of the system, its velocity defines the asymptotic current, $\tilde{J} = v_A$. In the multi-attractor case, the phase space contains several coexisting attractors, all of different types and different velocities. Each attractor has its own *basin of attraction* [19]. That is a part of the phase space, Σ_A , such that a trajectory launched from a point $(x_0, p_0, \Omega_0) \in \Sigma_A$ ends up, after some transient, on the corresponding attractor. Basins of different attractors are often entangled and form complex fractal-like structures [19,70].

Let us consider first a situation when symmetry \hat{S}_x holds. In the single-attractor case, the corresponding transformation maps the attractor onto itself, and, therefore, $v_A = 0$. There are two alternatives in the multi-attractor case. Namely, the transformation (i) either maps an attractor A onto itself, and therefore this attractor again is non-transporting or (ii) it maps an attractor onto its symmetry-related twin $A' = \hat{S}_x : A$, such that $v_A = -v_{A'}$. The symmetry also enforces the basins of attraction of two symmetry-related attractors to be mapped onto each another by the same transformation. Therefore, a distribution of initial conditions $\mathcal{F}(x_0, p_0, t_0)$ which occupies the same volume in both basins (note that it must not even be strictly symmetric point by point), will yield zero current [25].

By violating symmetry \hat{S}_x we remove the above constraints and expect a nonzero current [4,8]. In the case of a single limit-cycle attractor, the transition to the ratchet regime must necessarily involve a bifurcation [19], i.e. a sudden change of the attractor structure, since it is impossible to tune continuously between zero and any nonzero rational numbers n/m . Therefore, this bifurcation will happen only after some finite parameter tuning. So it may happen that for these restrictive topological reasons the overall current will stay zero even though all symmetries have already been broken.

In the case when two symmetry-related limit cycles coexist, the transition to the ratchet regime can be smooth. A violation of the symmetry will cause the desymmetrization of the basins of attraction so that the averaging with a symmetry-respecting distribution function, $\mathcal{F}(x_0, p_0, \Omega_0)$, Eq. (33), will result in a finite asymptotic current. Further increase of an asymmetry parameter will lead to a bifurcation after which one of the attractors disappears [25]. In the case of a single chaotic attractor, the transition to the ratchet regime can be continuous as well. Variations of the asymmetry parameter(s) may cause different bifurcations, with a birth of a new attractor and death of an old one, via, for example, a period-doubling bifurcation or an inverse tangent bifurcation [19]. There is a multitude of possible bifurcation scenarios [72], and each of them can show up upon parameter variations. A bifurcation changes the attractor structure, thus leading to sudden changes of the current, up to current reversals [44,45,73,71,74], see Fig. 4.

3.5.3. Transport in the overdamped limit

The symmetries in the overdamped limit, $m = 0$, were elaborated in great detail in Refs. [25,40], while a big variety of overdamped ratchet models is reviewed in Refs. [4,8]. Below we only briefly outline this limit by using the rocking ratchet set-up introduced in Section 3.3.1, as a model.

The dynamics of a particle is described by the following equation,

$$\gamma \dot{x} = f(x) + E(t). \quad (51)$$

The asymptotic evolution, similar to the above considered general dissipative case, is governed by attractors [19], and symmetry \hat{S}_x acts here in the same manner as before. Surprisingly, time-reversal symmetry \hat{S}_t Eq. (32) is acting again, which appears to be odd. The time reversal operation will map an attractor; i.e., a manifold, which attracts trajectories from a part

¹¹ There is also a possibility to produce a quasiperiodic attractor, but for that one needs either a driving force with non-zero constant component [19] or quasiperiodic driving [59], see Section 3.4.

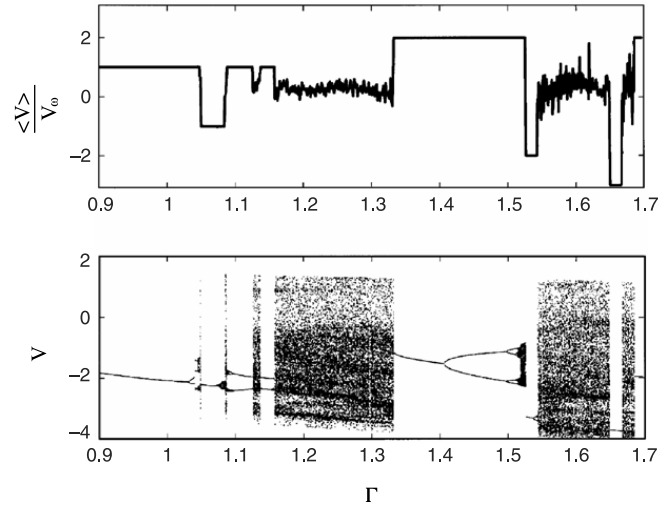


Fig. 4. (Top) Asymptotic velocity of a dissipative ratchet vs. driving amplitude, $E_1 \equiv \Gamma$. The equations of motion are given by (34)–(36). The velocity is measured in units of $v_\omega = L/T = \omega$; (Bottom) Bifurcation diagram, i.e. stroboscopic values of the particle velocity, $v(t_i) = p(t_i)/m$, plotted at the instants of time $t_i = (i + 1/2)T$, $i = 1, 2, \dots$. Note the bifurcation from the chaotic attractor to the limit cycle at the point $\Gamma \approx 1.65$, which leads to a current reversal. The parameters are $m = 1.1009$, $f_1 = 1$, $f_2 = 0.5$, $\Delta = \pi/2$, $\gamma = 0.1109$, $\omega = 0.67$, and $E_2 = 0$. The initial conditions are $\{x(0) = 0, p(0) = 1.1009\}$. Source: Adapted from Ref. [71].

(or whole) of the phase space, onto a repeller [19], an unstable manifold which repels trajectories and seemingly does not influence the asymptotic dynamics on large time scales. Therefore, the line of reasoning used before for Hamiltonian systems does not apply here: Contributions from two symmetry-related manifolds do not cancel each other because their statistical weights are different. The resolution of this paradox is that the time-reversal symmetry, also termed ‘supersymmetry’ in Refs. [40,4], imposes certain restrictions not directly on the equations of motion themselves but on their asymptotic solutions. We will address this issue in Section 3.6.2, when discussing the approach based on the Fokker–Planck equation.

Recently, time-reversal symmetry \hat{S}_t was used for the real-time control of microsphere transport in a fluid [51]. The bi-harmonic potential force,

$$f(x) = f_1 \cos(x) + f_2 \cos(2x + \Delta), \quad (52)$$

has been realized with a periodic pattern of fringes produced by interference of several laser beams. A rocking ratchet was introduced by means of phase modulations of the beams, Eq. (39), which procedure resulted in the appearance of a three-state tilting force,

$$E(t) = \begin{cases} E_0 & \text{if } 0 \leq t < \tau_1, \\ 0 & \text{if } \tau_1 \leq t < \tau_1 + \tau_0, \\ -E_0 & \text{if } \tau_1 + \tau_0 \leq t < T - \tau_0, \\ 0 & \text{if } T - \tau_0 \leq t < T, \end{cases} \quad (53)$$

with the period $T = 2(\tau_0 + \tau_1)$. The function $E(t)$ has zero mean and possesses all three possible symmetries, Eqs. (4)–(6). It is symmetric around the point $t = \tau_1/2$, antisymmetric around the point $t = \tau_1 + \tau_0/2$, and, consequently, is shift-symmetric under the shift $\tau = \tau_1 + \tau_0 = T/2$. The bi-harmonic form of the potential force (52) violates symmetry \hat{S}_x by default. Symmetry \hat{S}_t , Eq. (32), holds when $\Delta = \pm\pi/2$. Any other choice of Δ violates the time-reversal symmetry and may lead to the appearance of net transport of the microsphere. In addition, the shift of Δ by $\pm\pi$ should reverse the direction of the motion. The obtained experimental results perfectly validated all these predictions, see Fig. 5 (and Ref. [51] for more details).

3.6. Transport with noise and fluctuations

Many applications require statistical descriptions of transport properties, especially when the system of interest is coupled to a heat bath so that the system evolution is essentially stochastic. Thermal noise will change the dynamics of a deterministic dissipative system by allowing the latter to explore the phase space outside the attractor(s). This results in a self-averaging of the dynamics over the phase space so that the system asymptotic state is no longer localized on the attractor(s) but should be described by a certain distribution function, $P(x, p, t)$. This function depends on the temperature of the heat bath \mathcal{T} , $P(x, p, t; \mathcal{T})$. The symmetries of the equations of motion of the noise free case will be recovered in corresponding evolution equations for the distribution function P .

We recapitulate that in the Hamiltonian noise-free limit the phase space is mixed, and regular islands of a Hamiltonian system enclose their ‘cores’, marginally stable elliptic periodic orbits. These orbits are characterized by velocities $v = nL/mT$,

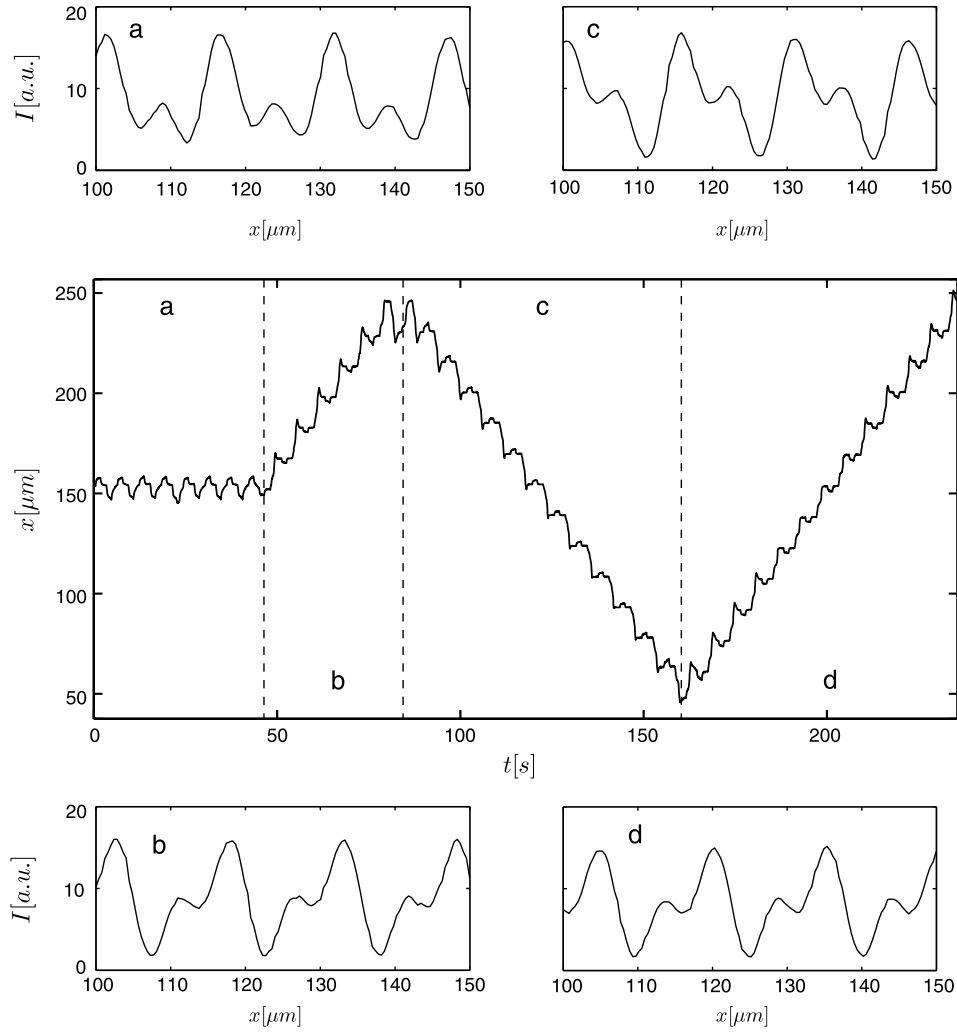


Fig. 5. Central part: Monitored position of a glass microsphere vs. time obtained with optical realization of the overdamped rocking ratchet, Eqs. (51)–(53) [51]. The dashed lines indicate instants of time when the parameter Δ of the optical force, Eq. (52), was changed to a new value. The four time regions correspond to (a) $\Delta = \pi/2$, (b) $\Delta = 0$, (c) $\Delta = \pi$, and (d) $\Delta = 0$. Top and bottom plots show the profiles of optical forces corresponding to different values of Δ .
Source: Adapted from Ref. [51].

given by pairs of co-prime integers, n and m . Weak dissipation (with still no noise) transforms the chaotic layer into a set of limit-cycle attractors, which are located inside the former regular islands [68,26]. The velocities of these limit cycles are equal to the velocities of their predecessors, the elliptic orbits, while their basins of attraction form complex fractal-like structures in the region of the phase space which was occupied by the Hamiltonian chaotic layer. Additional thermal noise induces jumps between the attractors [75], and in between two consecutive jumps the trajectory may stick to one of attractor for a relatively long time. If the coupling to the bath is weak, the trajectory mainly explores the phase-space region corresponding to the former chaotic layer. The joint effect of weak damping, weak noise and complex geometric structure of the attractor basins results in velocity probability distribution which is far from the conventional Maxwell's distribution [76,26]. While it is tempting to perform direct numerical integrations of stochastic differential equations like the Langevin equation, such approaches appear to be notoriously hard, since all kinds of transient effects, convergence rates and relaxation times, and other technical issues, will typically make this approach not very efficient.

Statistical approaches, based on the direct evaluation of the distribution function, $P(x, p, t)$, can lead to the needed asymptotic average characteristics of the system. Below we explain how the symmetry analysis can be generalized within two complementary statistical formalisms. We will consider first the method based on the kinetic Boltzmann equation, an approach frequently used in condensed matter physics [77]. Next we will review an approach based on the Fokker–Planck equation, a popular tool of computational statistical physics [22]. As an illustration we use the tilting-ratchet setup with bi-harmonic potential and driving,

$$V(x) = V_1 \cos(x) + V_2 \cos(2x + \Delta), \quad (54)$$

$$E(t) = E_1 \cos(\omega t) + E_2 \cos(2\omega t + \theta). \quad (55)$$

3.6.1. Molecular chaos assumption and the Boltzmann equation

The kinetic Boltzmann equation for the case of additive drive reads [23]

$$\hat{\mathcal{L}}P \equiv \partial_t P + \dot{x}\partial_x P + \dot{p}P = \mathcal{J}(P, F), \quad (56)$$

$$\dot{x} = p, \quad \dot{p} = g(x, t) = -V'(x) + E(t), \quad (57)$$

where $P = P(x, p, t)$ is the nonequilibrium distribution function, $F = F(x, p)$ is some equilibrium distribution function,

$$F(x, p) \equiv F_x(x)F_p(p) = \frac{e^{-p^2/2}}{\sqrt{2\pi}} \cdot \frac{e^{-V(x)}}{\mathcal{E}}, \quad \mathcal{E} = \int_0^{2\pi} e^{-V(x)} dx, \quad (58)$$

and $\mathcal{J}(P, F)$ is a collision integral. We use a collision integral of the type [77]

$$\mathcal{J}(P, F) = -\gamma(P - F). \quad (59)$$

The dissipation constant γ determines the characteristic relaxation time, $\tau = \gamma^{-1}$. The dissipative linear equations (56) has a unique limit-cycle solution, $P_A(x, p, t + T) = P_A(x, p, t)$. The asymptotic current is given by the attractor velocity,

$$\begin{aligned} J &= \langle (p/m) \cdot P_A(x, p, t) \rangle_{x,p,t} \\ &= \frac{1}{T\sqrt{2\pi}\mathcal{E}} \int_0^T \int_{-\infty}^{\infty} \int_0^{2\pi} (p/m) \cdot P_A(x, p, t) dt dp dx. \end{aligned} \quad (60)$$

In the overdamped limit, where γ^{-1} sets the shortest timescale of the system dynamics, the limit-cycle solution can be obtained by expanding the function $P_A(x, p, t)$ into a power series over γ^{-1} . In the case $V_2 = 0$ and $E_2 \neq 0$, the first non-zero term of the expansion appears in seventh order of γ^{-1} [23],

$$J \simeq -\frac{45}{4\gamma^7} \frac{I_1(V_0)}{I_0(V_0)} E_2 E_1^2 \cos(\theta) \quad (61)$$

where $I_n(z)$ is the modified Bessel function of n th order [78]. The average current is proportional to the term $\cos(\theta)$, reflecting the fact that the current disappears when $\theta = \pm\pi/2$, i.e. when symmetry \hat{S}_t holds, see Table 1.

The dissipative case cannot be handled analytically in the general case. However, Eq. (56) can be solved numerically by using the expansion of the distribution function $P_A(x, p, \Omega)$ into a series over Hermitian polynomials in p -space and into Fourier series in the x -space. Then, after a proper basis truncation, one ends up with a system of ordinary linear differential equations for the expansion coefficients $A_{n,m}(t)$, where n and m denotes the order of the Hermitian polynomial and Fourier component, correspondingly. The set of equations can be propagated numerically, and, after some transient evolution, it will converge to a limit-cycle attractor, $A_{n,m}(t + T) = A_{n,m}(t)$. This corresponds to the attractor solution, $P_A(x, p, t)$, from which one could calculate the asymptotic current by using Eq. (61).¹²

In Fig. 6 we show the dependence of the asymptotic current J on θ for different values of the dissipation strength. The results demonstrate the crossover between the overdamped and dissipative cases. In the case of strong dissipation, $\gamma = 4$, the asymptotic current vanishes when θ is close to $\pm\pi/2$, i.e. when the symmetry \hat{S}_t is restored at the overdamped limit. When the dissipation is weak, $\gamma = 0.3$, ratchet current drops to zero at the vicinities of points $\theta = 0, \pm\pi$, when the symmetry \hat{S}_t is restored at the Hamiltonian limit. It is noteworthy that the transition from the overdamped limit to the limit of weak dissipation leads to an overall current enhancement of more than two orders of magnitude. Another interesting result is that the dependence $J(\theta)$ preserves its smooth, sine-like form so that the effect of dissipation can be quantified with a phase-lag θ_0 and some overall prefactor,

$$J \sim J_\gamma^0 \sin[\theta - \theta_0(\gamma)], \quad (62)$$

where $\theta_0 = 0$ in the Hamiltonian limit and $\theta_0 = \pm\pi/2$ in the overdamped limit.

3.6.2. From Langevin dynamics to the Fokker–Planck equation

The coupling to a heat bath can be accounted for by introducing noise terms in the rhs of Eq. (16),

$$m\ddot{x} + \gamma\dot{x} = g(x, t) + \xi(t), \quad (63)$$

where $\langle \xi(t)\xi(t') \rangle = 2\gamma k_B \mathcal{T} \delta(t - t')$. Thermal noise $\xi(t)$ has all possible symmetries in the statistical sense. From any particular realization of the noise, $\xi(t)$, we can obtain another one, $\xi'(t)$, by applying to the former either of the transformations, Eqs. (23), (14). The realization $\xi'(t)$ can be taken as another noise realization produced by the same heat bath. In this sense the symmetry properties of Eq. (63) are completely the same as of its deterministic predecessor, Eq. (16).

¹² There is an alternative approach based on the so-called method of characteristics. The expansion method is optimal for the case of moderate dissipation, $\gamma/\omega \geq 0.01$, but both methods demonstrate a good agreement in the range $\gamma/\omega \gtrsim 10^{-2} - 10^{-1}$ [23].

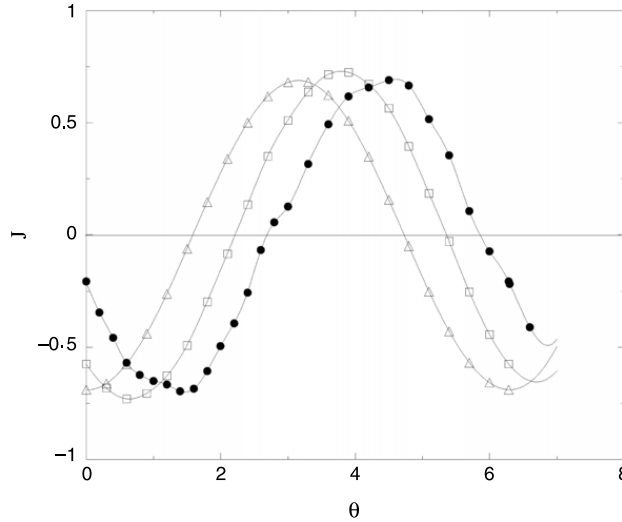


Fig. 6. Dependence of the asymptotic current J , Eq. (60), on the phase shift θ for different values of dissipation parameter: $\gamma = 0.3$ (filled circles), $\gamma = 1$ (squares), and $\gamma = 4$ (triangles). Note that the current values are scaled by a factor of 4.86 ($\gamma = 1$) and 181.6 ($\gamma = 4$). The parameters of Eqs. (54)–(57) are $V_1 = 6$, $V_2 = 0$, $E_1 = -2.6$, $E_2 = -2.04$, $\omega = 0.85$.
Source: Adapted from Ref. [23].

The transport properties of the system (63) can be evaluated in terms of the probability distribution function, $P(x, p, t)$, by using the Fokker–Planck equation (FPE). Below we briefly review main results. The interested reader can find a detailed analysis in Ref. [24].

For the dissipative cases the FPE reads [22]

$$\left\{ \frac{\partial}{\partial t} + \frac{\partial}{\partial x} \frac{p}{m} - \frac{\partial}{\partial p} \left[\frac{\gamma}{m} p - g(x, t) \right] - \gamma m k_B \mathcal{T} \frac{\partial^2}{\partial p^2} \right\} P(x, p, t) = 0, \quad (64)$$

where k_B is the Boltzmann constant. The respective FPE for the overdamped limit, when inertia is negligible, $m = 0$, reads [22]

$$\left\{ \gamma \frac{\partial}{\partial t} + \frac{\partial}{\partial x} g(x, t) - k_B \mathcal{T} \frac{\partial^2}{\partial x^2} \right\} P(x, t) = 0. \quad (65)$$

Eqs. (64) and (65) are linear, dissipative, and preserve the norm, $\int P dx dp$ for Eq. (64) and $\int P dx$ for Eq. (65) [79]. In addition, the equations possess discrete time- and space-translation symmetries so that operations $x \rightarrow x + L$ and $t \rightarrow t + T$ leave the equations invariant. For given boundary conditions and a fixed norm, any initial distribution, $P(\dots, 0)$, will converge to a single time-periodic attractor solution, $P_A(\dots, t) = P_A(\dots, t + T)$. The current can be calculated from a spatially periodic solution of the type $P(x, \dots) = P(x + L, \dots)$ [4].

The averaged asymptotic current on the attractor $P_A(x, p, t)$ is given by Eq. (60) for the dissipative case, and by [4]:

$$J = \gamma^{-1} \langle g(x, t) \cdot P_A(x, t) \rangle_{T, L}, \quad (66)$$

in the overdamped limit.

It is easy to see that the FPE for the general dissipative case, Eq. (64), inherits all the symmetries of the corresponding equations of motions, including those for the Hamiltonian limit, $\gamma = 0$. However, the time-reversal symmetry for the overdamped limit, Eq. (32), cannot be detected with Eq. (65). This symmetry imposes certain restrictions not directly on symmetries the equation itself but on its solutions. Consider the case of rocking ratchet, Eq. (54). The corresponding attractor solution, $P_A(x, t)$, is periodic both in time and space. We define an operator

$$\hat{W} = \frac{-\frac{\partial}{\partial x}}{\gamma \frac{\partial}{\partial t} - \frac{\partial^2}{\partial x^2} + E(t) \frac{\partial}{\partial x}}. \quad (67)$$

Then the attractor solution is the solution of a Lippmann–Schwinger-type integral equation [80],

$$P_A(x, t) = 1 + \hat{W} f(x) P_A(x, t). \quad (68)$$

Both operators, $\partial/\partial t$ and $\partial/\partial x$, are anti-Hermitian in the space of x , t -periodic functions. Provided the conditions for \hat{S}_t hold, i.e. $E(t)$ is antisymmetric, see Table 1, the operator \hat{W} has the following properties:

$$\hat{W}^\dagger = -\hat{W}(-t), \quad \hat{W}(x + x_0) = \hat{W}(x). \quad (69)$$

Expanding Eq. (68) in a formal series in $f(x)$ we obtain

$$P_s = 1 + \sum_{n=1}^{\infty} (\hat{W}f(x))^n. \quad (70)$$

With Eq. (66) we finally obtain for the average current

$$J = \sum_{n=1}^{\infty} \int f(x) (\hat{W}f(x))^n dx dt. \quad (71)$$

Since all terms in (71) are real-valued, we conclude that all integrals with even n vanish when the symmetry \hat{S}_t holds, i.e. the function $f(x)$ is shift-symmetric, and these terms contain odd powers of f only. All integrals with odd n vanish because of the conditions (69). Thus we conclude that indeed the average current exactly vanishes when \hat{S}_t holds.

Eqs. (64), (65) can be solved numerically, by expanding $P(x, p, t)$ into the Fourier series over x and t , and into the Hermite polynomial series over p . This will result in a system of linear algebraic equations for the expansion coefficients, which can be solved then by using standard numerical diagonalization routines [24].

3.7. Experiments with cold atoms

Fast progress in the field of experimental manipulations with cold and ultracold atoms served a new class of physical systems which fulfill the conditions required to observe symmetry-controlled directed transport. The dynamics of the corresponding systems is weakly dissipative, or even, on certain time scales, near perfectly Hamiltonian, thus allowing one to get in touch with classical Hamiltonian and quantum dynamics *in vivo*. Laser created periodic optical potentials provide a possibility to explore nonequilibrium transport induced by violation of time–space symmetries. In this section we review a series of experiments with rocking cold atom ratchets which have perfectly validated the results of the symmetry analysis for classical ratchets in the regime of weak dissipation. Again, before starting the discussion, we will flash through some basic information on the cold atom optics (for more information see Ref. [14]).

An atom with nonzero spin has several internal states, determined by the spin projection on a given direction. The transition between two different states can be induced by an external electromagnetic field, i.e. by light. The electromagnetic field also shifts energy levels of the atoms, which leads to an effective interaction between the light and the atom. A periodic potential for the atom can be created using counter-propagating laser beams which form standing light waves. The periodic interference pattern introduces a spatial modulation of the energy shift, thus creating a potential. The parameters of optical potentials can be tuned by changing the parameters of the lasers—intensities, relative shifts, etc. [14,16].

In experiments with cold atom ratchets, optical lattices serve two ends: They (i) create periodic potentials for atoms and (ii) provide a possibility to reduce the kinetic energy of the atoms by cooling them down to mKelvin temperatures. The latter was possible due to the *Sisyphus cooling* phenomena [81]. As an illustration we use the simplest case when an atom has only two internal states, a ground state, with the spin projection $J_g = 1/2$, and an excited state, $J_e = 3/2$. Imagine now that the atom is placed into an optical potential created by two counter-propagating laser beams, both with the same wavelength λ but of mutually orthogonal polarizations. The interference between beams results in a $\lambda/2$ –periodic potential with spatially-dependent elliptic polarization. When in the ground state $J_g = \pm 1/2$, the atom feels a periodic potential

$$V_{\pm}(x) = \frac{V_0}{2} [-2 \pm \cos(k_L x)], \quad (72)$$

where $k_L = \pi/\lambda$, and the potential depth V_0 can be tuned by changing the laser intensity and frequency.¹³ If the laser frequency is close to the frequency of the transition $J_g \rightarrow J_e$, the corresponding electromagnetic field may induce a transition between the two internal states of the atom. Consider the situation when the atom, initially located at the point $x = 0$, has a positive velocity and it is in the ground state $J_g = -1/2$. Atom starts to climb the potential slope $V_{-}(x)$ (dashed line in Fig. 7), by transferring its kinetic energy into potential energy. At the potential summit, the light field consists of the σ_{+} -component only, and the probability of the transition $J_g = -1/2 \rightarrow J_g = +1/2$, through two consecutive events of absorption and emission, is maximal. This transition results in a loss of the potential energy by the atom. After the emission the atom is subjected to the potential $V_{+}(x)$ (solid line in Fig. 7), where it appears at the bottom of a potential well. The process repeats again and again, like in the ancient story about king Sisyphus [83]. Finally, after several cycles of absorption and emission, the atom ends up in a state where it does not have enough energy to climb the potential slope, thus remaining localized at the bottom of one of the potential wells.

In the Sisyphus cooling machinery, fluctuation and dissipation mechanisms are closely interwoven as they are produced by the same chain of stochastic transitions between atom internal states. The overall effect is quantified by the frequency of the transitions, also called *scattering rate* Γ . Its value depends on the intensity of the laser field I_l and the difference

¹³ A bi-harmonic potential of the form $V(x) = \frac{1}{2}[V_1 \cos(kx) + V_2 \cos(2kx + \Delta)]$, with the tunable phase Δ , can be created by using dispersive properties of multiphoton Raman transitions [82,47].

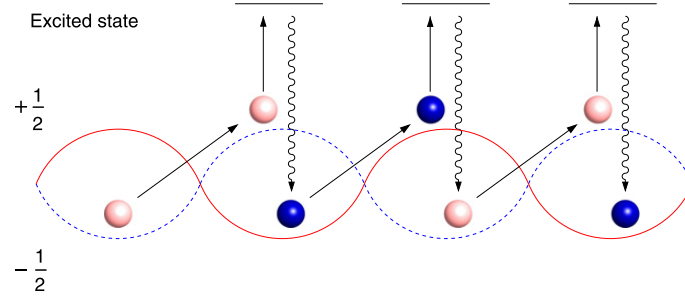


Fig. 7. Sisyphus cooling of an atom with two internal states defined by the projections of its spin, $J_g = -1/2$ and $J_e = +1/2$, in a lin ⊥ lin optical lattice [81]. The atom (ball) travels from the left to the right through the lattice and its state is indicated by the color of the ball, blue for J_g and red for J_e . The upwards arrows denote absorptions of photons, while downwards wave arrows mark the spontaneous emission events. (For interpretation of the references to color in this figure legend, the reader is referred to the web version of this article.)

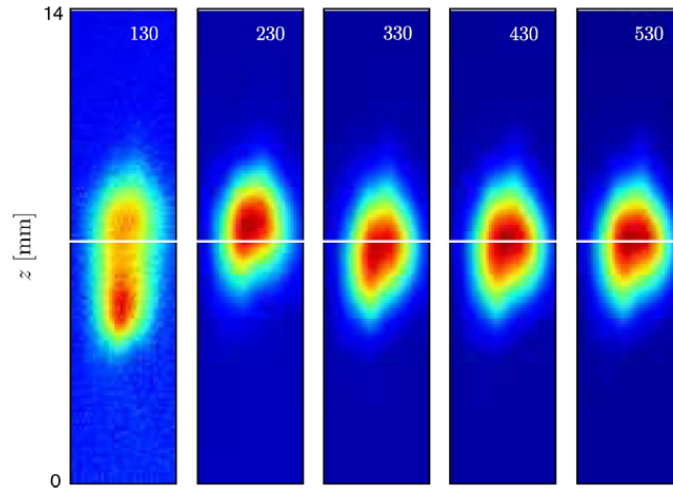


Fig. 8. Fluorescence images of the atomic cloud obtained in experiments with a rocking ratchet setup, Eq. (74), after the exposition to the driving during 26 ms. Different panels correspond to different values of the driving frequency ω (in kHz units). The white line marks the initial position of the cloud's center of mass. The phase shift is $\theta = \pi/2$ in all cases. (For interpretation of the references to color in this figure legend, the reader is referred to the web version of this article.)

Source: Courtesy of Ferruccio Renzoni.

between the laser frequency and the frequency of the transition, $\Delta = \omega_l - \omega_0$, $\Gamma \propto I_l / \Delta^2$. The potential height scales as $U_0 \propto I_l / \Delta$ [14]. Therefore, it is possible to change the decoherence strength by changing simultaneously the intensity I_l and the detuning Δ while keeping their ratio, i.e. the potential strength, constant.

A driving force can be realized in different ways, depending on a particular ratchet setup one wants to implement. The multiplicative driving, $g(x, t) = E(t)f(x)$, can be implemented by modulating the intensity of the lasers periodically in time [47]. The additive driving, $g(X, t) = f(x) + E(t)$, can be introduced through phase modulations of one of the beams, in a manner similar the described in Section 3.3.3. The modulations result in a shaking potential $V(x) \propto \cos(kx - \alpha(t))$ so that in the co-moving frame, $x' = x - \alpha(t)/k$, an atom of mass m experiences a tilting force $E(t) = -m\ddot{\alpha}(t)/k$. A bi-harmonic function $\alpha(t)$ will produce a bi-harmonic driving $E(t)$, with the same phase shift θ . Finally, due to the periodicity of the driving, $\alpha(t + T) = \alpha(t)$, the averaged velocities of an atom are the same in the lab and co-moving frames, $\langle \dot{x} \rangle = \langle \dot{x}' \rangle$. This elegant idea has been implemented in a series of experiments reported in Refs. [49,38]. The spatial positions of the atoms were monitored through the direct imaging by using a charge-couple-device (CCD) camera. From these images, the position of the cloud center of mass was calculated, thus allowing to detected the transport of the atomic cloud along the optical lattice [49], see Fig. 8.

3.7.1. Cold atom ratchets with periodic driving

The rocking ratchet set-up, used in the experiments with cold atom ratchets [49,38,84], corresponds to a simple-harmonic potential force,

$$f(x) = f_1 \sin(k_L x), \quad (73)$$

and a bi-harmonic driving function,

$$E(t) = E_1 \cos(\omega t) + E_2 \cos(2\omega t + \theta). \quad (74)$$

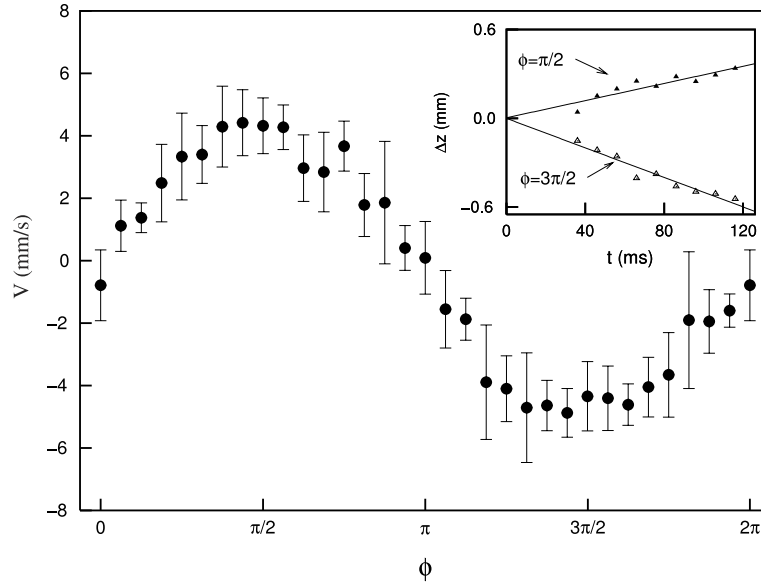


Fig. 9. Average velocity of the atomic cloud center-of-mass as a function of the phase θ (denoted by ϕ here). Inset: the displacement of the center-of-mass as a function of time for two different values of the phase θ . The potential is $V(x) = V_0 \cos(kx)$, with the bi-harmonic drive of the form $E(t) = E_1 \cos(\omega t) + E_2 \cos(2\omega t + \theta)$. Source: Adapted from Ref. [49].

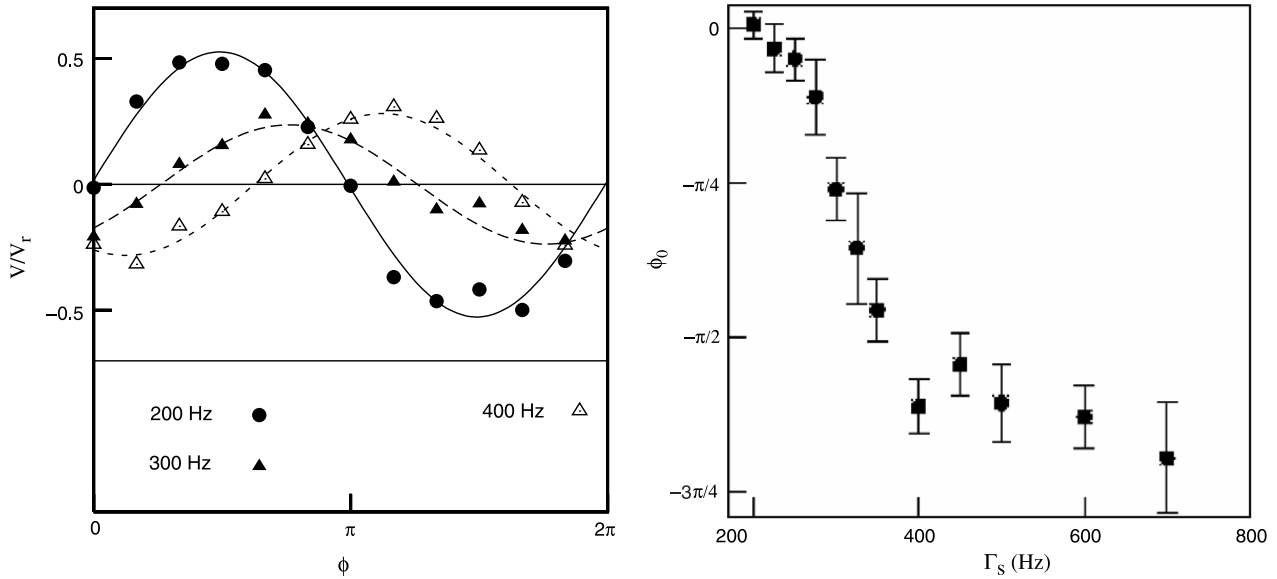


Fig. 10. (Left panel) Average velocity of the atomic cloud center of mass as a function of θ (denoted by ϕ here) for different scattering rates Γ . Lines correspond to the fitting obtained with Eq. (75); (right panel) phase lag $\theta_0(\Gamma)$ (denoted by ϕ_0 here) as a function of the scattering rate. Source: Adapted from Ref. [39].

The measured dependence of the center-of-mass velocity of the atomic vs θ has a well-pronounced sine-like shape (50), see Fig. 9. It is important to understand, however, that the dynamics of atoms in an optical lattice is far from being exactly Hamiltonian. The decoherence of the atomic dynamics, created by emission–absorption events, is always present. Moreover, it plays a key role because it is responsible for the cooling of the atoms. From the classical model it follows that the overall effect of dissipation and fluctuations can be absorbed into the phase lag θ_0 , Eq. (62). The effect of decoherence, induced by the interaction between an atom and the electromagnetic field of a laser beam, is then replaced by dissipation and fluctuations, exerted on the classical particle by a heat bath, see Eq. (63). By looking at the experimental data, Fig. 9, we can conclude that the decoherence effects were not able to produce a tangible shift of the sine-like dependence (expected at the Hamiltonian limit).

The decoherence quantifier, the scattering rate Γ [14], is a tunable parameter which can be controlled in experiment. This naturally leads to the following question: Would it be possible, by increasing Γ , to see the effect of dissipation-induced phase lag, similar to that observed in computational studies of the stochastic classical model, Eq. (62)? This question was positively answered with cold atoms [39]. The main result of the experiments is shown in Fig. 10. By fitting the data points

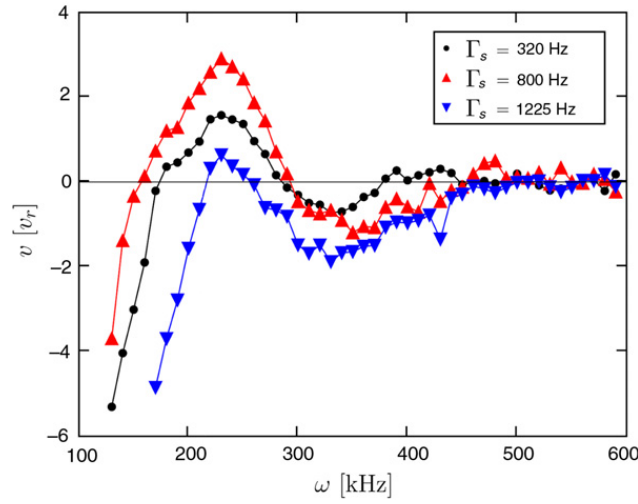


Fig. 11. Average velocity of the center of mass of the atomic cloud as a function of the driving frequency ω for different scattering rates, Γ_s . The phase shift is $\theta = \pi/2$. The fluorescence images corresponding to $\Gamma_s = 320$ kHz are shown in Fig. 8. (For interpretation of the references to color in this figure legend, the reader is referred to the web version of this article.)

Source: Courtesy of Ferruccio Renzoni.

obtained for different values of θ with the target function

$$J(\theta; \Gamma) \sim J_r^0 \sin[\theta - \theta_0(\Gamma)], \quad (75)$$

the dependence $\theta_0(\Gamma)$ was extracted, see the right panel of Fig. 10. The phase lag is close to zero for the smallest examined scattering rate, it lowers down to $\theta_0 = -\pi/2$ with the increase of the scattering rate, and then even goes below this value, finally approaches $\theta_0 = -3\pi/4$. This deviation from the results obtained for the classical ratchet, see Fig. 6, which say that the phase lag cannot go below the threshold $\theta_0 = -\pi/2$ (corresponding to the overdamped limit), is noteworthy. This discrepancy demonstrates that the analogy between the classical stochastic model and the quantum system, explored in the experiments, should not be overstretched. A proper modeling requires more appropriate numerical approaches, for example, quantum or quasiclassical Monte-Carlo methods [85,14] (see also Refs. [86,87] for alternative approaches to decoherence-induced phenomena in quantum ratchets).

Directed current of cold atoms depends not only on θ but on the other parameters of the driving function as well. Multiple current reversals have been detected in the experiments upon tuning amplitudes [38] and frequency of $E(t)$ [88], see Fig. 11. It has been observed that the dependence $J(\theta)$, Eq. (75), preserves its smooth sine-like upon the variations of the driving frequency [89]. Therefore, the dependence of the atomic current on ω can again be absorbed into the phase lag, $\theta_0(\Gamma, \omega)$.

A realization of the gating ratchet with cold cesium atoms, Eqs. (40), (41), was presented in Ref. [58]. The obtained experimental results again confirmed the predictions of the symmetry analysis. Finally, the results obtained with cold atom version of the kicked rotor (a particular example of the multiplicative setup, Section 3.3.2), were reported in Ref. [90].

3.7.2. Cold atom ratchets with quasiperiodic driving

Quasiperiodic driving, Section 3.4, provides another chance to probe the symmetry analysis with cold-atom ratchets. In principle, an arbitrary time-dependent driving function $E(t)$ can be generated by modulating the relative phases of the laser beams. By using additional acousto-optic modulators (AOMs), it is possible to obtain signals with different frequencies, $\omega_1, \omega_2, \omega_3, \dots$ [91]. If the ratio ω_2/ω_1 is an irrational number then the driving is quasiperiodic. It is evident, however, that the ideal quasiperiodicity is a mere mathematical abstraction which is absent in the real life. Effective cutoffs appear due to unavoidable parameters fluctuations during an experiment. Thus, the ratio ω_1/ω_2 can always be approximated by a rational number p/q , with p, q being two co-prime integers. However, as the duration of the experiment is always finite, one could, by choosing p and q sufficiently large, obtain a driving which is quasiperiodic on the time scale of the experiment. This idea was realized in another series of experiments with cold cesium atoms [92].

The first type of the driving function examined in the experiments was a sum of three harmonics,

$$E(t) = E_1 \cos(\omega_1 t) + E_2 \cos(2\omega_1 t + \theta) + E_3 \cos(\omega_2 t + \delta). \quad (76)$$

Let us start the symmetry analysis of this setup from the case when ω_1/ω_2 is a rational number. For $E_3 = 0$ we have a standard bi-harmonic setup, Eq. (74), with the time-reversal symmetry holding for $\theta = 0, \pm\pi$ in the limit of vanishing dissipation. When $E_3 \neq 0$ and $\delta = 0, \pm\pi$, the time-reversal symmetry is still present. For $\delta \neq 0, \pm\pi$, the symmetry is broken and the directed current can appear at the former symmetry points $\theta = 0, \pm\pi$. Thus the third harmonics produces an additional shift effect of the current dependence $J(\theta)$. By taking the decoherence effects into account, we arrive at the following target function [92]:

$$J \sim J_{\Gamma, \delta}^0 \sin[\theta - \theta_0(\Gamma, \delta)]. \quad (77)$$

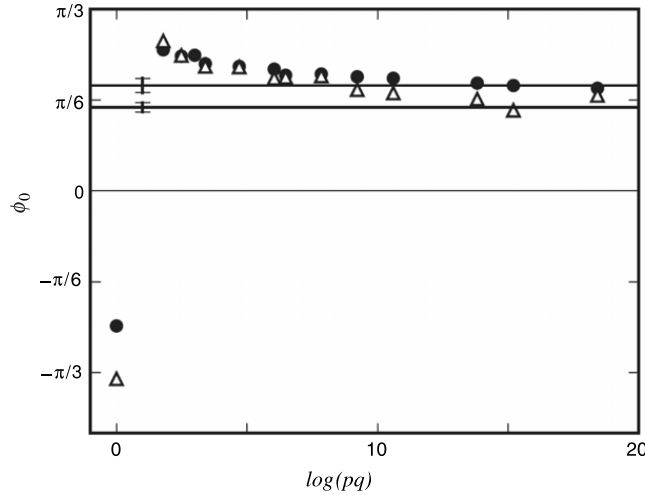


Fig. 12. Phase lag $\theta_0(\Gamma, \delta)$ (denoted ϕ_0 here), Eq. (77), as a function of the product pq , where p and q are co-primes determined by the ratio $\omega_1/\omega_2 = p/q$. The quasiperiodic limit corresponds to $pq \rightarrow \infty$. The two data sets correspond to different amplitudes of the driving. The phase of the driving at frequency ω_2 , Eq. (76), is $\delta = \pi/2$. The phase lag was estimated by fitting the current dependence on θ with Eq. (77). The two horizontal lines indicate the phase shift θ_0 for the bi-harmonic drive, i.e. in the absence of the driving at frequency ω_2 , $E_3 = 0$. Source: Adapted from Ref. [92].

The difference between this expression and that one introduced before, Eq. (75), is that now θ_0 depends not only on the strength of the decoherence, determined by the scattering rate Γ , but also on the phase shift of the third harmonics δ .

Let us turn now to the case of quasiperiodic driving, when ω_1/ω_2 is an irrational number. As discussed in Section 2.2, in this case the phases $t_1 = \omega_1 t$ and $t_2 = \omega_2 t$ can be treated as independent variables. The tri-harmonic driving, Eq. (76), is invariant under the transformation $t_2 \rightarrow -t_2$, for any value of δ and for $\theta = 0, \pm\pi$. In the Hamiltonian limit, we should return to the dependence of the ratchet current given by Eq. (62). In the quasiperiodic limit, the third harmonics does not induce any additional lag, which is determined now by the strength of decoherence solely. This prediction was confirmed by the results of the experiments, see Fig. 12. It was found that upon the approach of the quasiperiodic limit, when the ratio ω_1/ω_2 tends to be more and more irrational, the dependence of the lag on the phase of the third harmonics disappears and the phases t_1 and t_2 behave as two independent variables.

A different form of the driving function,

$$E(t) = E_1 \cos(\omega_2 t + \delta)[a \sin(\omega_1 t) + b \sin(2\omega_1 t)] + E_2 \sin(\omega_2 t + \delta)[a \cos(\omega_1 t) + 2b \cos(2\omega_1 t)] \quad (78)$$

was also examined in Ref. [92]. Consider ω_1/ω_2 to be a rational number, p/q . The period of the function $E(t)$ is $T = qT_1 = pT_2$, where $T_1 = 2\pi/\omega_1$ and $T_2 = 2\pi/\omega_2$. Time-shift transformations, $t \rightarrow t + T/2$, change phase variables, $t_1 \rightarrow t_1 + q\pi$ and $t_2 \rightarrow t_2 + p\pi$. It is easy to check that the function $E(t)$ possesses shift-symmetry (6) whenever q is even and p is odd. Therefore, in the limit of vanishing dissipation, when q is even and p is odd, symmetry \hat{S}_x , Eq. (26), holds and the ratchet current should disappear. Assume now that q is odd. Symmetry \hat{S}_x is already broken but the time-reversal symmetry, \hat{S}_t , Eq. (26), remains. Its validity depends on the phase δ : It holds when $q\delta = (n + 1/2)\pi$, with n integer. The current is expected to show the familiar sine-like dependence on $q\delta - \pi/2$, perhaps with an additional lag accounting for the decoherence-induced shift effect. In the quasiperiodic limit, as before, we can think of two independent variables, $t_1 = \omega_1 t$ and $t_2 = \omega_2 t$. The function (78) is shift-symmetric with respect to t_2 , i.e. it changes sign under the transformation $t_2 \rightarrow t_2 + \pi$. Therefore, the ratchet transport should disappear in the limit $pq \rightarrow \infty$. The results of experiments [92], Fig. 13, confirmed that indeed the rectification is lost in the quasiperiodic limit due to the restoration of the shift-symmetry of $E(t)$.

4. Directed transport in two and three spatial dimensions

In this section we generalize the symmetry analysis to the case of two- and three-dimensional potentials. Two new features can be expected right from the start. First, the current is a vector now and it has a certain length and is pointing at certain direction. Second, the new angular dependence may lead to a rotational motion, i.e. to a vorticity. Both linear and vortex currents may become nonzero. Moreover, they may be intricately coupled to each other in the manner similar to the spin-orbit coupling effect [93]. Quantum optics also gives practical reasons to extend the symmetry analysis in this direction. Nowadays, by using several laser beams, experimentalists can routinely fabricate two- and three-dimensional optical potentials of very different symmetries and shapes [16,17] that can be driven in addition [14]. These advances served a testing ground to study weakly-dissipative ratchets with two- and three-dimensional periodically driven potentials.

In this section we consider the dynamics of a classical particle in a $d = \{2, 3\}$ -dimensional space-periodic potential, which is driven by a zero-mean ac-field. The particle may contribute to a directed current along a certain direction, and, at the same time, it could perform a rotational vortex-like motion. The main issue we want to address here is how to simultaneously

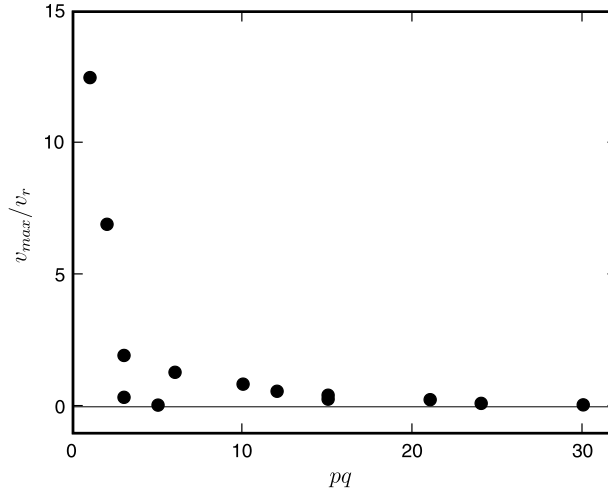


Fig. 13. Maximum average velocity of the atomic cloud as a function of pq , where p and q are the co-primes defined by the ratio of the driving frequencies, $p/q = \omega_2/\omega_1$. The maximum velocity was estimated by fitting the current dependence on q with the function $v(q) \sim \sin(q\delta - \pi/2)$. Source: Adapted from Ref. [92].

control two different transport modes. By using the symmetry analysis, we will first identify the symmetries which ensure that either translational or vortex components along certain directions are strictly zero. Then, by using a 2d model, we will show how, by breaking these symmetries one by one, we can control the particle motion generating either directed or vortex currents or both simultaneously. Finally, we will review an experimental realization of this idea with cold atoms and two-dimensional optical potentials [94].

4.1. Symmetry analysis

We start with a model of a classical particle exposed to a potential force and fluctuations produced by the coupling to a heat bath,

$$m\ddot{\mathbf{r}} + \gamma\dot{\mathbf{r}} = \mathbf{g}(\mathbf{r}, t) + \boldsymbol{\xi}(t), \quad \mathbf{g}(\mathbf{r}, t) = -\nabla V(\mathbf{r}, t). \quad (79)$$

Here $\mathbf{r} = \{x, y, z\}$ is the coordinate vector of the particle. The force $\mathbf{g}(\mathbf{r}, t) = \{g_\alpha(\mathbf{r}, t)\}$, $\alpha = x, y, z$, is time- and space-periodic:

$$\mathbf{g}(\mathbf{r}, t) = \mathbf{g}(\mathbf{r}, t + T) = \mathbf{g}(\mathbf{r} + \mathbf{L}_\alpha, t), \quad \alpha = x, y, z. \quad (80)$$

\mathbf{L}_α are the lattice vectors. The absence of dc-components of the force vector implies

$$\langle \mathbf{g}(\mathbf{r}, t) \rangle_{\mathbf{L}, T} \equiv \int_0^T \int_{\mathbf{L}} \mathbf{g}(\mathbf{r}, t) dt dxdydz = 0 \quad (81)$$

where the spatial integration is performed over the unit cell of the lattice.

The current is a vector now, $\mathbf{J} = \{J_\alpha\}$, with the components given by the corresponding components of the average velocity vector $\mathbf{v} = \dot{\mathbf{r}}$ of the particle,

$$J_\alpha = \lim_{t \rightarrow \infty} \frac{v_\alpha}{t}. \quad (82)$$

The conditions for the current to be absent, i.e. $\mathbf{J} \equiv \mathbf{0}$, and the corresponding symmetries can be obtained by direct generalizations of the symmetry analysis for the 1d case, discussed in the previous section. Namely, there are two fundamental symmetry transformations,

$$\hat{\mathbf{S}}_r[\boldsymbol{\Xi}, \tau] : \mathbf{r} \rightarrow -\mathbf{r} + \boldsymbol{\Xi}, \quad t \rightarrow t + \tau, \quad (83)$$

$$\hat{\mathbf{S}}_t[\boldsymbol{\Xi}, \tau] : \mathbf{r} \rightarrow \mathbf{r} + \boldsymbol{\Xi}, \quad t \rightarrow -t + \tau, \quad (84)$$

parametrized by a shift vector $\boldsymbol{\Xi} = \{\chi_\alpha\}$ and scalar parameter τ , with both depending on the shape of the force function $\mathbf{g}(\mathbf{r}, t)$. Any of the transformations that change the sign of \mathbf{J} , Eq. (82), such that when the system (79) is invariant under either of the transformations, yield a zero of the average corresponding ratchet current.

Consider as an example the additive case,

$$\mathbf{g}(\mathbf{r}, t) = -\nabla V(\mathbf{r}) + \mathbf{E}(t) \equiv \mathbf{f}(\mathbf{r}) + \mathbf{E}(t). \quad (85)$$

Similar to the one-dimensional case, symmetry \hat{S}_r holds when the potential force is *anti-symmetric*, $\mathbf{f}(-\mathbf{r} + \mathbf{r}') = -\mathbf{f}(\mathbf{r})$, and the driving function is *shift-symmetric*, $\mathbf{E}(t + T/2) = -\mathbf{E}(t)$. The symmetry \hat{S}_t holds at the Hamiltonian limit, $\gamma = 0$, if the driving force is *symmetric*, $\mathbf{E}(-t + t') = \mathbf{E}(t)$. Finally, the symmetry \hat{S}_t holds at the overdamped limit, $m = 0$, if the potential force is *shift-symmetric*, $\mathbf{f}(\mathbf{r} + \boldsymbol{\Xi}) = -\mathbf{f}(\mathbf{r})$ and the driving force is *anti-symmetric*, $\mathbf{E}(t + t') = -\mathbf{E}(-t)$. All of the above can be re-formulated in terms of the potential, $V(\mathbf{r}) = V(x, y)$, taking into account the relations between the symmetries of the function and its derivative/integral, see Section 2.1.

The system can be coupled to a heat bath in the standard way, by adding to the rhs of Eq. (79) a random Gaussian vector, $\boldsymbol{\xi}(t) = \{\xi_x, \xi_y, \xi_z\}$, $\langle \xi_\alpha(t) \xi_\eta(t') \rangle = 2\gamma k_B \mathcal{T} \delta(t - t') \delta_{\alpha\eta}$, $\alpha, \eta = \{x, y, z\}$. The statistical description of the system evolution is provided by the Fokker–Planck equation (FPE) [22]:

$$\left\{ \frac{\partial}{\partial t} + \nabla_{\mathbf{r}} \cdot \frac{\mathbf{p}}{m} - \nabla_{\mathbf{p}} \cdot [\gamma \mathbf{v} - \mathbf{g}(\mathbf{r}, t)] - \gamma m D \Delta_{\mathbf{p}} \right\} P(\mathbf{r}, \mathbf{p}, t) = 0, \quad (86)$$

where $\mathbf{p} = m\dot{\mathbf{r}}$ and $D = k_B \mathcal{T}$. The respective FPE for $m = 0$ reads

$$\left\{ \gamma \frac{\partial}{\partial t} + \nabla_{\mathbf{r}} \cdot \mathbf{g}(\mathbf{r}, t) - D \Delta_{\mathbf{r}} \right\} P(\mathbf{r}, t) = 0. \quad (87)$$

Similar to their one-dimensional counterparts, Section 3.6.2, these linear differential equations have unique, space- and time-periodic attractor solutions, $P_A(\mathbf{r}, \mathbf{p}, t)$ and $P_A(\mathbf{r}, t)$, correspondingly [22]. The asymptotic currents can then be written as

$$\mathbf{J} = \langle \mathbf{v} \cdot P_A(\mathbf{r}, \mathbf{p}, t) \rangle_{T,L}, \quad m = 1, \quad (88)$$

$$\mathbf{J} = \gamma^{-1} \langle \mathbf{g}(\mathbf{r}, t) \cdot P_A(\mathbf{r}, t) \rangle_{T,L}, \quad m = 0. \quad (89)$$

It is easy to see that the FPE for the underdamped case, Eq. (86), inherits all the symmetries of the corresponding equations of motions, Eq. (79), including the Hamiltonian limit, $\gamma \rightarrow 0$. The time-reversal symmetry for the overdamped case, Eq. (87), can be explained in the same manner used for the 1d case, Eqs. (68)–(71).

There is a new possibility to control the current. Namely, we can align the ratchet current \mathbf{J} along a desirable direction. This can be achieved by setting the adjacent components of the current vector to zero. For that one has to define the symmetry operations which change the signs of adjacent current component only. If such a symmetry is present then the current along the corresponding directions is absent. As an illustration, consider a generalization of the symmetry \hat{S}_x , which acts in the following manner:

$$\hat{S}_x[\boldsymbol{\Xi}, \tau] : x \rightarrow -x + \chi_x, \quad y \rightarrow y + \chi_y, \quad t \rightarrow t + \tau. \quad (90)$$

Whenever Eq. (79) is invariant under this transformation, the x -component of the current is absent, $J_x = 0$. If there are no further symmetries then a ratchet current will appear along the y -direction. The extension of this idea to the 3d case, with the symmetries of the type $\hat{S}_{x,y}$, is straightforward.

As an illustration, we consider a 2d rocking ratchet,

$$H(r, p, t) = \frac{\mathbf{p}^2}{2} + V(x, y) + \mathbf{E}(t) \cdot \mathbf{r}, \quad (91)$$

with the potential

$$V(x, y) = \cos(x)[1 + \cos(2y)]. \quad (92)$$

The rocking force, $\mathbf{E}(t)$, has components

$$E_{x,y}(t) = E_{x,y}^{(1)} \sin(t) + E_{x,y}^{(2)} \sin(2t + \theta_{x,y}). \quad (93)$$

When $E_x^{(2)} = E_y^{(1)} = 0$ and $\theta_y = 0$, the symmetry $\hat{S}_x[\mathbf{0}, \pi]$ holds. This implies that $J_x = 0$ and the directed transport is confined to the y -axis.

At variance to the one-dimensional case, particles in two and three dimensions can perform rotational motion. Even in the case when the directed current is absent, $\mathbf{J} = 0$, the particle can still perform unbiased diffusion in the coordinate space. In order to distinguish between directed transport and spatial diffusion on one side, and *rotational currents* on the other side, we use the angular velocity

$$\boldsymbol{\Omega}(t) = [\dot{\mathbf{r}}(t) \times \ddot{\mathbf{r}}(t)] / \dot{\mathbf{r}}^2(t), \quad \mathbf{J}_{\Omega} = \langle \boldsymbol{\Omega}(t) \rangle_t, \quad (94)$$

as a quantifier for the particle vorticity. $\boldsymbol{\Omega}(t)$ is invariant under translations in space and time, and describes the speed of rotation with which the velocity vector $\dot{\mathbf{r}}(t)$ encompasses the origin.

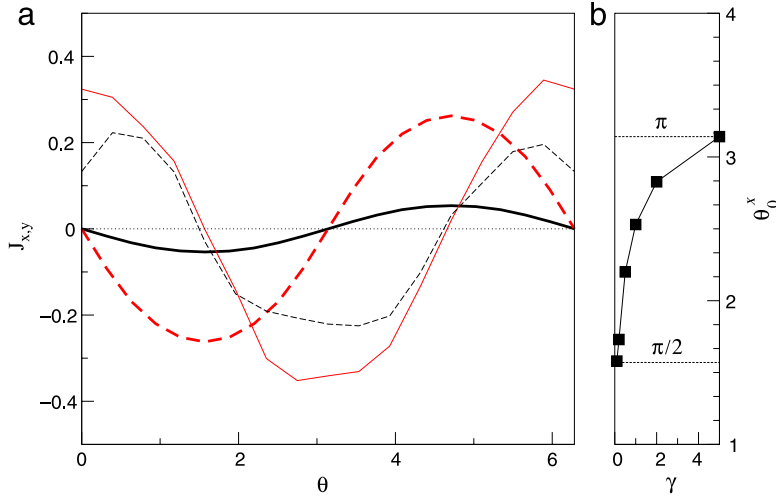


Fig. 14. (Color online) (a) Dependences of the current components, J_x (solid line) and J_y (dashed line), on $\theta_x = \theta_y := \theta$ for the system (91)–(93). Curves correspond to the overdamped ($m = 0$, $\gamma = 1$, thick lines) and underdamped ($m = 1$, $\gamma = 0.1$, thin lines) cases, respectively. (b) The phase lag θ_0^x , cf. Eq. (98), as a function of the dissipation strength γ . The parameters are $D = 1$, $E_x^{(1)} = -E_x^{(2)} = 2$, $E_y^{(1)} = -E_y^{(2)} = 2.5$. Source: Adapted from Ref. [95].

We now search for symmetry operations which leave the equation of motion, Eq. (79), invariant, while changing the sign of the angular velocity $\Omega(t)$. The sign can be inverted by (i) the time-reversal transformation, $t \rightarrow -t$, together with an optional space-inversion, $\mathbf{r} \rightarrow \pm \mathbf{r}$. The corresponding symmetry transformation is

$$\hat{\mathbf{R}}_t^\pm[\mathcal{E}, \tau] : \mathbf{r} \rightarrow \pm \mathbf{r} + \mathcal{E}, \quad t \rightarrow -t + \tau. \quad (95)$$

Note that the symmetry $\hat{\mathbf{R}}_t^+$ formally is identical to the symmetry $\hat{\mathbf{S}}_t$, Eq. (84). There are two extra symmetries for $d = 2$. Namely, the following operations change sign of $\Omega(t)$: (ii) the permutation of the variables, $\{x, y\} \rightarrow \{y, x\}$, and (iii) the mirror reflections, $\hat{\sigma}_x : \{x, y\} \rightarrow \{-x, y\}$ or $\hat{\sigma}_y : \{x, y\} \rightarrow \{x, -y\}$. The corresponding symmetries are:

$$\hat{\mathbf{R}}_p[\mathcal{E}, \tau] : \mathbf{r} \rightarrow \hat{\mathcal{P}}\mathbf{r} + \mathcal{E}, \quad t \rightarrow -t + \tau. \quad (96)$$

$$\hat{\mathbf{R}}_{x,y}[\mathcal{E}, \tau] : \mathbf{r} \rightarrow \hat{\sigma}_{x,y}\mathbf{r} + \mathcal{E}, \quad t \rightarrow -t + \tau. \quad (97)$$

The rotational symmetries can also be expressed in terms of the potential, $V(x, y)$, and driving vector, $\mathbf{E}(t)$. As an illustration, we consider the Hamiltonian version of the two-dimensional ratchet with additive driving, Eq. (91). If the driving function is symmetric, $\mathbf{E}(-t + \tau) = \mathbf{E}(t)$, then, in the Hamiltonian limit, symmetry $\hat{\mathbf{R}}_t^+$ holds, independent of the symmetry properties of $V(x, y)$. However, symmetry $\hat{\mathbf{R}}_t^-$ holds only when the drive function is anti-symmetric, $\mathbf{E}(-t + \tau) = -\mathbf{E}(t)$, and the potential is symmetric, $V(x, -y + \chi_y) = V(-x + \chi_x, y) = V(x, y)$. Note that this symmetry does not forbid the ratchet current since the corresponding transformation does not change the sign of \mathbf{J} . Symmetry $\hat{\mathbf{R}}_p$ holds when both functions, potential and drive vector, possess the permutation symmetry, $V(x, y) = V(y, x)$ and $E_x(t) = E_y(t)$. The analysis for the dissipative and overdamped limit can be performed in the similar manner. The final outcome of the symmetry analysis is presented with Table 3, where we list the conditions for the functions $V(x, y)$ and $\mathbf{E}(t)$ have to satisfy for the corresponding rotational symmetries be present. We leave it as an exercise to the reader to figure out the rotational symmetries for the 2d version of the multiplicative set-up, Eq. (37).

4.2. Applications: numerical studies





















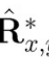


As an illustration, we consider a two-dimensional version of the rocking ratchet, Eqs. (91)–(93). The potential (92) is shift-symmetric, with $\mathcal{E} = \{\pm\pi, 0\}$. The symmetry $\hat{\mathbf{S}}_t$ is already broken since the driving vector \mathbf{E} is not shift-symmetric. Therefore we expect $\mathbf{J} \neq 0$ for the case of nonzero dissipation, $\gamma > 0$.













In Fig. 14 we show the results of numerical integration of Eqs. (86) and (87). By applying operations $\hat{\mathbf{S}}_t$ and $\theta \rightarrow \theta + \pi$, one can see that $\mathbf{J}(\theta + \pi) = -\mathbf{J}(\theta)$, which allows for the inversion of the current direction by shifting θ , see Fig. 14(a). In the overdamped limit $m = 0$, symmetry $\hat{\mathbf{S}}_t$ is restored for $\theta = 0, \pm\pi$, and therefore $\mathbf{J}(-\theta) = -\mathbf{J}(\theta)$ (thick lines in Fig. 14(a)). Upon approaching the Hamiltonian limit, $\gamma \rightarrow 0$, the points where $\mathbf{J} = 0$ shift from $\theta = 0, \pi$ to $\theta = \pm\pi/2$, where the symmetry $\hat{\mathbf{S}}_t$ is restored again (thin lines in Fig. 14(a)). In the underdamped regime, the asymptotic current can be approximated with the target function

$$J_\alpha \propto J_\alpha^0 \sin[\theta - \theta_0^\alpha(\gamma)], \quad \alpha = \{x, y\}. \quad (98)$$

Table 3

(Color online) Conditions for the rotational symmetries, Eqs. (95)–(97), to hold for the two-dimensional ratchet with additive driving, Eq. (91). Asterisk indicates that one of the symmetries $\hat{\mathbf{R}}_{x,y}$, Eq. (97), holds when the potential $V(x, y)$ is symmetric with respect to the relevant variable, x or y . Tornado icon indicates the cases when all symmetries are broken and the nonzero rotational current, Eq. (94), can be expected. Note that any other combination, not included in the tables, corresponds to the case when all the symmetries are broken.

	HAMILTONIAN				DISSIPATIVE			
	$\gamma = 0, m > 0$				$\gamma, m > 0$			
E_P	$\hat{\mathbf{R}}_P$				$\hat{\mathbf{R}}_P$			
E_s	$\hat{\mathbf{R}}_t^+$	$\hat{\mathbf{R}}_t^+$	$\hat{\mathbf{R}}_t^+$	$\hat{\mathbf{R}}_t^+$				
E_a		$\hat{\mathbf{R}}_t^-$						
E_{sh}		$\hat{\mathbf{R}}_{x,y}^*$				$\hat{\mathbf{R}}_{x,y}^*$		
	V_P	V_s	V_a	V_{sh}	V_P	V_s	V_a	V_{sh}

	OVERDAMPED			
	$\gamma > 0, m = 0$			
E_P	$\hat{\mathbf{R}}_P$			
E_s			$\hat{\mathbf{R}}_t^-$	
E_a				$\hat{\mathbf{R}}_t^-$
E_{sh}		$\hat{\mathbf{R}}_{x,y}^*$		
	V_P	V_s	V_a	V_{sh}

The phase lag is equal to $\theta_0^{x,y} = \pi/2$ in the Hamiltonian limit and $\theta_0^{x,y} = 0, \pm\pi$ in the overdamped limit, respectively, cf. Fig. 14(b).

The realization of the current direction control is presented with Fig. 15. For the system given by Eqs. (91)–(93) with $E_x^{(2)} = E_y^{(1)} = 0, \theta_y = 0$, the symmetry $\hat{\mathbf{S}}_x[0, \pi]$ implies that the current along the x -direction is absent, $J_x = 0$, and the directed transport is happening along the y -axis only, see Fig. 15, curve (i).

To illustrate the control of the rotational current, we use the tilting setup with the following potential and drive functions:

$$V(x, y) = [-3(\cos x + \cos y) + \cos x \cos y]/2, \quad (99)$$

$$E_x(t) = E_x^{(1)} \cos t, \quad E_y(t) = E_y^{(1)} \cos(t + \theta). \quad (100)$$

We have numerically integrated the corresponding stochastic equations of motions, Eq. (79), and averaged the results over $N = 10^5$ different realizations. Fig. 16 shows the dependence of the rotational current (94) on the relative phase θ . The system is invariant under the transformation $\hat{\mathbf{S}}_r$, therefore the directed current is absent, $\mathbf{J} = 0$. However, for the underdamped case, $\gamma \neq 0$, all the relevant symmetries, Eqs. (95)–(97), are violated, and the resulting rotational current (94) is nonzero. Note that the symmetry $\hat{\mathbf{R}}_t$ is restored when $\theta = 0, \pm\pi$, thus the current disappears in the Hamiltonian and overdamped limits for these values of θ . The right inset in Fig. 16 shows a single stochastic trajectory, which shows how the particle is acquiring an average nonzero angular momentum.

The overdamped limit, $m = 0$, is singular for the function (94) since the velocity of a Brownian particle, $\dot{\mathbf{r}}(t)$, is a nowhere differentiable function. The overdamped limit can be approached by increasing γ at a fixed $m = 1$. Numerical simulations show that when $\gamma/m \geq 5$ the rotational current completely reflects the symmetries corresponding to the overdamped case, see the dependence $\theta_0(\gamma)$ depicted in Fig. 16(b).

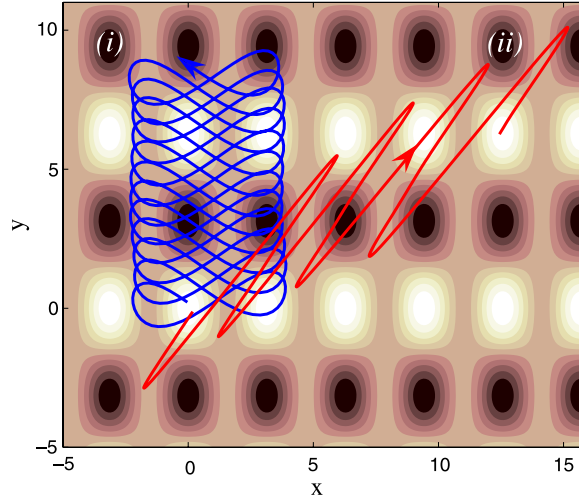


Fig. 15. (Color online) Time evolution of the mean particle positions $\bar{\mathbf{r}}(t) = \int \mathbf{r} \mathcal{F}_A(\mathbf{r}, \mathbf{v}, t) d\mathbf{r} d\mathbf{v}$, for the system given by Eqs. (91)–(93). The trajectories are superimposed on the contour plot of the potential (92). Curve (i) corresponds to the parameters $E_x^{(1)} = 3$, $E_x^{(2)} = E_y^{(1)} = 0$, $E_y^{(2)} = 3.5$, $\theta_y = 0$, and curve (ii) to the set of parameters of Fig. 14(a). Both trajectories were obtained by averaging over 10^6 independent realizations. The other parameters are $D = m = 1$, $\gamma = 0.1$.
Source: Adapted from Ref. [95].

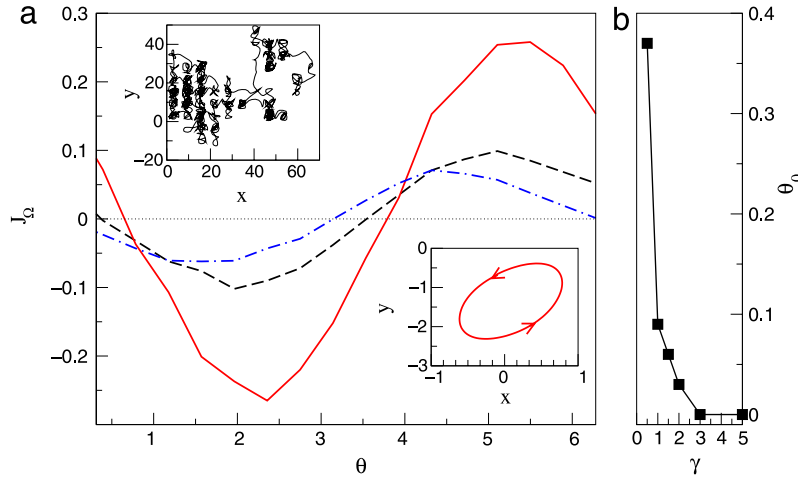


Fig. 16. (Color online) (a) Dependence $J_\Omega(\theta)$, Eq. (94), for (79), (99)–(100), with $m = 1$, $D = 0.5$, $E_x^{(1)} = 0.4$, $E_y^{(1)} = 0.8$ and $\gamma = 0.2$ (solid line), $\gamma = 0.05$ (dashed line), and $\gamma = 2$ (dashed–dotted line). Insets: the trajectory (left inset) and the corresponding attractor solution, $\bar{\mathbf{r}}(t)$, (right inset) for the case $\gamma = 0.2$ and $\theta = \pi/2$. We performed an averaging over $N = 10^5$ independent stochastic realizations in order to obtain the attractor. (b) The phase lag for the rotational current θ_0 as a function of the dissipation strength γ .
Source: Adapted from Ref. [95].

We did not address the exact Hamiltonian limit, $\gamma = 0$, here. The phase–space dimension of the system (79) equals five for $d = 2$ and seven for $d = 3$. At the same time invariant tori have the dimension three for $d = 2$ and four for $d = 3$ [20]. It is known that there are no topological constraints on the Hamiltonian evolution in such cases [96,97]. Already in the $2d$ case, the Hamiltonian dynamics of an ac-driven particle, even initiated within the region of low kinetic energy, is not restricted to a finite-volume chaotic manifold [97,96]. Therefore, an unbounded, possibly very slow, diffusion in the momentum subspace may take place [96,98,99]. Direct numerical integrations of the equations of motion are not very conclusive since the time scale of the momentum diffusion could be huge [99]. The sum rule [32] also does not apply here because of the absence of compact invariant manifold over which the system can self-average itself. The relevant phase space structures and the evolution of ac-driven 2- and 3-d Hamiltonian systems are less explored up to date [99,100], and effects caused by symmetry breaking in such systems certainly deserves further studies.¹⁴

To conclude this section, we briefly overview other existing models. The case of two-dimensional stochastic rocking ratchets under the influence of a colored noise has been studied in Ref. [102]. Since equivalent, in a statistical sense, colored noises, $\zeta_x(t)$ and $\zeta_y(t)$, have been used as driving forces, the symmetry $\hat{\mathbf{R}}_P$ (96) can be violated only by an asymmetric potential. Yet all potentials considered in Ref. [102] were invariant under the permutation transformation \hat{P} . As

¹⁴ Here recent computational advances could be of help [101].

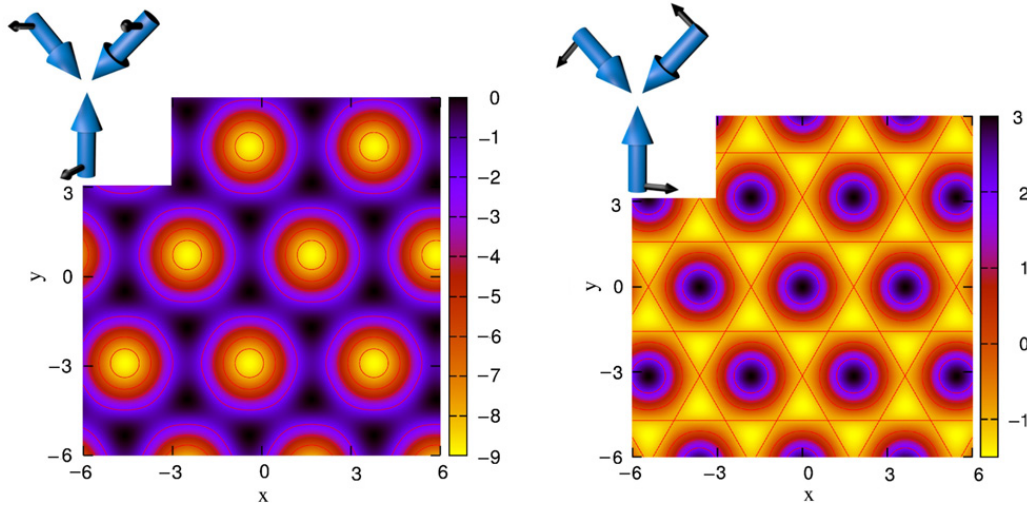


Fig. 17. Three-beam configurations and the corresponding two-dimensional optical potentials. Big blue arrows indicate the directions of the beam wave-vectors while the small black arrows denote the polarization of the beams. In both cases the beams are confined to x - y plane. When the polarization vectors point in the z -direction, the corresponding optical potential appears as a triangular lattice. When the polarization vectors span x - y plane in (counter) clockwise manner, the resulting potential takes form of a hexagonal honeycomb lattice. (For interpretation of the references to color in this figure legend, the reader is referred to the web version of this article.)

a consequence, vortex structures for the velocity field presented in Ref. [102] are completely symmetric (clockwise vortices are mapped into counterclockwise ones by \hat{P}) and, therefore, the average rotation for any trajectory would be equal to zero.

There are some studies of directed motion of particles, both quantum and classical, in two-dimensional arrays of asymmetric scatterers [103,104]. The symmetries were broken along one direction only. Naturally, a directed current occurred in the direction with broken symmetries. In the series of papers [105–109], particle transport in periodic arrays of scattering semi-disks and obstacles, under the additional influence of an ac-drive of zero mean, has been considered. It has been shown that by tuning the polarization direction of the ac drive it was possible to change the direction of the current. In the papers [110–112] the dynamics of colloidal suspensions of ferromagnetic particles, placed in an external time-periodic magnetic field has been studied. It was shown, both theoretically [111,112] and experimentally [110], that due to the symmetry breaking induced by the shape of the time-dependent magnetic field, particles perform directed rotations. These rotations cause a non-zero macroscopic torque of the carrier liquid, which effect was measured in experiment [110].

Finally, in Ref. [113] evolution of electrons in spatially elongated quantum dots, modeled either by a elliptically-symmetric single-well potential or by the Bunimovich stadium, under the influence of a linearly polarized microwave radiation was studied. The radiation field plays the role of ac drive, $\mathbf{E}(t) = \{E_x(t), E_y(t)\} = \{A \cos \varphi, A \sin \varphi\} \cos \omega t$, with the angle φ describing the polarization with respect to the symmetry axis of the dot. Note, that such a system lacks spatial periodicity, and, therefore does not fall into the class of directed transport models, described by Eq. (79). However, it supports unidirectional rotation of electrons due to the symmetry breaking of the rotational transport component, induced by the field when its direction does not coincide with the symmetry axes of the stadium, e.g. $\varphi \neq 0, \pi/2$. As a result, a non-zero magnetization, caused by the unidirectional rotations, appears.

4.3. Experiments with cold atoms

The creation of two- and three-dimensional optical potentials is a well-developed procedure in experimental physics of cold atoms, and since the late 1990s it is routinely performed in many laboratories [14,114]. The corresponding technique is based on an extension of the idea used to create one-dimensional optical potentials, see Section 3.7. An atom is immersed into an electromagnetic field, created by N lasers of the same wavelength, $\lambda = 2\pi/\omega_L$,

$$\mathbf{E}(\mathbf{r}, t) = \sum_{j=1}^N E_j^0 \mathbf{e}_j \text{Re}\{\exp[-i(\omega_L t - \mathbf{k}_j \cdot \mathbf{r} - \phi_j)]\}, \quad (101)$$

where E_j^0 , \mathbf{e}_j , \mathbf{k}_j are the intensity, polarization vector and wave-vector of the j th beam. The electric dipole interaction between the atom and the field lead to the creation of a spatially-dependent potential,

$$V(\mathbf{r}) \propto \overline{\mathbf{E}^2(\mathbf{r}, \phi_j)}, \quad (102)$$

where $\overline{\dots}$ stands for the averaging over the fast phase $\omega_L t$. Three laser beams of equal intensities are already enough to create two-dimensional periodic potentials of tunable topology and strength [14]. Two most popular set-ups are shown in Fig. 17. In both cases beams intersect in the x - y plane at an angle of 120° to each other. When the polarization vectors of

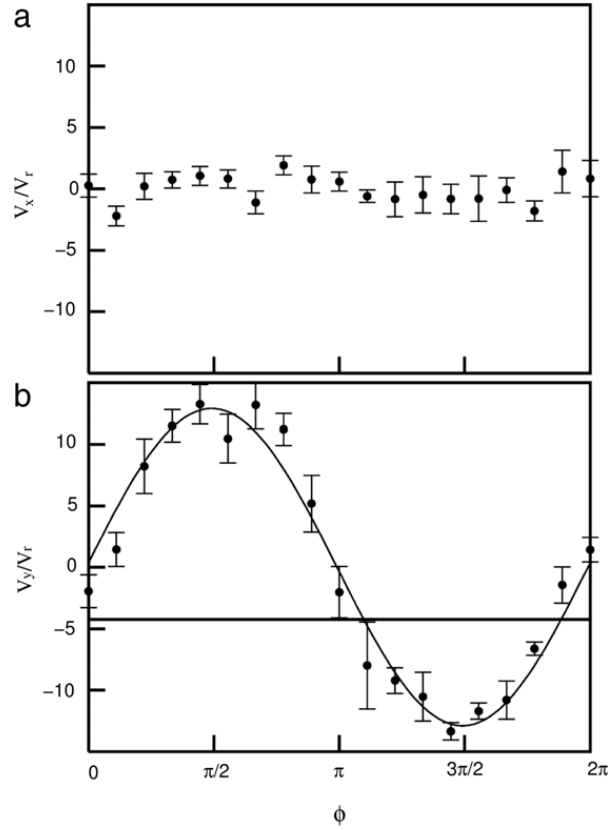


Fig. 18. Components of the average velocity of the atomic cloud center of mass as a function of θ_y (denoted by ϕ here) measured in experiments with a two-dimensional optical rocking ratchet-like potential, Eqs. (91), (93), and cold cesium atoms. The driving vector has components $E_x^{(2)} = E_y^{(1)} = 0$. The solid line is a fit of the data with the function $v_y = v_{\max} \sin(\theta + \theta_0)$.
Source: Adapted from Ref. [94].

the beams (black arrows) point along the z -direction, the resulting potential forms a triangular optical lattice,¹⁵ left panel of Fig. 17. When the beams are polarized in the x - y plane, in a clockwise or counter-clockwise manner, a hexagonal potential appears [114], right panel of Fig. 17. The relative beam phases ϕ_j are key parameters. For a three-beam setup, the number of relative phases is two, i.e. $\phi_1 - \phi_2$ and $\phi_2 - \phi_3$. The number of independent space translations for a 2-d periodic potential is also two. Hence, variations of the phases can only induce a global shift of the potential but cannot change the potential topography [14]. Therefore one can realize a two-dimensional rocking ratchet, Eq. (91). Namely, periodic modulations of the relative phases allows to introduce rocking forces, both in x and y directions, in a controllable manner. The idea is similar to that used for the experimental realization 1-d cold atom ratchets, Section 3.7: by shaking the potential with a time-periodic phase, $a_\alpha(t + T) = a_\alpha(t)$, $\alpha = \{x, y\}$, one introduces a rocking force along the α -direction, $f_\alpha(t) \propto \ddot{a}_\alpha(t)$, in the co-moving frame, $\tilde{\alpha} = \alpha - a_\alpha(t)$. The asymptotic current is the same in both frames, laboratory and co-moving, $J_{\tilde{\alpha}} = J_\alpha$. In an experiment, the relative phases can be controlled by using three acousto-optical modulators [14].

This idea has been realized by the group of F. Renzoni [94]. The driving vector was of the standard bi-harmonic form, Eq. (93), with amplitudes $E_{x,y}^{(1,2)}$ and phases $\theta_{x,y}$ as tunable parameters. An optical potential $V(x, y)$ of the hexagonal topology, right panel of Fig. 17, was used in the experiments. The potential is symmetric in both direction, x and y . For the driving vector with $E_x^{(2)} = E_y^{(1)} = 0$, symmetry $\hat{\mathbf{S}}_x[\mathbf{0}, \pi]$, Eq. (90), forbids directed current in the x -direction. In the Hamiltonian limit, transport of atoms along the y -direction is controlled by the symmetry $\hat{\mathbf{S}}_t[\mathbf{0}, \pi]$, such that $J_y = 0$ whenever $\theta_y = 0, \pm\pi$. The experimental results shown in Fig. 18 perfectly followed the prediction of the symmetry analysis.

A more subtle control of the current direction was realized by using the following idea. Consider a bi-harmonic drive vector (93) with phases $\theta_{x,y} = \pi/2$ and fixed ratios between the harmonic amplitudes, $E_x^{(1)}/E_x^{(2)} = E_y^{(1)}/E_y^{(2)} = 3/4$. This setup breaks all relevant symmetries and therefore a directed current should appear. The only control parameter left is the ratio between the harmonic amplitudes in mutually orthogonal directions, $q = E_x^{(1)}/E_x^{(2)}$. By tuning q to zero (infinity) it was possible to direct the current along the $x(y)$ -direction. Intermediate values of q correspond to the atomic transport along diagonal directions, see Fig. 19. Note that both transport modes, along x and y directions, are not independent but dynamically coupled. Therefore the overall two-dimensional transport cannot be considered as a ‘product’ of two mutually independent, one-dimensional rectification processes.

¹⁵ The topography of a potential is defined by the structure of the potential minima.

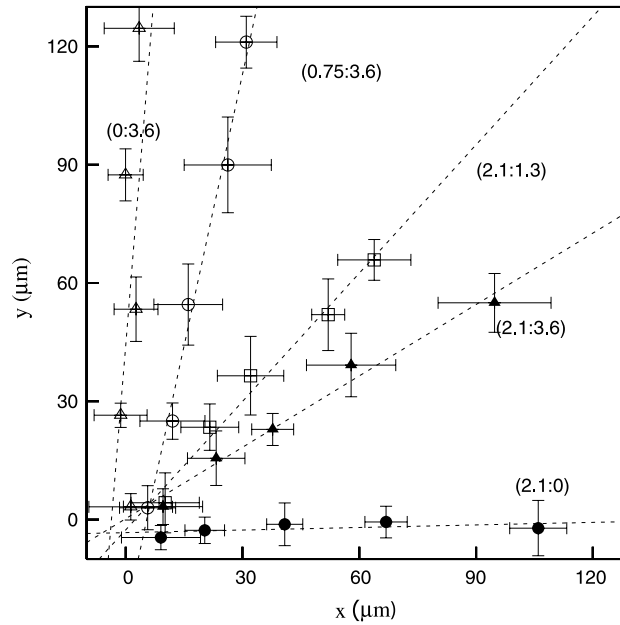


Fig. 19. Performance of a two-dimensional cold atom rocking ratchet, Eqs. (91), (93). The plot shows positions of the atomic cloud center-of-mass at different instants of time. The different data sets correspond to different ratios between the driving amplitudes, $q = E_x^{(1)} : E_x^{(2)}$. Points were obtained by taking fluorescence images of the atomic cloud, see Fig. 8, at intervals of 0.5 ms. The lines are the best fits of the data with linear functions $y = (v_y/v_x)x$. Source: Adapted from Ref. [94].

Realizations of a peculiar ratchet-like mechanism with cold atoms moving in two- and three-dimensional optical lattices were reported in Ref. [115]. There were no ac-driving forces, and the rectification effect appeared due to decoherence-induced transitions of atoms between two different optical potentials. If the optical potentials were shifted in such a way that their relative phases in x , y and z -directions were different from $k\pi$, $k = 0, \pm 1$, the presence of an optical pumping mechanism, which induces transitions of atoms between potentials, led to the appearance of a net motion of the atomic cloud. By tuning the relative phases, it was possible to shuttle atoms into desirable directions.

5. Quantum ratchets

Experimental realizations of ac-driven ratchets with cold atoms discussed in the previous two sections [49,38,39,50,94] are in a good agreement with the numerical results obtained for the classical models. There are two key factors responsible for this accordance. First of all, it is the initial state of the atomic cloud used in experiments, namely its temperature. The de Broglie wavelength of a cesium atom at the temperature of the order of tens μK is of the order of 10 nm while the spatial period of the optical potentials L is of the order of μm . The atom therefore can be well approximated by a point-like particle. Even at several μK the corresponding de Broglie wavelength is of the order of 100 nm, which is still smaller than L . Only by cooling atoms down to nK temperatures, i.e. by entering into the Bose–Einstein condensation regime, one could get atomic wavelengths of the order of ten μm , which are now larger than the potential period. Below this temperature atoms start behave themselves as genuine quantum objects. At the same time the kinetic energy of the atom becomes of the order of the recoil energy $E_R = \hbar^2 k_L^2 / 2m$, which means that the atom evolves within the potential range and feels the potential shape. Last but not least factor responsible for downgrading the atomic evolution to the classical limit was the decoherence [39]. Strong interaction between the laser field and atoms induced a chain of stochastic adsorption/emission events with a characteristic rate comparable to the period of the driving which process destroyed the coherence of the quantum evolution.

Therefore, there are two conditions which have to be respected in order to grasp quantum ratchets in experiment. First, the atomic cloud has to be cooled down to the BEC-transition temperature so that the distribution of the atom momenta is narrow with respect to the energy scale set by the potential height, and the atomic de Broglie wavelength becomes of the order (or even larger than) the optical potential period L . After that the tunneling between potential wells becomes essential and starts contribute to the transport process. Second, a further detuning of the optical potential is needed [16] in order to make decoherence effects negligible on the time scale of experiment.

Both demands are within the reach of modern ultra-cold atom optics [15], and the creation of an atomic Bose–Einstein condensates (BECs) followed by the consecutive loading of the BEC into an optical confinement, is an almost everyday routine in many laboratories across the world. Quite naturally, a realization of ac-driven coherent quantum ratchets was reported in 2009 [47].

In this section we present an extension of the symmetry-analysis to the case of coherent quantum ratchets [116], outline the peculiarities of the quantum rectification process, and review the first experimental realizations of a multiplicative quantum ratchet with a Bose–Einstein condensate of rubidium atoms [47].

5.1. Symmetry analysis

We start with a quantum particle moving in a time and space periodic potential. The Hamiltonian is

$$H(\hat{x}, \hat{p}, t) = \frac{\hat{p}^2}{2} + V(\hat{x}, t), \quad (103)$$

where $V(\hat{x}, t) = V(\hat{x} + \hat{L}, t) = V(\hat{x}, t + T)$, and \hat{L} is the translation operator over the distance L . The corresponding Schrödinger equation reads

$$i\hbar \frac{\partial}{\partial t} |\psi(t)\rangle = H(t) |\psi(t)\rangle. \quad (104)$$

The Hamiltonian (103) is formally identical to its classical version, with the only difference that the position and momentum are operators now not numbers. Despite this similarity, there are two technical issues that make the symmetry analysis in the quantum case different from the previous classical case.

The first issue concerns the definition of the quantum current. It is not a variable of the equation of motion like in the classical limit but an expectation value of a certain operator. Namely, the current for a given initial wave function is quantified through the instantaneous momentum expectation value,

$$J(t; t_0) = \frac{1}{m} \langle \psi(t, t_0) | \hat{p} | \psi(t, t_0) \rangle. \quad (105)$$

Second, the evolution of the quantum system is governed by the equation which includes the potential $V(\hat{x}, t + T)$ while the evolution of the classical system is governed by Eq. (16) that has a force as an input, i.e. the derivative of the potential $g(x, t) = -\partial_x V(x, t)$. In the case of a multiplicative setup, Eq. (37), both functions, potential and force, are time- and space-periodic. So are the corresponding equations of motion, and there is no visible difference with respect to the symmetry analysis. However, in the case of additive setup, Eq. (34), where the classical force function is time-space periodic, the original potential,

$$V(\hat{x}, t) = V(\hat{x}) - \hat{x}E(t), \quad (106)$$

is not. This problem can be resolved by resorting to a gauge transformation [117], $|\psi\rangle \rightarrow \exp(-\frac{i}{\hbar} \hat{x} \int_{t_0}^t E(t') dt') |\psi\rangle$, which yields a new Hamiltonian,

$$H(\hat{x}, \hat{p}, t) = \frac{[\hat{p} - A(t; t_0)]^2}{2} + V(\hat{x}). \quad (107)$$

The new momentum operator is time-dependent now, $\hat{p} = \hat{p} + A(t; t_0)$, with a time-periodic vector potential, $A(t; t_0) = A(t + T; t_0) = -\int_{t_0}^t E(t') dt' + A(t_0)$ where the constant $A(t_0)$ is chosen such that the time average of $A(t)$ over one temporal period of the drive vanishes. Since the vector potential is of zero mean, the time averaged expectation values of the momentum operators, \hat{p} and $\hat{\tilde{p}}$, are identical. Note the explicit parametric dependence of the vector potential on the parameter t_0 ('starting time' henceforth) which determines the initial phase of the driving field, $E(t_0)$. As we will show, this parameter plays an important role in the dynamics of coherent quantum ratchets.

The solution of the Schrödinger Eq. (104) for a given initial state $|\psi(t_0)\rangle$ can be formally written as $|\psi(t + t_0)\rangle = U(t, t_0) |\psi(t_0)\rangle$, where $U(t, t_0)$ is the propagation or evolution operator. Hamiltonian (103) is periodic in time with period T , and the system evolution can be evaluated by using eigenfunctions of the Floquet operator, $U(T, t_0)$, which propagates the system over one period of the driving, $|\psi_\alpha(t)\rangle = e^{-i\frac{E_\alpha}{\hbar}t} |\phi_\alpha(t)\rangle$, $|\phi_\alpha(t + T)\rangle = |\phi_\alpha(t)\rangle$ [118–120]. The eigenfunctions can be obtained by solving the eigenvalue problem for the Floquet operator,

$$U(T, t_0) |\phi_\alpha(t_0)\rangle = e^{-iE_\alpha T/\hbar} |\phi_\alpha(t_0)\rangle, \quad (108)$$

with the eigenvalues $e^{-iE_\alpha T/\hbar}$. Their phase are known as quasienergies, $E_\alpha \in [-\hbar\omega/2, \hbar\omega/2]$. When $\hbar \ll 1$, Floquet states of the quantum system can be associated with different invariant manifolds of its classical version, see Fig. 20.

The set of Floquet states, $\{|\phi_\alpha(t)\rangle\}$, forms a complete orthonormal basis and the state of the quantum system at any instant of time is

$$|\psi(t; t_0)\rangle = \sum_{\alpha} C_{\alpha}(t_0) e^{-iE_{\alpha}t/\hbar} |\phi_{\alpha}(t_0 + t)\rangle, \quad (109)$$

where the coefficients $\{C_{\alpha}(t_0)\}$ are given by the expansion of the initial state over the Floquet basis,

$$|\psi(t_0)\rangle = \sum_{\alpha} C_{\alpha}(t_0) |\phi_{\alpha}(t_0)\rangle. \quad (110)$$

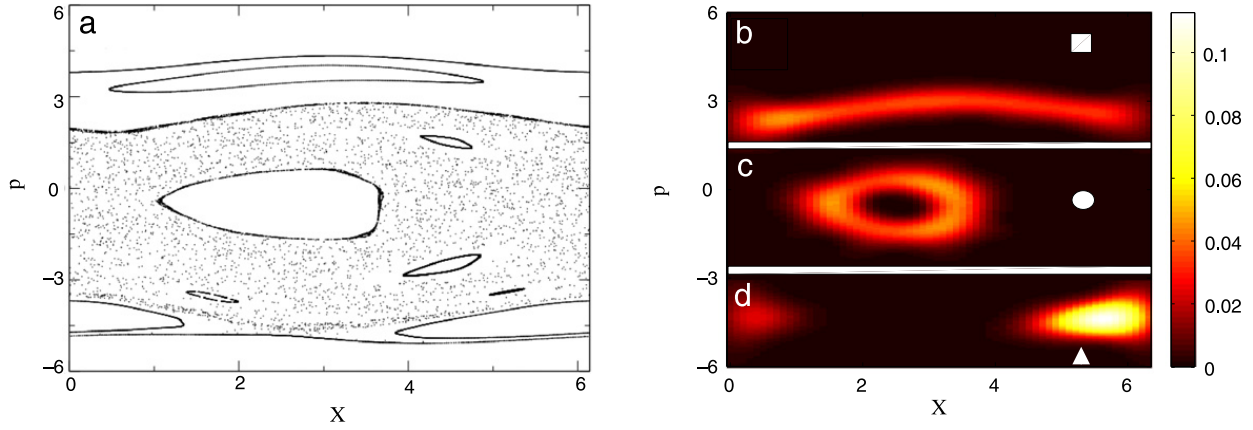


Fig. 20. (Color online) (a) Poincaré section of the Hamiltonian system (122), (123) in the classical limit and (b–d) Husimi distributions [121] of different Floquet states of the quantum version, $\hbar = 0.2$. The parameters are $E_1 = E_2 = 2$, $\omega = 2$, $\theta = -\pi/2$ and $t_0 = 0$. Source: Adapted from Ref. [116].

The expansion coefficients explicitly depend on t_0 so that even when the shape of the initial wave function, $|\psi(t_0)\rangle$, is fixed, the expansion over the Floquet basis still depends on the starting time. This is because Floquet states, although retaining their initial shapes after one round of the driving, are time-dependent vectors. Due to the discrete translational invariance of the Hamiltonian in x -space, all Floquet states can be arranged into subsets, characterized by different values of quasimomentum κ : $|\phi_\alpha(x + 2\pi)\rangle = e^{i\hbar\kappa} |\phi_\alpha(x)\rangle$, $\kappa \in [-\pi/L, \pi/L]$. The quasimomentum subspaces are invariant under the evolution of the Schrödinger equation.

We start the analysis with the case $\kappa = 0$ (the general case $\kappa \neq 0$ will be considered later on). The case of zero quasimomentum corresponds either to (i) an initial state which was uniformly smeared over the whole, strictly speaking, infinite potential $U(x, t = t_0)$ or (ii) to the case when the evolution of the system is confined a potential in a form of a ring of the length L . The first situation can be well approximated with an initial cloud of atoms distributed over a distance much larger than the spatial period of the potential.

Consider now transport properties of Floquet states. Similar to the invariant manifolds of classical deterministic systems, every Floquet state can be labeled by its averaged velocity, $\bar{v}_\alpha = (1/mT) \int_0^T p_\alpha(t) dt$, where $p_\alpha(t) = \langle \phi_\alpha(t) | \hat{p} | \phi_\alpha(t) \rangle$. Combining this definition with Eqs. (105) and (109), we arrive at the following expression for the current,

$$J(t; t_0) = \frac{1}{m} \sum_{\alpha, \alpha'} C_\alpha(t_0) C_{\alpha'}^*(t_0) e^{-i(E_\alpha - E_{\alpha'})t/\hbar} \langle \phi_{\alpha'}(t + t_0) | \hat{p} | \phi_\alpha(t + t_0) \rangle. \quad (111)$$

It can be represented as the sum of diagonal and off-diagonal contributions,

$$J(t; t_0) = \frac{1}{m} \sum_{\alpha} |C_\alpha(t_0)|^2 p_\alpha(t + t_0) + \frac{1}{m} \sum_{\alpha \neq \alpha'} C_\alpha(t_0) C_{\alpha'}^*(t_0) e^{-i(E_\alpha - E_{\alpha'})t/\hbar} \langle \phi_{\alpha'}(t + t_0) | \hat{p} | \phi_\alpha(t + t_0) \rangle. \quad (112)$$

Now we turn to the asymptotic averaged current,

$$\tilde{J}(t_0) = \lim_{t \rightarrow \infty} \frac{1}{t} \int_{t_0}^t J(\tau; t_0) d\tau. \quad (113)$$

We assume that the quasienergy spectrum of the system has no degeneracies, i.e. there are no pairs $\{\alpha, \alpha' \neq \alpha\}$ such that $E_\alpha = E_{\alpha'}$. This is a well-justified assumption supported by the extension of the von Neumann–Wigner theorem [122] to the case of periodically modulated Hamiltonians.¹⁶

Note that heretofore we consider the case of vanishing quasimomentum $\kappa = 0$ only. The symmetry action is more involved for nonzero quasimomentum, and this case will be addressed later on. The immediate consequence of this assumption is that as time grows, all interference terms collected into the second sum on the rhs of Eq. (112) are averaging themselves out. Thus, in the asymptotic limit $t \rightarrow \infty$, the diagonal part is only left,

$$\tilde{J}(t_0) = \sum_{\alpha} |C_\alpha(t_0)|^2 v_\alpha. \quad (114)$$

This result demarcates coherent quantum Hamiltonian ratchets from their classical counterparts in a clear-cut manner. While it was possible to assign a unique current value to the chaotic layer of the classical Hamiltonian ratchet, $J = v_{ch}$,

¹⁶ Nodgeneracy can be absent in some specific models, e.g. when the dynamics of a quantum ratchet is restricted to several *fixed* bands, with an enforced crossing between a pair of them [123,124].

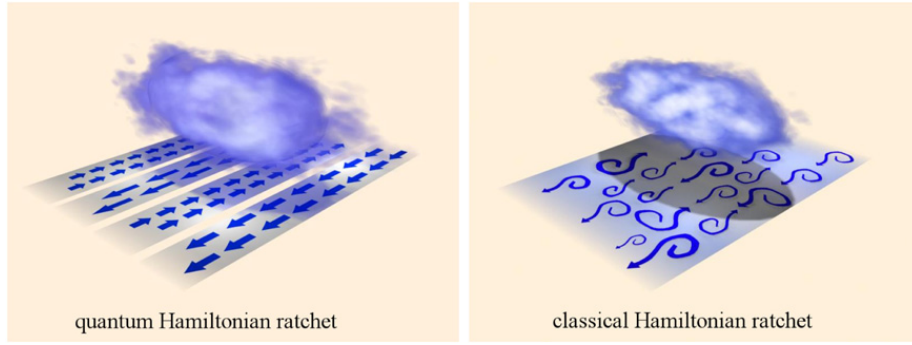


Fig. 21. (Color online) Performance of a quantum (left) and classical (right) Hamiltonian ratchets. In the quantum limit an ac-driven ratchet can be represented as a set of conveyor belts (Floquet states), each moving with a constant velocity. The asymptotic current, Eq. (114), depends on the way an initial wave packet is distributed among the belts. The asymptotic current in the chaotic layer of a classical Hamiltonian ratchet is of the same value for all initial conditions chosen within the layer, see Eq. (47).

see also Eq. (47), it is impossible to do so in the quantum limit. The stochasticity, which takes care of erasing memory on initial conditions and induces averaging over the chaotic region, is absent in the quantum world. The evolution of a coherent quantum system is governed by the linear equation, Eq. (104), so that the system keeps memory on its initial state imprinted into the set of coefficients $C_\alpha(t_0)$. Even in the asymptotic limit, the quantum ratchet current still depends not only on the shape of the initial wave function but also on the starting time t_0 , because of the explicit time-dependence of the Floquet basis. A quantum coherent ratchet can be thought as a set of moving conveyor belts – the Floquet states – and a cloud – the initial wave packet – is distributed among them so that every belt gets a certain load, see Fig. 21(a). The total current, Eq. (114), is a sum of the belt velocities weighted with the corresponding loads. A classical Hamiltonian ratchet can be thought of as a turbulent stream, which drags all particles with the same average velocity, v_{ch} , independently of their initial positions, see Fig. 21b. The same picture holds true when the classical system is coupled to a heat bath. The asymptotic solution of the corresponding Fokker–Planck equation, Eq. (64) or Eq. (65), consists of a single Floquet state only, $P_A(\dots, t) = P_A(\dots, t + T)$. All the other Floquet states have multipliers with nonzero imaginary parts and therefore die out in the course of time [79]. The asymptotic current does not depend on initial conditions in this case as well.

Having now the definition of the quantum current, we can turn to the symmetry analysis. Remarkably, the relevant symmetries are similar to the classical case [116,125]. Namely, there are two basic symmetries, Eq. (104),

$$\hat{S}_x[\hat{\chi}, \tau] : \{\hat{x}, \hat{p}, t\} \rightarrow \{-\hat{x} + \hat{\chi}, -\hat{p}, t + \tau\}, \quad (115)$$

and

$$\hat{S}_t[\hat{\chi}, \tau] : \{\hat{x}, \hat{p}, t\} \rightarrow \{\hat{x} + \hat{\chi}, -\hat{p}, -t + \tau\}, \quad (116)$$

where $\hat{\chi}$ is the translational operator over the distance χ . However, the ways the symmetries affect the system dynamics in the quantum limit are very different from how they realized themselves in classical ratchets. A symmetry, when present, is imprinted in the corresponding Floquet operator, $U(T, t_0)$, and thus influences transport properties of its eigenstates [116].

The presence of symmetry \hat{S}_x , also called ‘generalized parity’ [120], implies that the corresponding Floquet states obey:

$$|\phi_\alpha(-x, t)\rangle = \sigma_\alpha |\phi_\alpha(x, t + \tau)\rangle, \quad (117)$$

where $\sigma_\alpha = \pm 1$. The space reversal changes the sign of the momentum operator, $\hat{p} = -i\hbar\partial/\partial x$. The expectation values of the instantaneous velocity of a Floquet state at instants of times separated by τ are symmetry related, $v_\alpha(t) = -v_\alpha(t + \tau)$. Therefore, the average velocity, \bar{v}_α , of any Floquet state is equal to zero.

The symmetry \hat{S}_t involves complex conjugation and the Floquet states of the corresponding system obey:

$$|\phi_\alpha(x, T - t)\rangle = \sigma_\alpha |\phi_\alpha^*(x, t)\rangle. \quad (118)$$

Because of the complex conjugation operation, the momentum operator, $\hat{p} = -i\hbar\partial/\partial x$, changes its sign under the symmetry transformation. From Eq. (118) it follows that $v_\alpha(t) = -v_\alpha(T - t)$, so that the average velocity of any Floquet state is again zero, $\bar{v}_\alpha = 0$.

When all Floquet states are non-transporting, the asymptotic average current (114) vanishes for any initial wave function $\psi(t_0)$ and any choice of starting time t_0 .¹⁷ However, the transient, finite-time current $\tilde{J}(t, t_0) = 1/t \int_{t_0}^t J(\tau; t_0) d\tau$ can still be detected – even when one of the symmetries is present. It is the result of the interference between different Floquet states, see the second sum on the rhs of Eq. (112). The transient time depends on the values of the terms $\langle \phi_{\alpha'}(t) | \hat{p} | \phi_\alpha(t) \rangle$ and the

¹⁷ Note that heretofore we consider the case of vanishing quasimomentum $\kappa = 0$ only. The symmetry action is more involved for nonzero quasimomentum, and this case will be addressed later on.

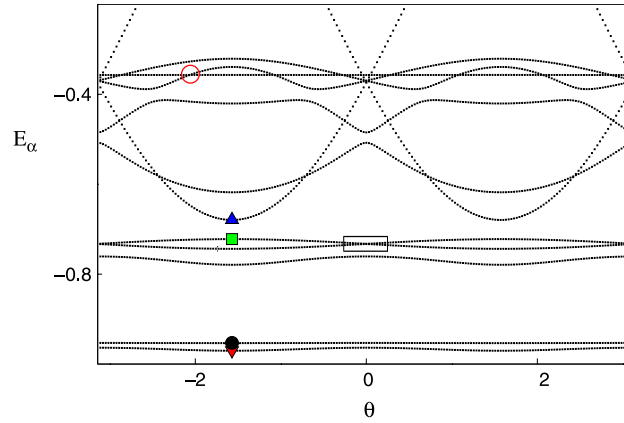


Fig. 22. (Color online) A part of the quasienergy spectrum vs. θ . The symbols indicate the corresponding Floquet states shown in Fig. 20(b–d). The empty red circle indicates an avoided crossing between two eigenstates.
Source: Adapted from Ref. [116].

statistics of the splittings, $\Delta E_{\alpha,\alpha'} = E_{\alpha} - E_{\alpha'}$. The effect can be very long-lasting in the absence of level repulsion as for the Poisson level-spacing distribution of integrable and near-integrable quantum systems [21].

Finally, we address the case of $\kappa \neq 0$ ¹⁸ [126]. In this case we deal with the set of Floquet bands $\epsilon_{\alpha}[\kappa]$, which extend over the Brillouin zone $\kappa \in [-\pi/L, \pi/L]$. By virtue of the Hellmann–Feynman theorem [119], the average velocity of the state is equal to the local slope of the corresponding Floquet band [32],

$$\bar{v}_{\alpha,\kappa} = \hbar^{-1} \frac{\partial E_{\alpha}(\kappa)}{\partial \kappa}. \quad (119)$$

The generalization of the basic symmetries is straightforward, and so we get

$$\hat{S}_x^{\kappa}[\hat{\chi}, \tau] : \{\hat{x}, \hat{p}, t, \kappa\} \rightarrow \{-\hat{x} + \hat{\chi}, -\hat{p}, t + \tau, -\kappa\}, \quad (120)$$

and

$$\hat{S}_t^{\kappa}[\hat{\chi}, \tau] : \{\hat{x}, \hat{p}, t, \kappa\} \rightarrow \{\hat{x} + \hat{\chi}, -\hat{p}, -t + \tau, -\kappa\}. \quad (121)$$

In words, both symmetries reverse quasimomentum values and map every Floquet band into itself, a negative branch onto a positive one and vice versa, $E_{\alpha}[\kappa] = E_{\alpha}[-\kappa]$. Therefore all Floquet bands are symmetric at $\kappa = 0$ when at least one of the symmetries holds. From this it immediately follows that all bands are flat at $\kappa = 0$ and the corresponding Floquet states are non-transporting. The symmetries transformations map these states onto themselves since $\kappa = -\kappa = 0$. However, a Floquet state with $\kappa \neq 0$ may possess a nonzero velocity $v_{\alpha}[\kappa]$ even in the case of symmetry (yet there is always a symmetry-related state with the opposite velocity on the same band at $\kappa' = -\kappa$). Both fundamental symmetries involve time transformations, \hat{S}_t^{κ} for sure and \hat{S}_x^{κ} in some cases. This means that even though the initial wave packet can be perfectly symmetric $\kappa = 0$, $\psi(t = 0; \kappa) = \psi(t = 0; -\kappa)$, this fact alone does not guarantee the absence of the asymptotic current in the symmetric cases. The contributions from the symmetry-related Floquet states to a symmetric wave packet are not equal in general, $C_{\alpha,-\kappa}(t_0) \neq C_{\alpha,\kappa}(t_0)$. Only the averaging over the initial phase t_0 or the presence of specific symmetry $\hat{S}_x^{\kappa}[\hat{\chi}, \tau = 0]$ can guarantee the absence of the asymptotic current.

5.2. Applications: numerical studies

We start with a quantum version of the rocking ratchet, Section 3.3.1. The potential

$$U(x) = 1 + \cos(x), \quad (122)$$

is driven by the bi-harmonic driving force,

$$E(t; t_0) = E_1 \cos(\omega[t - t_0]) + E_2 \cos(2\omega[t - t_0] + \theta). \quad (123)$$

All information on transport properties of the quantum ratchet is encoded in the eigenpectrum and eigenstates (i.e., Floquet states) of the corresponding Floquet operator, $U(T, t_0)$. The typical dependence of the quasienergies on the asymmetry parameter θ is shown in Fig. 22 [116]. The spectrum exhibits two symmetries, $E_{\alpha}(\theta) = E_{\alpha}(-\theta)$ and $E_{\alpha}(\theta) = E_{\alpha}(\theta + \pi)$, which are consequences of the bi-harmonic setup (123). While some bands show strong dependence on θ , others have

¹⁸ It is noteworthy that there was no need for that in the classical case. As long as only the averaged current is concerned, it is enough to solve the Fokker–Planck equation for the periodic boundary conditions, i.e. with $\kappa = 0$ [4].

rather flat profiles. The former host the Floquet states lying within the potential range, so the state energies $\langle\langle\phi_\alpha|H(t)|\phi_\alpha\rangle\rangle_T$ are comparable to V_0 . These states are strongly affected by the variations of θ . The latter bands bear Floquet states which either (i) have small energies and are mostly localized at the bottoms of the potential wells or (ii) have large energies and lie much above the potential. States of both kinds remain almost unaffected by variations of θ .

Fig. 20(b–d) shows Husimi distributions [121] of several Floquet states, whose quasienergies are marked by corresponding symbols in Fig. 22. For the symmetric case $\theta = 0, \pm\pi$, the set of Floquet states splits into two non-interacting symmetric and antisymmetric subsets, depending on the sign of σ_α in Eq. (115). Symmetric and antisymmetric Floquet bands alternate in the quasienergy spectrum and are separated by finite gaps.

For $\theta \neq 0, \pm\pi$, all the Floquet states become asymmetric. Upon deviation from the symmetry points, Floquet states acquire nonzero average velocities thus becoming transporting. Now one can detect a nonzero quantum current even by starting with an initial state of zero velocity. We restrict the consideration to the initial wave function in the form of a zero-momentum plane wave, $|\psi(t_0)\rangle = |0\rangle = \frac{1}{\sqrt{2\pi}}$.¹⁹ This initial state mainly overlaps with Floquet states of small kinetic energies, which in the quasiclassical limit, $\hbar \ll 1$, have their Husimi distributions localized in the chaotic layer region of the corresponding classical system. We will first discuss the results obtained for the current $J(t_0)$, Eq. (114), averaged over the starting time, $J = 1/T \int_0^T J(t_0) dt_0$, and then address the dependence of ratchet characteristics on t_0 . Fig. 23(a) shows the dependence of the average current on the phase θ . The average current J shows the expected symmetry properties, $J(\theta) = -J(\theta + \pi) = -J(-\theta)$, and looks like a smooth curve with several sharp peaks on top of it. These peaks are produced by avoided crossing (resonances) between two Floquet eigenstates, see the insets in Fig. 23(a). One state, which we denote $|1\rangle$, has relatively small kinetic energy and overlaps substantially with the initial wave function $|\psi(t_0)\rangle$. The other state, $|2\rangle$, has large kinetic energy and overlaps weakly with the initial state off the resonance point. At the resonance, these eigenstates ‘mix’ [128], see Fig. 23(b). This results in the appearance of a new hybrid shape for the state $|1\rangle$, which acquires a tangible velocity now. Its overlap with the initial state remains mostly unaffected, so the avoided crossing finally results in a strong current enhancement. This resonance-like effect can be taken as a quantum analog of the overlap between the chaotic layer and a ballistic resonance in the phase space of the classical Hamiltonian ratchet, Fig. 2(b). The width and position of the quantum resonance are tunable. By changing the amplitude of the second harmonics, E_2 , it is possible to split the resonance peak into two and then move two peaks apart [116].

Without additional averaging over the starting time, the asymptotic current depends on t_0 . However, the variation of the starting time will affect only the overlap of the Floquet states with the initial wave function. The structure of resonance peaks, being determined by avoided crossings between Floquet bands, is independent of the parameter t_0 . In Fig. 24 we show the asymptotic (however still initial-time dependent) current versus both θ and t_0 . As expected, the resonant current enhancement is present for all values of t_0 and the variations of the starting time only modify the current amplitude.

Finally, we consider a quantum ratchet with multiplicative driving [116],

$$H(x, p, t) = \frac{p^2}{2} + U(x)E(t - t_0), \quad (124)$$

where $U(x + L) = U(x)$ and $E(t + T) = E(t)$. Here, we use the potential

$$U(x) = K [\cos(x) + s \cos(2x + \phi)], \quad (125)$$

where θ is the parameter which destroys the potential symmetry away from $\theta = 0, \pm\pi$. The relevant symmetries for the classical limit of the Hamiltonian (124) are listed in Table 2, Section 3.3.2. Neither the bi-harmonic potential nor the bi-harmonic driving alone is sufficient to break both fundamental symmetries. With a single-harmonic drive symmetry \hat{S}_t survives while in the case of single-harmonic potential symmetry \hat{S}_t is still present. For the above potential we again use the function (123) for a drive, which choice ensures that for $\phi \neq 0, \pm\pi$ and $\theta \neq 0, \pm\pi$ all the relevant symmetries are violated.

Fig. 25 shows the average current J versus θ for the asymmetric potential, $\phi = -\pi/2$, at the deep quantum limit $\hbar = 1$. The current dependence possesses the symmetry $J(\theta) = -J(\theta + \pi) = -J(-\theta)$, and similar to the previously considered case of rocking quantum ratchets, we observe broad quantum resonances and a dependence of the asymptotic current on the initial time t_0 , see inset in Fig. 25(a).

5.3. Experiments with Bose–Einstein condensates

The first realization of a quantum Hamiltonian ratchet with multiplicative driving was reported in Ref. [47]. The setup used in the experiments corresponded to the model described by Eqs. (124), (125). The $\lambda/2$ spatial component of the optical potential was created by using the two counter propagating laser beams of wavelength λ , see Section 3.7. The second optical lattice with period $\lambda/4$ was realized by using dispersive properties of four-photon Raman transitions between ground state sub-levels of rubidium atoms [82,129]. Finally, the temporal modulations were induced by periodically changing the intensity of the beams. A Bose–Einstein condensate of rubidium atoms was first loaded into the optical lattice potential, and after finite-time exposition to the driving (from 26 to 100 periods of the drive function) the atoms were released and

¹⁹ One can use as the initial wave function the Bloch ground state of the undriven potential. Such a choice is relevant in the context of experiments [127].

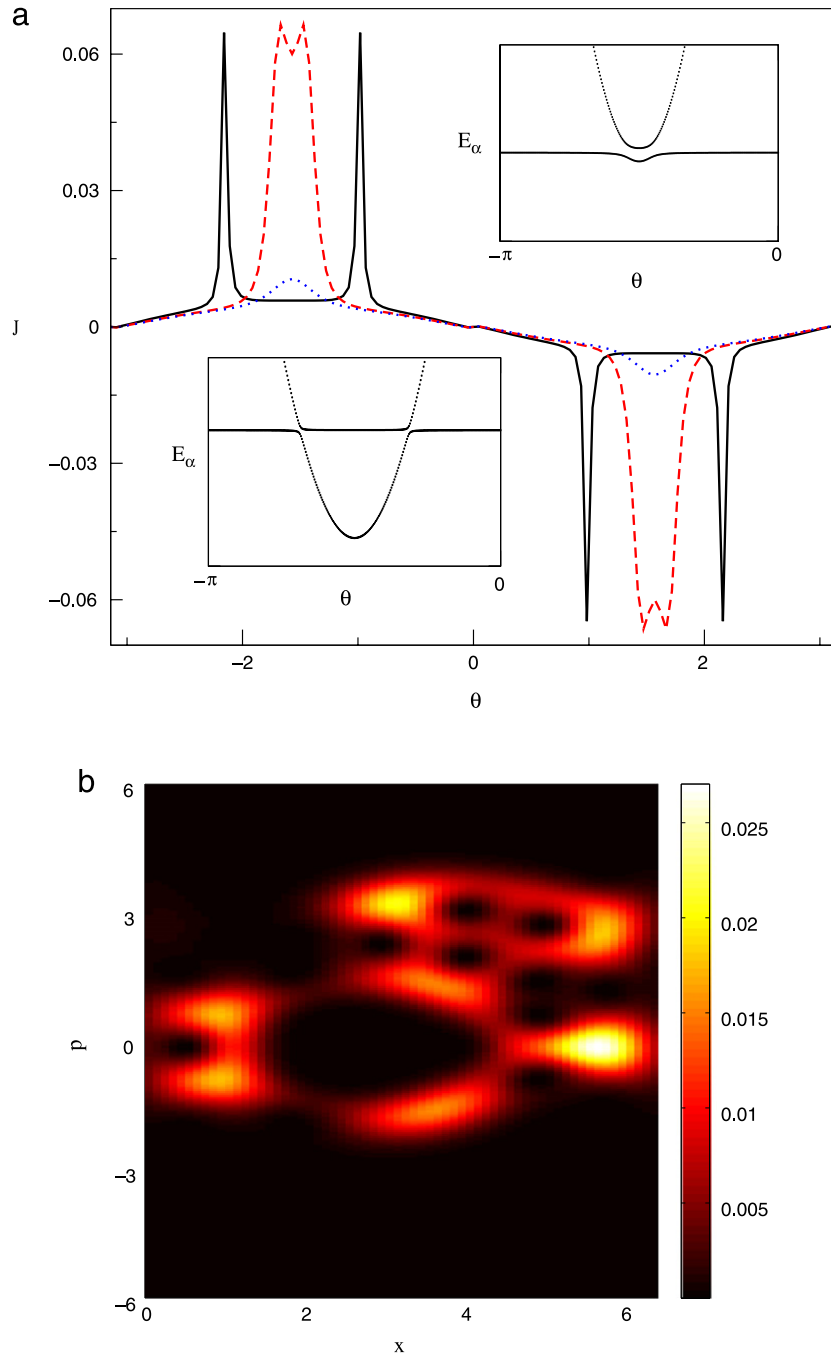


Fig. 23. (Color online) (a) The average current J (in units of the recoil momentum) vs. θ for different values of the second harmonic amplitude, E_2 : 0.95 (pointed line), 1 (dashed line) and 1.2 (solid line). Insets: the part of the quasienergy spectrum where the resonance takes place, for $E_2 = 1$ (top right) and $E_2 = 1.2$ (bottom left). The parameters are $E_1 = 3.26$ and $\omega = 3$. (b) Husimi function for the upper eigenstate that appears in (a) (top right inset) with $\theta = -\pi/2$.

Source: Adapted from Ref. [116].

freely expanded during 15 ms. After this time, an absorption image was recorded, see Fig. 26(a). The sharp diffraction peaks serve as evidence that the evolution of the atomic ensemble was coherent during the experiment. The mean velocity of the atomic cloud was calculated as $\bar{v} = \bar{p}/m_{Rb}$, with $\bar{p} = 2\hbar k \sum_s |c_s|^2$, where $|c_s|^2$ denotes the fraction of atoms in the s th order momentum state, $|2s\hbar k\rangle$. Time evolution of the mean velocity of the cloud, shown in Fig. 26(b), reveals two important features. First, it validates the predictions of the symmetry analysis. Namely, the current is absent when $\theta = 0$, so that symmetry \hat{S}_t , Eq. (116), holds, and (ii) inversion of θ reverses the current. The detected oscillations of the cloud mean velocity in time are attributed to the contribution from the interference between different Floquet states of the driven quantum system, see second term on the rhs of Eq. (112), thus serving as another evidence of the coherence of the system evolution.

The dependences of the atomic cloud velocity on the phases θ and ϕ are shown in Fig. 27. As predicted by the theory, when $\theta = 0$ or $\phi = 0$, the velocity is nearly zero. The velocity reaches maximum values when the values of both phases are close to

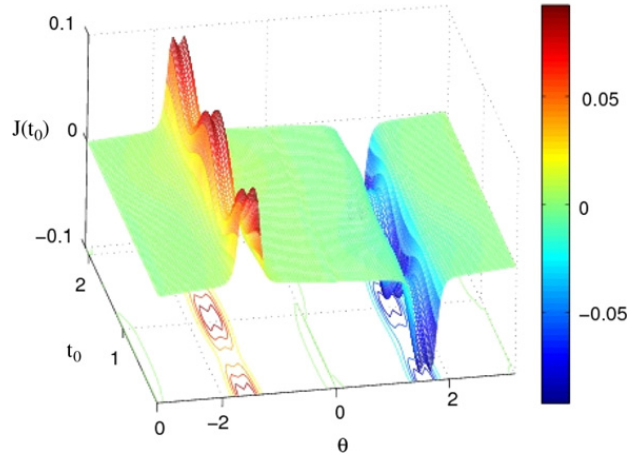


Fig. 24. (Color online) Current dependence on initial time t_0 and phase θ . The parameters are the same as in Fig. 23. Source: Adapted from Ref. [116].

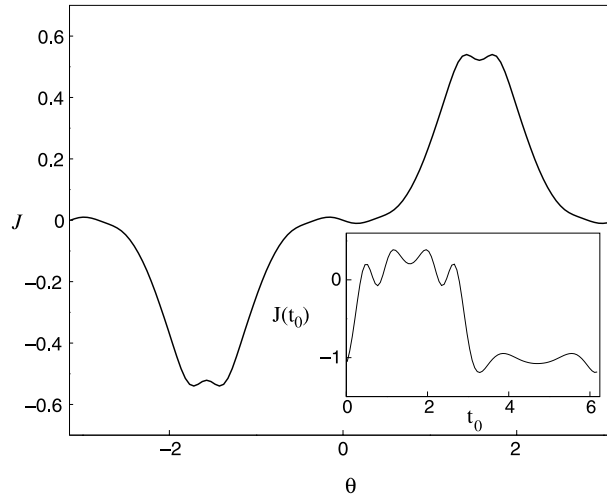


Fig. 25. The average current J vs. θ for the quantum flashing ratchet, Eqs. (124), (125). Inset: Asymptotic current as a function of the starting time t_0 at $\theta = -\pi/2$. The parameters are $E_1 = 2$, $E_2 = 1.5$, $\hbar = 1$, $\omega = 1$, $K = 1.5$, $s = 0.25$, $\phi = \pi/2$. Source: Adapted from Ref. [116].

$\pm\pi/2$, at which values the desymmetrization of Floquet states is expected to be maximal. An important feature of quantum ratchets, which has been observed before in numerical studies, is the dependence of the current on the starting time t_0 . This dependence is another trademark of the coherent quantum evolution. The absence of decoherence allows the system to maintain memory about the initial shape of the potential so that the latter is imprinted in the asymptotic characteristics. Fig. 28 presents the measured dependence of the cloud velocity on t_0 , which clearly corroborated this theoretical prediction. By tuning t_0 in the experiment it was possible to more than double the directed transport velocity. Finally, a resonant-like dependence of the atomic current on the frequency of the drive has been observed. Namely, a sharp maximum was detected for the value of driving frequency close to the recoil frequency ω_R and a smaller resonance peak was observed at $\omega \approx 2\omega_R$. Outside the resonances current value was almost negligible. Altogether the observed effects reproduced the full spectrum of features predicted for ac-driven quantum ratchets.

Finally, a realization of a kicked-rotor version of quantum multiplicative ratchet with a BEC of Rubidium atoms, was reported in Ref. [130].

6. Extensions and outlook

In this review we focused on classical and quantum Hamiltonian single-particle ratchets and their realization with cold and ultracold atomic gases. Many-particle effects in their role in the performance of classical Hamiltonian ratchets have been studied in Ref. [131]. To present date not much results on interacting quantum ratchets are collected [132]. Both on the mean-field level of the Gross-Pitaevsky equation [133,134] and on the genuine quantum many-body level [15], we anticipate intriguing novel results [135–137]. Interactions between particles may not only modify the performance of the ratchets qualitatively but, as well, can also introduce a new symmetry operation – *permutation* – which may discriminate

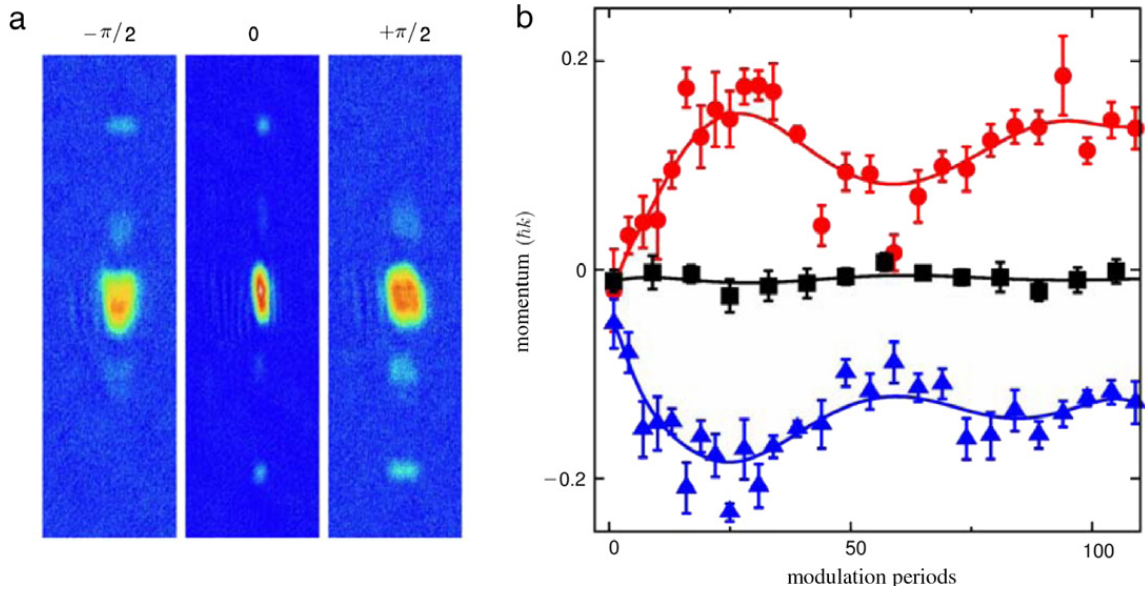


Fig. 26. (a) Time-of-flight images showing the atomic velocity distribution after 26 modulation periods of the ratchet potential for a relative phase between temporal harmonics $\theta = -\pi/2$ (left), $\theta = 0$ (middle), and $\theta = \pi/2$ (right); (b) Mean atomic momentum as a function of time for $\theta = -\pi/2$ (blue triangles), $\theta = 0$ (black squares) and $\theta = \pi/2$ (red dots). (For interpretation of the references to color in this figure legend, the reader is referred to the web version of this article.)

Source: Adapted from Ref. [47].

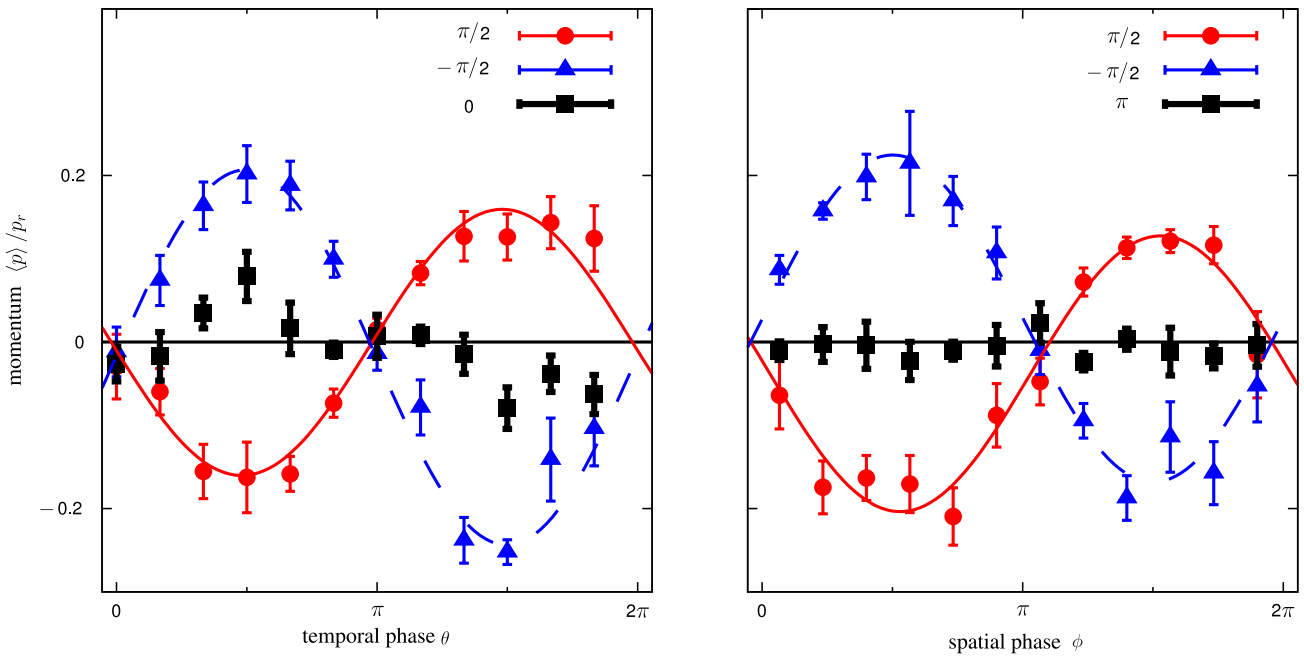


Fig. 27. (Color online) Mean atomic momentum versus temporal phase θ (left panel) and spatial phase ϕ (right panel). The values of the complementary phase are indicated in the right corner of each figure.

Source: Courtesy of Martin Weitz.

between fermionic and bosonic ratchets. An additional symmetry operation may further enhance the overall symmetry and prevent a particle current in situations where it exists in the single-particle regime. Another interesting property of many body systems is the appearance of two separately conserved quantities, namely particle number and energy. Both can be assigned with a current. Ratchets can therefore be designed to promote any of the two current types or even both simultaneously. In particular, the Mott insulator state [138,139] might prevent a flow of atoms, but allow for a directed energy transport.

As we already discussed in Section 4.1, in higher space dimensions vortex currents can be generated. This effect mimics a magnetic field acting on a charged particle. The symmetry-based approach could be relevant for the creation of artificial magnetic fields for neutral and spinless particles, e.g. for atoms [140] or even photons [141]. The symmetry analysis has already been used to synthesize non-Abelian gauge fields with rocking two-dimensional optical potentials [142]. The same

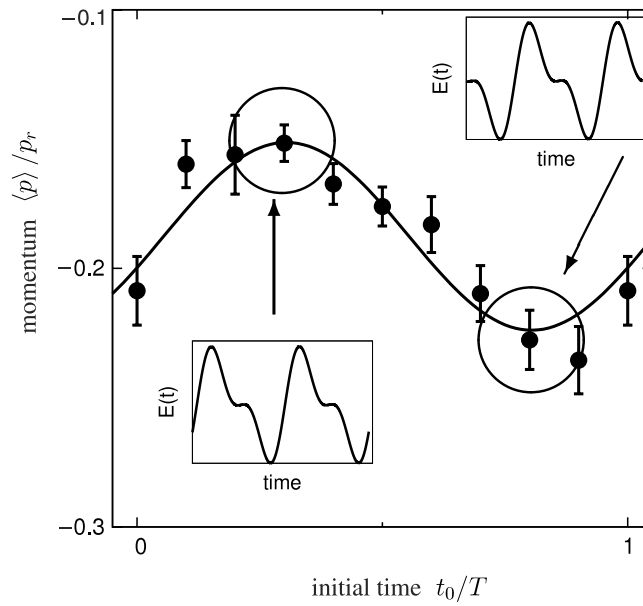


Fig. 28. Mean momentum of the BEC cloud as a function of starting time t_0 . Insets show the initial profiles of the driving field.
Source: Adapted from Ref. [47].

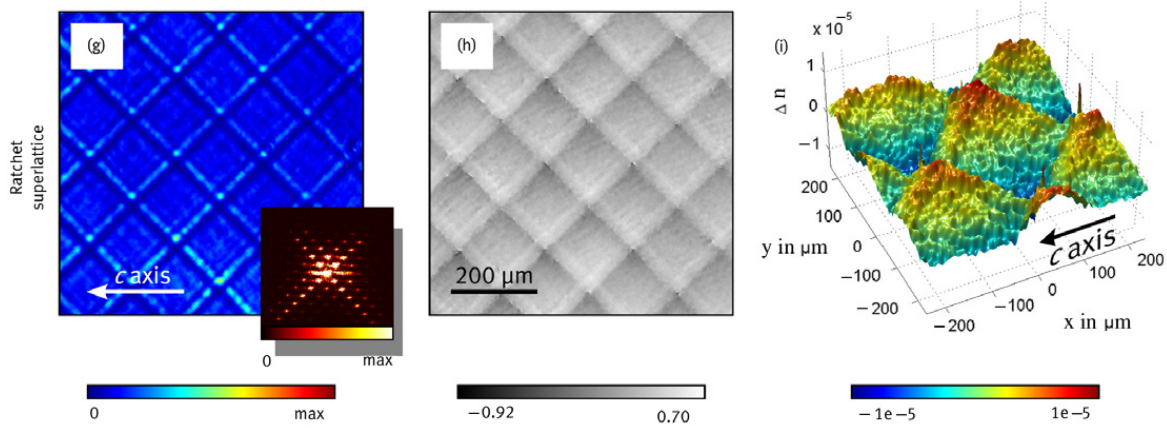


Fig. 29. (Color online) Two-dimensional photonic superlattice with an imprinted ratchet potential. Right panel shows the corresponding refractive index landscape.
Source: Adapted from Ref. [157].

idea can be implemented within other concepts like the spin–orbit coupling in condensed atoms [143], where the coupling strength can be tuned by ac-modulations of the laser intensity [144]. Floquet topological insulators and the fractional quantum Hall effect [145–147] provide further experimental candidates for an implementation of the symmetry analysis.

Notably, many of these essentially quantum effects can also be realized with pure optical setups, by using engineered networks of optical waveguides [148–150]. Different optical realizations of one-dimensional ac-driven quantum ratchets have been proposed [151,152]. In the setup suggested in Ref. [152], the role of time is played by the direction of light propagation and a time-dependent potential is created by spatial modulations of the refractive index along the paraxial direction. The time evolution of a ‘wave-packet’ can be visualized by looking into the spatial intensity of the beam inside the slab. An experimental realization of this idea has already been reported in Ref. [153]. Most interestingly, the analog of time-reversal breaking in an optical waveguide array with periodic modulations of refractive index has been implemented rather recently for the creation of photonic Floquet topological insulators [154]. Finally, optical versions of two-dimensional quantum ratchets can be built with two-dimensional photonic crystals [155–157], cf. Fig. 29.

An alternative experimental test bed for the ratchet concept with ultracold atoms is provided by the ‘atomic wire’ or the ‘atomic chip’ technology [158]. A current-carrying wire produces a magnetic field curling around it, and a potential minimum of the field can be created above the wire by applying an additional dc magnetic component. As a result, a pipe-like potential appears on top of the wire which confines atoms in the transverse direction. The potential follows the wire. Upon slightly meandering this wire it produces a spatially modulated potential. Next, ac-modulations of the flowing current can create the needed ac-modulations of the potential in the transverse direction. The classical variant of a ratchet-based magnetic micro-pump was proposed in Ref. [159] where the corresponding symmetry analysis has been presented.

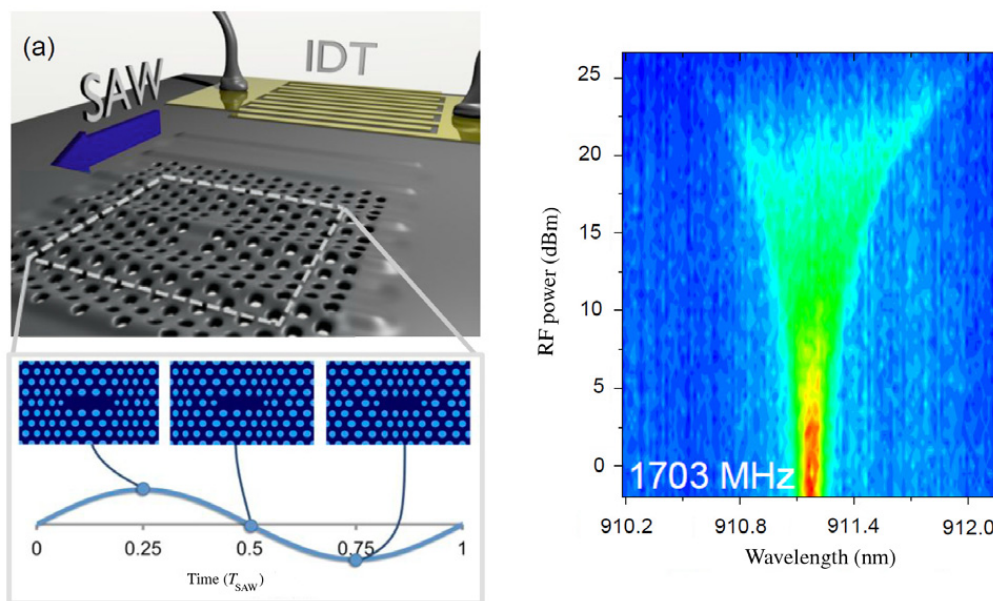


Fig. 30. (Color online) Left panel: Photonic crystal nanocavity modulated by a surface acoustic wave. The wave is generated by a radio-frequency pulse applied to an interdigital transducer. Lower sketch shows deformations of the nanocavity at different times during one modulation period. Right panel: Cavity emission spectra as a function of the pulse power for the driving frequency 1.7 GHz.

Source: Adapted from Ref. [169].

When traversing from classical to quantum ratchets, as detailed in Section 5, the current had to be re-defined via the Schrödinger equation. Other wave equations can be considered as well, and the ratchet concept can be adapted likewise to any other sort of physical current. For instance, the symmetry analysis was applied to the energy current generated by a nonlinear field equation which describes a long Josephson junction [160–162]. The predicted symmetry breaking was linked to the presence of solitons, and the corresponding soliton ratchet was subsequently successfully realized experimentally with a fluxon trapped in an annular Josephson junction which was driven by a microwave field [163]. A promising extension of this idea is the realization of soliton ratchets with matter-wave solitons in a dense Bose–Einstein condensate, in the regime of either attractive (ratchets with bright solitons) [164,165] or repulsive (ratchets with dark solitons) [166,167] interatomic interactions. A symmetry-based control of the directed motion of domain walls in ferromagnets has been studied in Ref. [168] by using the Landau–Lifshitz field equation as a model.

The symmetry approach is not restricted to the case of directed transport only. It can be also applied to any expectation value where zeros in asymptotic regimes emerge that are due to some symmetries, see the general recipe given in Section 2. A proper engineered ac-driving can then lift such symmetries so that the system yields a nonzero expectation value of a designated observable. A good example is the induced transverse magnetization of diluted $s = 1/2$ impurity spins [170]. Here, the applied magnetic field assumed both static and time-periodic components, which however were all perpendicular to the generated magnetization direction. The theoretical ‘prediction’ and explanation of this experimental observation was obtained independently 33 years later [171,172].²⁰ Symmetry analysis can also serve some purposes that are not directly related to a directed transport or polarization of an observable. For example, an interesting application of Hamiltonian ratchets for patterned deposition of particles was proposed in Refs. [173,174].

A perspective venue for the symmetry analysis is the developing field of tunable metamaterials [175]. The ability to change their properties in response to the exposition to voltage [176] and light [177,178] makes these materials appealing candidates for applications in many areas. The responses can be tangibly nonlinear [179] and reveal memory effects [180]. Thus ac-modulations of the controlling field can produce a whole new spectrum of tunable non-equilibrium responses that are absent in the stationary limit. Recent experiments with photonic crystal nanocavities driven by surface acoustic waves show how ac modulations indeed modify the spectrum of the light emitted from the cavity [169], see in Fig. 30, right panel. The experimental setup resembles the traveling potential ratchet discussed in Section 3.3.3. The observed effect of an increasing asymmetry of the spectral broadening with the increase of the driving strength poses a question about the origin of this dynamical symmetry-breaking phenomenon. Another intriguing issue concerns the possibility to observe the consequences of bi-harmonic driving with tunable asymmetry (see in Eq. (36)) in the emission spectrum of the cavity.

In order to properly address the experimental reality, especially of photonics (see the right panel in Fig. 29) and atomic chip technologies,²¹ the issue of disorder has to be taken into account. The role of a static potential disorder in the ac-driven

²⁰ One of us (SF) is indebted to Ennio Arimondo for a clarifying dinner discussion on the theoretical work with the final statement “Your theory has been experimentally verified 33 years ago”, and for the supplying the corresponding reference, Ref. [170].

²¹ Diminutive fluctuations in wire’s meandering and small roughness of the wire surface lead to a strong disorder in the created magnetic potential [158].

ratchet transport is presently an almost unexplored territory.²² We believe that further progress in this direction, especially in the quantum area, will create an intriguing research field at the interface between the Anderson localization [184–187], Floquet formalism [55,118–120] and quantum chaos [21].

Finally, the authors share the hope that this overview will inspire and invigorate readers to embark on this timely theme and enrich it with pursuing their own research.

Acknowledgments

It is a pleasure to thank our colleagues and collaborators Yaroslav Zolotaryuk, Oleg Yevtushenko, Ferruccio Renzoni, Martin Weitz, Sigmund Kohler, Tobias Salger and Christopher Grossert for helpful discussions, suggestions and comments. We acknowledge the financial support of the German Research Foundation (DFG) through the grants, HA1517/31-2, HA1517/35, DE1889/1. We authors thank the Max Planck Institute for the Physics of Complex Systems (Dresden), where parts of this work were accomplished, for its hospitality and kind support.

References

- [1] P. Hänggi, R. Bartussek, Brownian rectifiers: how to convert Brownian motion into directed transport, *Lect. Notes Phys.* 476 (1996) 294.
- [2] R.D. Astumian, Thermodynamics and kinetics of a Brownian motor, *Science* 276 (1997) 917.
- [3] R.D. Astumian, P. Hänggi, Brownian motors, *Phys. Today* 55 (11) (2002) 33.
- [4] P. Reimann, Brownian motors: noisy transport far from equilibrium, *Phys. Rep.* 361 (2002) 57–265.
- [5] M.V. Smoluchowski, Experimentell Nachweisbare der Üblichen thermodynamik widersprechende molekulärphänomene, *Phys. Z.* 13 (1912) 1069.
- [6] R. Feynman, *Feynman Lectures on Physics*, vol. 1, Addison Wesley, Longman, 1970.
- [7] P. Hänggi, F. Marchesoni, F. Nori, Brownian motors, *Ann. Phys. (Leipzig)* 14 (2005) 51.
- [8] P. Hänggi, F. Marchesoni, Artificial Brownian motors: controlling transport on the nanoscale, *Rev. Modern Phys.* 81 (2009) 387–442.
- [9] I. Goychuk, M. Grifoni, P. Hänggi, Nonadiabatic quantum Brownian rectifiers, *Phys. Rev. Lett.* 81 (1998) 649; Nonadiabatic quantum Brownian rectifiers, *Phys. Rev. Lett.* 81 (1998) 2837.
- [10] I. Goychuk, P. Hänggi, Quantum rectifiers from harmonic mixing, *Europhys. Lett.* 43 (1998) 503.
- [11] I. Goychuk, P. Hänggi, Minimal quantum Brownian rectifiers, *J. Phys. Chem. B* 105 (2001) 6642.
- [12] H. Linke, T.E. Humphrey, A. Löfgren, A.O. Sushkov, R. Newbury, R.P. Taylor, P. Omling, Experimental tunneling ratchets, *Science* 286 (1999) 2314.
- [13] V.S. Kharpai, S. Ludwig, J.P. Kotthaus, H.P. Tranitz, W. Wegscheider, Double-dot quantum ratchet driven by an independently biased quantum point contact, *Phys. Rev. Lett.* 97 (2006) 176803.
- [14] G. Grynberg, C. Robilliard, Cold atoms in dissipative optical lattices, *Phys. Rep.* 355 (2001) 335–451.
- [15] I. Bloch, J. Dalibard, W. Zwerger, Many-body physics with ultracold gases, *Rev. Modern Phys.* 80 (2008) 885–964.
- [16] O. Morsch, M. Oberthaler, Dynamics of Bose–Einstein condensates in optical lattices, *Rev. Modern Phys.* 78 (2006) 179–215.
- [17] P. Windpassinger, K. Sengstock, Engineering novel optical lattices, *Rep. Prog. Phys.* 76 (2013) 086401-1–086401-29.
- [18] M.C. Gutzwiller, *Chaos in Classical and Quantum Mechanics*, Springer, Berlin, 1991.
- [19] E. Ott, *Chaos in Dynamical Systems*, Cambridge University Press, Cambridge, 1992.
- [20] R.Z. Sagdeev, D.A. Usikov, G.M. Zaslavsky, *Nonlinear Physics: From the Pendulum to Turbulence and Chaos*, Harwood Academic, Chur, Switzerland, 1992.
- [21] H.-J. Stöckmann, *Quantum Chaos: An Introduction*, Cambridge University Press, 1999.
- [22] H. Risken, *The Fokker–Planck Equation: Methods of Solutions and Applications*, Springer, Berlin, 1984.
- [23] O. Yevtushenko, S. Flach, Y. Zolotaryuk, A. Ovchinnikov, Rectification of current in ac-driven nonlinear systems and symmetry properties of the Boltzmann equation, *Europhys. Lett.* 54 (2001) 141.
- [24] S. Denisov, P. Hänggi, J.L. Mateos, ac-driven Brownian motors: a Fokker–Planck treatment, *Amer. J. Phys.* 77 (2009) 602.
- [25] S. Flach, O. Yevtushenko, Y. Zolotaryuk, Directed current due to broken time–space symmetry, *Phys. Rev. Lett.* 84 (2000) 2358.
- [26] S. Denisov, S. Flach, O. Yevtushenko, A.A. Ovchinnikov, Y. Zolotaryuk, Broken space–time symmetries and mechanisms of rectification of ac fields by nonlinear (non)adiabatic response, *Phys. Rev. E* 66 (2002) 041104.
- [27] S. Denisov, Collective current rectification, *Physica A* 377 (2007) 429.
- [28] P. Curie, Symétrie dans les phénomènes physique: symétrie d'un champ électrique et d'un champ magnétique, *J. Phys. (Paris)* 3 (1894) 343.
- [29] J.G. Freire, C. Cabeza, A. Marti, T. Poschel, J.A.C. Gallas, Antiperiodic oscillations, *Sci. Rep.* 3 (2013) 1.
- [30] I. Goychuk, P. Hänggi, Directed current without dissipation: re-incarnation of a Maxwell–Loschmidt demon, *Lect. Notes Phys.* 557 (2000) 7–20.
- [31] T. Dittrich, R. Ketzmerick, M.-F. Otto, H. Schanz, Classical and quantum transport in deterministic Hamiltonian ratchets, *Ann. Phys. (Leipzig)* 9 (2000) 1.
- [32] H. Schanz, M.-F. Otto, R. Ketzmerick, T. Dittrich, Classical and quantum Hamiltonian ratchets, *Phys. Rev. Lett.* 87 (2001) 070601.
- [33] S. Denisov, S. Flach, Dynamical mechanisms of dc current generation in driven Hamiltonian systems, *Phys. Rev. E* 64 (2001) 056236.
- [34] T.S. Monteiro, P.A. Dando, N.A.C. Hutchings, M.R. Isherwood, Proposal for a chaotic ratchet using cold atoms in optical lattices, *Phys. Rev. Lett.* 89 (2002) 194102.
- [35] G.G. Carlo, G. Benenti, G. Casati, D.L. Shepelyansky, Quantum ratchets in dissipative chaotic systems, *Phys. Rev. Lett.* 94 (2005) 164101.
- [36] S. Savell'ev, F. Marchesoni, P. Hänggi, F. Nori, Signal mixing in a ratchet device: commensurability and current control, *Eur. Phys. J. B* 40 (2004) 403.
- [37] S. Savell'ev, F. Marchesoni, P. Hänggi, F. Nori, Nonlinear signal mixing in a ratchet devices, *Europhys. Lett.* 67 (2004) 179.
- [38] P.H. Jones, M. Goonasekera, F. Renzoni, Rectifying fluctuations in an optical lattice, *Phys. Rev. Lett.* 93 (2004) 073904.
- [39] R. Gommers, S. Bergamini, F. Renzoni, Dissipation-induced symmetry breaking in a driven optical lattice, *Phys. Rev. Lett.* 95 (2005) 073003.
- [40] P. Reimann, Supersymmetric ratchets, *Phys. Rev. Lett.* 86 (2001) 4992.
- [41] R. Bartussek, P. Hänggi, J.G. Kissner, Periodically rocked thermal ratchets, *Europhys. Lett.* 28 (1994) 459.
- [42] J. Luczka, R. Bartussek, P. Hänggi, White-noise-induced transport in periodic structures, *Europhys. Lett.* 31 (1995) 431.
- [43] P. Jung, J.G. Kissner, P. Hänggi, Regular and chaotic transport in asymmetric periodic potentials: inertia ratchets, *Phys. Rev. Lett.* 76 (1996) 3436.
- [44] J.L. Mateos, Chaotic transport and current reversal in deterministic ratchets, *Phys. Rev. Lett.* 84 (2000) 258.
- [45] M. Barbi, M. Salerno, Phase locking effect and current reversals in deterministic underdamped ratchets, *Phys. Rev. E* 62 (2000) 1988.
- [46] S. Denisov, J. Klafter, M. Urbakh, S. Flach, dc-current in Hamiltonian systems by Lévy flights, *Physica D* 170 (2001) 131.
- [47] T. Salger, S. Kling, T. Hecking, C. Geckeler, L.L. Morales-Molina, M. Weitz, Directed transport of atoms in a Hamiltonian quantum ratchet, *Science* 326 (2009) 1241.

²² Though some steps in this directions have been made in the classical corner of the research, see Refs. [181–183].

- [48] A. Ajdari, J. Prost, Mouvement induit par un potentiel périodique de basse symétrie: diélectrophorèse pulsée, *C. R. Acad. Sci. Paris* 315 (1992) 1635.
- [49] M. Schiavoni, L. Sanchez-Palencia, F. Renzoni, G. Grynberg, Phase control of directed diffusion in a symmetric optical lattice, *Phys. Rev. Lett.* 90 (2003) 094101.
- [50] F. Renzoni, Cold atom realizations of Brownian motors, *Contemp. Phys.* 46 (2005) 161–171.
- [51] A.V. Arzola, K. Volke-Sepulveda, J.L. Mateos, Experimental control of transport and current reversals in a deterministic optical rocking ratchet, *Phys. Rev. Lett.* 106 (2011) 168104.
- [52] Q. Niu, Towards a quantum pump of electric charges, *Phys. Rev. Lett.* 64 (1990) 1812.
- [53] B.L. Altshuler, L.I. Glazman, Pumping electrons, *Science* 283 (1999) 1864.
- [54] D.J. Thouless, Quantization of particle transport, *Phys. Rev. B* 27 (1983) 6083.
- [55] S. Kohler, J. Lehmann, P. Hänggi, Driven quantum transport on the nanoscale, *Phys. Rep.* 406 (2005) 379–443.
- [56] M. Strass, P. Hänggi, S. Kohler, Nonadiabatic electron pumping: maximal current with minimal noise, *Phys. Rev. Lett.* 95 (2005) 130601.
- [57] M. Borromeo, F. Marchesoni, Noise-assisted transport on symmetric periodic substrates, *Chaos* 15 (2005) 026110.
- [58] R. Gommers, V. Lebedev, M. Brown, F. Renzoni, Gating ratchet for cold atoms, *Phys. Rev. Lett.* 100 (2008) 040603.
- [59] E. Neumann, A. Pikovsky, Quasiperiodically driven Josephson junctions: strange nonchaotic attractors, symmetries and transport, *Eur. Phys. J. B* 26 (2002) 219.
- [60] S. Flach, S. Denisov, Symmetries and transport with quasiperiodic driving, *Acta Phys. Pol. B* 35 (2004) 1437.
- [61] W.C. Swope, H.C. Andersen, P.H. Berens, K.R. Wilson, A computer simulation method for the calculation of equilibrium constants for the formation of physical clusters of molecules: application to small water clusters, *J. Chem. Phys.* 76 (1982) 637.
- [62] B. Leimkuhler, S. Reich, *Simulating Hamiltonian Dynamics*, Cambridge University Press, 2005.
- [63] H. Schanz, T. Dittrich, R. Ketzmerick, Directed chaotic transport in Hamiltonian ratchets, *Phys. Rev. E* 71 (2005) 026228.
- [64] M.F. Shlesinger, G. Zaslavsky, J. Klafter, Strange kinetics, *Nature* 363 (1993) 31.
- [65] J.D. Meiss, E. Ott, Markov-tree model of transport in area-preserving maps, *Physica D* 20 (1986) 387.
- [66] G. Zumofen, J. Klafter, Laminar - localized - phase coexistence in dynamical systems, *Phys. Rev. E* 51 (1995) 1818.
- [67] S. Denisov, J. Klafter, M. Urbakh, Some new aspects of Lévy walks and flights: directed transport, manipulation through flights and population exchange, *Physica D* 187 (2004) 89.
- [68] U. Feudel, C. Grebogi, B.R. Hunt, J.A. Yorke, Map with more than 100 coexisting low-period periodic attractors, *Phys. Rev. E* 54 (1996) 71.
- [69] C.S. Rodrigues, A.P.S. de Moura, C. Grebogi, Emerging attractors and the transition from dissipative to conservative dynamics, *Phys. Rev. E* 80 (2009) 026205.
- [70] J. Aguirre, R.L. Viana, M.A.F. Sanjuan, Fractal structures in nonlinear dynamics, *Rev. Modern Phys.* 81 (2009) 333–386.
- [71] H.A. Larrondo, C.M. Arizmen, F. Family, Current basins of attraction in inertia ratchets, *Physica A* 320 (2003) 119.
- [72] J.M.T. Thompson, H.B. Stewart, Y. Ueda, Safe, explosive, and dangerous bifurcations in dissipative dynamical systems, *Phys. Rev. E* 49 (1994) 1019.
- [73] J.L. Mateos, Current reversals in chaotic ratchets: the battle of the attractors, *Physica A* 325 (2003) 92.
- [74] A. Celestino, C. Manchein, H.A. Albuquerque, M.W. Beims, Ratchet transport and periodic structures in parameter space, *Phys. Rev. Lett.* 106 (2011) 234101.
- [75] S. Kraut, U. Feudel, Multistability, noise, and attractor hopping: the crucial role of chaotic saddles, *Phys. Rev. E* 66 (2002) 015207.
- [76] R. Graham, T. Tél, On the weak-noise limit of Fokker–Planck models, *J. Stat. Phys.* 35 (1984) 729.
- [77] E. Lifshitz, L. Pitaevsky, *Physical Kinetics*, Pergamon, Oxford, New York, 1981.
- [78] M. Abramowitz, I.A. Stegun (Eds.), *Handbook of Mathematical Functions with Formulas, Graphs, and Mathematical Tables*, Dover Press, New York, 1965.
- [79] P. Jung, Periodically driven stochastic systems, *Phys. Rep.* 234 (1993) 175–295.
- [80] S. Weinberg, *The Quantum Theory of Fields*, Cambridge University Press, Cambridge, 1995.
- [81] J. Dalibard, C. Cohen-Tannoudji, Laser cooling below the Doppler limit by polarization gradients: simple theoretical models, *J. Opt. Soc. Amer. B* 6 (1989) 2023.
- [82] G. Ritt, C. Geckeler, T. Salger, G. Cennini, M. Weitz, Fourier synthesis of conservative atom potentials, *Phys. Rev. A* 74 (2006) 063622.
- [83] <http://en.wikipedia.org/wiki/Sisyphus>.
- [84] F. Renzoni, Ratchets from the cold: Brownian motors with cold atoms in optical lattices, *Europhys. News* 43 (2012) 26–30.
- [85] S. Marksteiner, K. Ellinger, P. Zoller, Anomalous diffusion and Lévy walks in optical lattices, *Phys. Rev. A* 53 (1996) 3409.
- [86] S. Denisov, S. Kohler, P. Hänggi, Underdamped quantum ratchets, *Europhys. Lett.* 85 (2009) 40003.
- [87] A. Kato, Y. Tanimura, Quantum suppression of ratchet rectification in a Brownian system driven by a bi-harmonic force, *J. Phys. Chem.* 117 (2013) 13132.
- [88] R. Gommers, P. Douglas, S. Bergamini, M. Goonasekera, P.H. Jones, F. Renzoni, Resonant activation in a nonadiabatically driven optical lattice, *Phys. Rev. Lett.* 94 (2005) 143001.
- [89] A. Wickenbrock, D. Cubero, N.A.A. Wahab, P. Phoonthong, F. Renzoni, Current reversals in a rocking ratchet: the frequency domain, *Phys. Rev. E* 84 (2011) 021127.
- [90] P.H. Jones, M. Goonasekera, D.R. Meacher, T. Jonckheere, T.S. Monteiro, Directed motion for delta-kicked atoms with broken symmetries: comparison between theory and experiment, *Phys. Rev. Lett.* 98 (2007) 073002.
- [91] F. Renzoni, Driven ratchets for cold atoms, *Adv. Atom. Mol. Opt. Phys.* 57 (2009) 1–32.
- [92] R. Gommers, S. Denisov, F. Renzoni, Quasiperiodically driven ratchets for cold atoms, *Phys. Rev. Lett.* 96 (2006) 240604.
- [93] D.J. Griffiths, *Introduction to Quantum Mechanics*, second ed., Prentice Hall, New York, 2004.
- [94] V. Lebedev, F. Renzoni, Two-dimensional rocking ratchet for cold atoms, *Phys. Rev. A* 80 (2009) 023422.
- [95] S. Denisov, Y. Iolotaryuk, S. Flach, O. Yevtushenko, Vortex and translational currents due to broken time–space symmetries, *Phys. Rev. Lett.* 100 (2008) 224102.
- [96] V.I. Arnold, Instability of dynamical systems with several degrees of freedom, *Sov. Mat. Dokl.* 5 (1964) 581.
- [97] A.J. Lichtenberg, M.A. Leiberman, *Regular and Stochastic Motion*, Springer, New York, 1982.
- [98] S. Bolotin, D. Treschev, Unbounded growth of energy in nonautonomous Hamiltonian systems, *Nonlinearity* 12 (1999) 365.
- [99] J.N. Mather, Arnold diffusion: announcement of results, *J. Math. Sci.* 124 (2004) 5275.
- [100] A. Delshams, G. Hugué, A geometric mechanism of diffusion: rigorous verification in a priori unstable Hamiltonian systems, *J. Differential Equations* 250 (2011) 2601.
- [101] A. Seibert, S. Denisov, A.V. Ponomarev, P. Hänggi, Mapping the Arnold web with a graphic processing unit, *Chaos* 21 (2011) 043123.
- [102] A.W. Ghosh, S.V. Khare, Breaking of general rotational symmetries by multidimensional classical ratchets, *Phys. Rev. E* 67 (2003) 056110.
- [103] I. Derenyi, R.D. Astumian, ac separation of particles by biased Brownian motion in a two-dimensional sieve, *Phys. Rev. E* 58 (1998) 7781.
- [104] C.J. Olson, C. Reichhardt, B. Janko, F. Nori, Collective interaction-driven ratchet for transporting flux quanta, *Phys. Rev. Lett.* 87 (2001) 177002.
- [105] A.D. Chepelianskii, D.L. Shepelyansky, Directing transport by polarized radiation in the presence of chaos and dissipation, *Phys. Rev. B* 71 (2005) 052508.
- [106] G. Cristadoro, D.L. Shepelyansky, Nonequilibrium stationary states with ratchet effect, *Phys. Rev. E* 71 (2005) 036111.
- [107] M.V. Entin, L.I. Magarill, Photocurrent in nanostructures with asymmetric antidots: exactly solvable model, *Phys. Rev. B* 73 (2006) 205206.
- [108] A.D. Chepelianskii, Directed transport born from chaos in asymmetric antidot structures, *Eur. Phys. J. B* 52 (2006) 389.
- [109] A.D. Chepelianskii, M.V. Entin, L.I. Magarill, D.L. Shepelyansky, Photogalvanic current in artificial asymmetric nanostructures, *Eur. Phys. J. B* 56 (2007) 323.
- [110] A. Engel, H.W. Müller, P. Reimann, A. Jung, Ferrofluids as thermal ratchets, *Phys. Rev. Lett.* 91 (2003) 060602.
- [111] A. Engel, P. Reimann, Thermal ratchet effects in ferrofluids, *Phys. Rev. E* 70 (2004) 051107.
- [112] V. Becker, A. Engel, Role of interactions in ferrofluid thermal ratchets, *Phys. Rev. E* 75 (2007) 031118.

- [113] A.D. Chepelienskii, D.L. Shepelyansky, Magnetization of ballistic quantum dots induced by a linear-polarized microwave field, *Eur. Phys. J. B* 55 (2007) 261.
- [114] G. Grynberg, B. Lounis, P. Verkerk, J.-Y. Courtois, C. Salomon, Quantized motion of cold cesium atoms in two- and three-dimensional optical potentials, *Phys. Rev. Lett.* 70 (1993) 2249.
- [115] P. Sjölundlund, S.J.H. Petra, C.M. Dion, S. Jonsell, M. Nysten, L. Sanchez-Palencia, A. Kastberg, Demonstration of a controllable three-dimensional Brownian motor in symmetric potentials, *Phys. Rev. Lett.* 96 (2006) 190602.
- [116] S. Denisov, L. Morales-Molina, S. Flach, P. Hänggi, Periodically driven quantum ratchets: symmetries and resonances, *Phys. Rev. A* 75 (2007) 063424.
- [117] W.C. Henneberger, Perturbation method for atoms in intense light beams, *Phys. Rev. Lett.* 21 (1968) 838.
- [118] J.H. Shirley, Solution of the Schrödinger equation with a Hamiltonian periodic in time, *Phys. Rev.* (1965) B979.
- [119] H. Sambe, Steady states and quasienergies of a quantum-mechanical system in an oscillating field, *Phys. Rev. A* 7 (1973) 2203.
- [120] M. Grifoni, P. Hänggi, Driven quantum tunneling, *Phys. Rep.* 304 (1998) 229–358.
- [121] C.K. Zachos, D.B. Fairlie, T.L. Curtright, *Quantum Mechanics in Phase Space*, World Scientific, Singapore, 2005.
- [122] J. von Neumann, E. Wigner, Über merkwürdige diskrete eigenwerte, *Phys. Z.* 30 (1929) 467.
- [123] M. Heimsoth, C.E. Creffield, F. Sols, Weakly driven quantum coherent ratchets in cold-atom systems, *Phys. Rev. A* 82 (2010) 023607.
- [124] C.E. Creffield, F. Sols, Directed transport in driven optical lattices by gauge generation, *Phys. Rev. A* 84 (2011) 023630.
- [125] S. Denisov, L. Morales-Molina, S. Flach, Quantum resonances and rectification in ac-driven ratchets, *Europhys. Lett.* 79 (2007) 10007.
- [126] F. Zhan, S. Denisov, A.V. Ponomarev, P. Hänggi, Quantum ratchet transport with minimal dispersion rate, *Phys. Rev. A* 84 (2011) 043617.
- [127] T. Salger, S. Kling, S. Denisov, A.V. Ponomarev, P. Hänggi, M. Weitz, Tuning the mobility of a driven Bose–Einstein condensate via diabatic Floquet bands, *Phys. Rev. Lett.* 110 (2013) 135302.
- [128] T. Timberlake, L.E. Reichl, Changes in Floquet-state structure at avoided crossings: delocalization and harmonic generation, *Phys. Rev. A* 59 (1999) 2886.
- [129] T.S.C. Geckeler, S. Kling, M. Weitz, Atomic Landau–Zener tunneling in Fourier-synthesized optical lattices, *Phys. Rev. Lett.* 99 (2007) 190405.
- [130] I. Dana, V. Ramareddy, I. Talukdar, G.S. Summy, Experimental realization of quantum-resonance ratchets at arbitrary quasimomenta, *Phys. Rev. Lett.* 100 (2008) 024103.
- [131] B. Liebchen, F.K. Diakonos, P. Schmelcher, Interaction-induced current reversals in driven lattices, *New J. Phys.* 14 (2012) 103032.
- [132] C.E. Creffield, F. Sols, Controlled generation of coherent matter-currents using a periodic driving field, *Phys. Rev. Lett.* 100 (2008) 250402.
- [133] L.P. Pitaevskii, S. Stringari, *Bose–Einstein Condensation*, Clarendon Press, Oxford, 2003.
- [134] S. Giorgini, L.P. Pitaevskii, S. Stringari, Theory of ultracold atomic Fermi gases, *Rev. Modern Phys.* 80 (2008) 1215.
- [135] D. Poletti, G. Benenti, G. Casati, P. Hänggi, B. Li, Steering Bose–Einstein condensates despite time symmetry, *Phys. Rev. Lett.* 102 (2009) 130604.
- [136] C.E. Creffield, F. Sols, Coherent ratchets in driven Bose–Einstein condensates, *Phys. Rev. Lett.* 103 (2009) 200601.
- [137] A.V. Ponomarev, S. Denisov, P. Hänggi, Quantum machine using cold atoms, *J. Comput. Theor. Nanosci.* 7 (2010) 2441.
- [138] M. Greiner, O. Mandel, T. Esslinger, T.W. Hansch, I. Bloch, Quantum phase transition from a superfluid to a Mott insulator in a gas of ultracold atoms, *Nature* 415 (2002) 39.
- [139] M. Greiner, O. Mandel, T.W. Hansch, I. Bloch, Collapse and revival of the matter wave field of a Bose–Einstein condensate, *Nature* 419 (2002) 51.
- [140] J. Dalibard, F. Gerbier, G. Juzeliunas, P. Ohberg, Artificial gauge potentials for neutral atoms, *Rev. Modern Phys.* 83 (2011) 1523.
- [141] K. Fang, Z. Yu, S. Fan, Realizing effective magnetic field for photons by controlling the phase of dynamic modulation, *Nature Photon.* 6 (2012) 782.
- [142] P. Hauke, O. Tieleman, A. Celi, C.C. Olschlager, J. Simonet, Non-abelian gauge fields and topological insulators in shaken optical lattices, *Phys. Rev. Lett.* 109 (2012) 145301.
- [143] Y.-J. Lin, K. Jimenez-Garcia, I.B. Spielman, Spin–orbit-coupled Bose–Einstein condensates, *Nature* 471 (2011) 83.
- [144] Y. Zhang, G. Chen, C. Zhang, Tunable spin–orbit coupling and quantum phase transition in a trapped Bose–Einstein condensate, *Sci. Rep.* 3 (2013) 1937.
- [145] M.Z. Hasan, C.L. Kane, Topological insulators, *Rev. Modern Phys.* 82 (2010) 3045–3067.
- [146] T. Kitagawa, E. Berg, M. Rudner, E. Demler, Topological characterization of periodically driven quantum systems, *Phys. Rev. B* 82 (2010) 235114.
- [147] N.H. Lindner, G. Refael, V. Galitski, Floquet topological insulator in semiconductor quantum wells, *Nat. Phys.* 7 (2011) 490.
- [148] M. Onoda, S. Murakami, N. Nagaosa, Hall effect of light, *Phys. Rev. Lett.* 93 (2004) 083901.
- [149] S. Longhi, Quantum-optical analogies using photonic structures, *Laser Photon. Rev.* 3 (2009) 243.
- [150] X. Yin, Z. Ye, J. Rho, Y. Wang, X. Zhang, Photonic spin Hall effect at metasurfaces, *Science* 339 (2013) 1405.
- [151] A.V. Gorbach, S. Denisov, S. Flach, Optical ratchets with discrete cavity solitons, *Opt. Lett.* 31 (2006) 1702.
- [152] S. Longhi, Rectification of light refraction in curved waveguide arrays, *Opt. Lett.* 34 (2009) 458.
- [153] F. Dreisow, Y.V. Kartashov, M. Heinrich, V.A. Vysloukh, A. Tünnermann, S. Nolte, L. Torner, S. Longhi, A. Szameit, Spatial light rectification in an optical waveguide lattice, *Europhys. Lett.* 101 (2013) 44002.
- [154] M.C. Rechtsman, J.M. Zeuner, Y. Plotnik, Y. Lumer, D. Podolsky, F. Dreisow, S. Nolte, M. Segev, A. Szameit, Photonic Floquet topological insulators, *Nature* 496 (2013) 196.
- [155] A. Forchel, Photonic crystals: switching light with light, *Nature Mater.* 2 (2003) 13.
- [156] J. Riedrich-Möller, L. Kipfstuhl, C. Hepp, E. Neu, C. Pauly, F. Mücklich, A. Baur, M. Wandt, S. Wolff, M. Fischer, S. Gsell, M. Schreck, C. Becher, One- and two-dimensional photonic crystal microcavities in single crystal diamond, *Nature Nanotechnol.* 7 (2011) 69.
- [157] M. Boguslawski, A. Kelberer, P. Rose, C. Denz, Multiplexing complex two-dimensional photonic superlattices, *Opt. Express* 20 (2012) 27331.
- [158] J. Fortagh, C. Zimmermann, Magnetic microtraps for ultracold atoms, *Rev. Modern Phys.* 79 (2007) 235.
- [159] S.J. Lade, Ratchet-based magnetic micropump, *Europhys. Lett.* 92 (2010) 33001.
- [160] S. Flach, Y. Zolotaryuk, A. Miroshnichenko, M. Fistul, Broken symmetries and directed collective energy transport in spatially extended systems, *Phys. Rev. Lett.* 88 (2002) 184101.
- [161] M. Salerno, Y. Zolotaryuk, Soliton ratchetlike dynamics by ac forces with harmonic mixing, *Phys. Rev. E* 65 (2002) 056603.
- [162] M.V. Fistul, A.E.A.E. Miroshnichenko, S. Flach, ac field-induced quantum rectification effect in tunnel junctions, *Phys. Rev. B* 68 (2003) 153107.
- [163] A.V. Ustinov, C. Coqui, A. Kemp, Y. Zolotaryuk, M. Salerno, Ratchet-like dynamics of fluxons in annular Josephson junctions driven by bi-harmonic microwave fields, *Phys. Rev. Lett.* 93 (2004) 087001.
- [164] D. Poletti, T.J. Alexander, E.A. Ostrovskaya, B. Li, Y.S. Kivshar, Dynamics of matter-wave solitons in a ratchet potential, *Phys. Rev. Lett.* 101 (2008) 150403.
- [165] J. Abdullaev, D. Poletti, E.A. Ostrovskaya, Y.S. Kivshar, Controlled transport of matter waves in two-dimensional optical lattices, *Phys. Rev. Lett.* 105 (2010) 090401.
- [166] S. Burger, K. Bongs, S. Dettmer, W. Ertmer, K. Sengstock, Dark solitons in Bose–Einstein condensates, *Phys. Rev. Lett.* 83 (1999) 5198.
- [167] C. Becker, S. Stellmer, P. Soltan-Panahi, S. Dörscher, M. Baumert, E.-M. Richter, J. Kronjäger, K. Bongs, K. Sengstock, Oscillations and interactions of dark and dark-bright solitons in Bose–Einstein condensates, *Nat. Phys.* 4 (2008) 496.
- [168] Y. Zolotaryuk, M.M. Osmanov, Directed motion of domain walls in biaxial ferromagnets under the influence of periodic external magnetic fields, *Eur. Phys. J. B* 79 (2011) 257.
- [169] D.A. Fuhrmann, S.M. Thon, Hyochu Kim, D. Bouwmeester, P.M. Petroff, A. Wixforth, H.J. Krenner, Dynamic modulation of photonic crystal nanocavities using gigahertz acoustic phonons, *Nature Photonics* 5 (2011) 605.
- [170] E. Arimondo, Angular momentum detection of non-linear phenomena in paramagnetic resonance, *Ann. Phys. (Paris)* 3 (1968) 425.
- [171] S. Flach, A. Ovchinnikov, Static magnetization induced by time-periodic fields with zero mean, *Physica A* 292 (2001) 268.
- [172] S. Flach, A.E. Miroshnichenko, A.A. Ovchinnikov, ac-driven quantum spins: resonant enhancement of transverse dc magnetization, *Phys. Rev. B* 65 (2002) 104438.
- [173] C. Petri, F. Lenz, F.K. Diakonos, P. Schmelcher, Directed transport and localization in phase-modulated driven lattices, *Phys. Rev. E* 81 (2010) 046219.

- [174] B. Liebchen, C. Petri, F. Lenz, P. Schmelcher, Patterned deposition of particles in spatio-temporally driven lattices, *Europhys. Lett.* 94 (2011) 40001.
- [175] A.D. Boardman, V.V. Grimalsky, Y.S. Kivshar, S.V. Koshevaya, M. Lapine, N.M. Litchinitser, V.N. Malnev, M. Noginov, Y.G. Rapoport, V.M. Shalaev, Active and tunable metamaterials, *Laser Photonics Rev.* 5 (2011) 287.
- [176] H.-T. Chen, J.F. O'Hara, A.K. Azad, A.J. Taylor, R.D. Averitt, D.B. Shrekenhamer, W.J. Padilla, Experimental demonstration of frequency-agile terahertz metamaterials, *Nature Photon.* 2 (2008) 295.
- [177] W.J. Padilla, J. Taylor, C. Highstrete, M. Lee, R.D. Averitt, Dynamical electric and magnetic metamaterial response at terahertz frequencies, *Phys. Rev. Lett.* 96 (2006) 107401.
- [178] I.V. Shadrivov, P.V. Kapitanova, S.I. Maslovski, Y.S. Kivshar, Metamaterials controlled with light, *Phys. Rev. Lett.* 109 (2012) 083902.
- [179] N.I. Zheludev, Y.S. Kivshar, From metamaterials to metadevices, *Nature Mater.* 11 (2012) 917.
- [180] T. Driscoll, Hyun-Tak Kim, Byung-Gyu Chae, Bong-Jun Kim, Yong-Wook Lee, N.M. Jokerst, S. Palit, D.R. Smith, M. Di Ventra, D.N. Basov, Memory metamaterials, *Science* 325 (2009) 1518.
- [181] F. Marchesoni, Transport properties in disordered ratchet potentials, *Phys. Rev. E* 56 (1997) 2492.
- [182] M.N. Popescu, C.M. Arizmendi, A.L. Salas-Brito, F. Family, Disorder induced diffusive transport in ratchets, *Phys. Rev. Lett.* 85 (2000) 3321.
- [183] C.M. Arizmendi, F. Family, A.L. Salas-Brito, Quenched disorder effects on deterministic inertia ratchets, *Phys. Rev. E* 63 (2001) 061104.
- [184] P.W. Anderson, Absence of diffusion in certain random lattices, *Phys. Rev. Lett.* 109 (1958) 1492.
- [185] G. Roati, C. D'Errico, L. Fallani, M. Fattori, C. Fort, M. Zaccanti, G. Modugno, M. Modugno, M. Inguscio, Anderson localization of a non-interacting Bose–Einstein condensate, *Nature* 453 (2008) 895.
- [186] L. Sanchez-Palencia, Quantum gases: joint forces against disorder, *Nat. Phys.* 6 (2010) 328.
- [187] M. Segev, Y. Silberberg, D.N. Christodoulides, Anderson localization of light, *Nature Photon.* 7 (2013) 197.